

**MEASUREMENTS OF DIFFUSION COEFFICIENTS OF ORGANIC DYES IN PROXIES OF
ATMOSPHERIC PARTICLES**

by

Dagny Anna Ullmann

B.Sc., Christian-Albrechts-Universität zu Kiel, 2013

A THESIS SUBMITTED IN PARTIAL FULFILLMENT OF
THE REQUIREMENTS FOR THE DEGREE OF

MASTER OF SCIENCE

in

THE FACULTY OF GRADUATE AND POSTDOCTORAL STUDIES
(Chemistry)

THE UNIVERSITY OF BRITISH COLUMBIA
(Vancouver)

June 2017

© Dagny Ullmann, 2017

Abstract

Atmospheric particles play a significant role in the atmosphere and climate. To be able to better predict their rate of growth and reactivity, information on diffusion coefficients of organic molecules in these particles is needed.

Diffusion coefficients of organic tracer molecules were measured in sucrose water solutions, which served as proxies for atmospheric particles. Diffusion coefficients of rhodamine 6G (hydrodynamic radius = 5.89 Å), an organic tracer molecule, ranged from $1.50 \cdot 10^{-14}$ to $4.73 \cdot 10^{-9}$ cm²/s as the water activity ranged from 0.38 to 0.8, respectively, in sucrose water solutions. The measured diffusion coefficients were compared to diffusion coefficients calculated using the Stokes-Einstein equation, which has often been used in the past to estimate diffusion coefficients in atmospheric particles. A breakdown of the Stokes-Einstein equation was observed at a water activity of 0.38 or a viscosity of $3.3 \cdot 10^6$ Pa s or T_g/T of 0.94 (T_g being the glass transition temperature and T the temperature of the measurement).

In addition, diffusion coefficients of intrinsic fluorophores were measured in brown limonene secondary organic material (SOM) which is thought to be important in the atmosphere. The SOM was generated by the oxidation of limonene followed by aging with NH₃ vapour. The diffusion coefficients of the intrinsic fluorophores in brown limonene SOM ranged from $3.82 \cdot 10^{-12}$ to $8.32 \cdot 10^{-9}$ cm²/s as the water activity ranged from 0.38 to 0.9. From the diffusion coefficients mixing times of large organics in brown limonene SOM were calculated, which ranged from 0.001 to 2.6 s across water activities of 0.9 and 0.38. Hence, mixing times of large

organics are short and atmospheric particles consisting of brown limonene SOM are well mixed in the atmosphere when water activities range from 0.38 to 0.9.

Furthermore, the hydrodynamic radius of the intrinsic fluorophores within brown limonene SOM was determined to be $7.34 \pm 1.47 \text{ \AA}$. This hydrodynamic radius is consistent with suggested structures for the intrinsic fluorophores.

Lay Summary

How will the climate change in the future? Climate researchers have developed models to answer that question and predict climate change accurately. The research conducted in this thesis is providing information on atmospheric particles (particles suspended in air) to improve climate models. Atmospheric particles can either cool down climate by scattering sunlight or can heat up climate by absorbing sunlight. The knowledge of growth rates and reactivity of atmospheric particles is needed to improve the quality of climate models. Growth rates and reactivity of atmospheric particles depend on the mobility of molecules inside an atmospheric particle, which can be measured in terms of diffusion coefficients. In this thesis, diffusion coefficients of organic molecules within proxies of atmospheric particles were determined. Using the diffusion coefficients, mixing times of large organic molecules and the radius of a diffusing molecule unknown prior to this study was calculated.

Preface

Chapter 2 is part of a co-authored peer-reviewed journal article. The details of my contribution are provided below the citations:

Chapter 2 (Second author on a journal article): Chenyakin, Y., Ullmann, D. A., Evoy, E., Renbaum-Wolff, L., Kamal, S., and Bertram, A. K.: Diffusion coefficients of organic molecules in sucrose–water solutions and comparison with Stokes–Einstein predictions, *Atmos. Chem. Phys.*, 17, 2423-2435, doi:10.5194/acp-17-2423-2017, 2017.

- Prepared samples of R6G in sucrose water solutions and performed fluorescence recovery after photobleaching experiments on these samples
- Conducted data analysis with the help of Dr. Saied Kamal
- Writing of the text regarding the experiments on R6G was shared with my supervisor
- Contribution of other authors:
 - Y. Chenyakin and A.K. Bertram identified the research question and developed the experimental setup and wrote the main body of the publication
 - Y. Chenyakin performed experiments on calcein and fluorescein and conducted data analysis with the help of Dr. Saied Kamal

Chapter 3 and 4 are to be submitted for publication. The details of my contributions to these research chapters are provided below:

- Identified research question with help from my supervisor

- SOM samples were produced by Mallory Hinks from the Department of Chemistry, University of California, Irvine, CA, USA
- Designed additional experimental setup for the preparation of R6G samples
- Prepared samples of SOM at various relative humidities
- Performed fluorescence recovery after photobleaching experiments
- Conducted data analysis with the help of Dr. Saied Kamal
- Prepared all figures for the manuscript
- Shared writing of the manuscript with my supervisor
- Prof. Allan Bertram and Dr. Saied Kamal derived the correction for fluorescence data of the fluorescent organic molecule in brown limonene SOM

Table of Contents

Abstract	ii
Lay Summary.....	iv
Preface.....	v
Table of Contents	vii
List of Tables	xii
List of Figures	xv
List of Symbols	xxiii
List of Acronyms	xxvi
Acknowledgements	xxvii
Chapter 1: Introduction	1
1.1 Atmospheric Particles	1
1.1.1 Formation, Composition and Sizes	1
1.1.2 Effects of Atmospheric Particles on Humans and Climate	2
1.2 The Importance of Molecular Motion Within Atmospheric Particles	4
1.3 Theories of Molecular Motion	6
1.4 Overview of this Thesis	7
Chapter 2: Diffusion Coefficients of Rhodamine 6G in Sucrose Water Solutions, a Proxy for Atmospheric Particles.....	9
2.1 Introduction	9

2.2	Experimental	12
2.2.1	Sample Preparation	12
2.3	Introduction to Fluorescence Recovery After Photobleaching (FRAP).....	17
2.3.1	FRAP Measurements.....	18
2.3.2	Analysis of the FRAP Data	20
2.3.3	Cylindrical Geometry of the Photobleaching Region.....	26
2.3.4	Corrections for Nonlinearity of the Fluorescence Intensity as a Function of Concentration of R6G	27
2.4	Results and Discussion	33
2.4.1	Diffusion Coefficients of R6G in Sucrose Water Solutions	33
2.4.2	Breakdown of the Stokes-Einstein Equation	33
2.4.3	Comparison with Diffusion Coefficients of Other Molecules in Sucrose Water Solutions.....	36
2.4.4	Breakdown of the Stokes-Einstein Equation for Molecules of Different Hydrodynamic Radii	37
Chapter 3: Diffusion Coefficients and Mixing Times of Fluorescent Organic Molecules in Brown Limonene Secondary Organic Material.....		41
3.1	Introduction	41
3.2	Experimental	44
3.2.1	Generation and Collection of Brown Limonene SOM	44

3.2.2	Preparation of Thin Films of Brown Limonene SOM at Water Activities Ranging from 0.38 to 0.9	45
3.2.3	Measurements of Diffusion Coefficients Using rFRAP	46
3.2.4	Analysis of the Images from the rFRAP Recovery Experiments	48
3.2.5	Effect of Laser Power on Measured Diffusion Coefficients	52
3.2.6	Corrections for Non-linearity of the Fluorescence Intensity as a Function of Concentration of the Intrinsic Fluorophores	52
3.3	Results and Discussion	55
3.3.1	Diffusion Coefficients of Intrinsic Fluorophores within Brown Limonene SOM	55
Chapter 4: The Hydrodynamic Radius of Intrinsic Fluorophores in Brown Limonene SOM		59
4.1	Introduction	59
4.2	Experimental	60
4.2.1	Preparation of Brown Limonene SOM Samples at Water Activities of 0.7, 0.8 and 0.9.....	60
4.2.2	Introduction of R6G into Brown Limonene SOM Samples	61
4.2.3	rFRAP Experiments: Measurements of Diffusion Coefficients of R6G and the Intrinsic Fluorophores in Brown Limonene SOM.....	63
4.2.4	Analysis of rFRAP Images Recorded for the Samples Containing R6G	64
4.2.5	Correction for Reversible Photobleaching.....	66
4.2.6	Corrections for Non-linearity of Fluorescence Intensity as a Function of Concentration of R6G	66

4.3	Results and discussion	70
4.3.1	Example of Experimental Data.....	70
4.3.2	Measured Diffusion Coefficients of the Intrinsic Fluorophores in Brown Limonene SOM.....	73
4.3.3	Measured Diffusion Coefficients of R6G in Brown Limonene SOM	74
4.3.4	Calculation of the Hydrodynamic Radius of Intrinsic Fluorophores in Brown Limonene SOM.....	75
4.3.5	Comparison with Previous Suggestions of the Molecular Structures and Formulas for the Light Absorbing Compounds and Intrinsic Fluorophores in Brown Limonene SOM	76
Chapter 5: Conclusion and Future Work.....		78
5.1	Measurement of Diffusion Coefficients in Proxies of Atmospheric Particles	78
5.2	Average Hydrodynamic Radius of the Intrinsic Fluorophores in Brown Limonene SOM.....	79
5.3	Consideration of Future Work	79
Bibliography.....		81
Appendices		97
Appendix A.....		97
A.1	Parameterization of the viscosity of sucrose in water as a function of water activity.....	98
A.2	Determination of water activities of sucrose solutions.....	99
A.3	Polynomial fit for diffusion coefficients of water from Price <i>et al.</i>	99

Appendix B	100
Appendix C	101

List of Tables

Table 2.1: Information on rhodamine 6G (R6G) including the molecular weight (MW), the chemical structure and the hydrodynamic radius.....	12
Table 2.2: Saturated salt solutions used for conditioning and storing samples at specific water activities in sealed glass jars.	15
Table 2.3: Best fit parameters for concentration vs. normalized fluorescence intensity data in Figure 2.10. $c = c_0 + A \cdot e^{B \cdot x}$, where c is the concentration and x is the normalized fluorescence intensity. The R^2 value indicated the quality of the fit.	30
Table 2.4: Hydrodynamic radius (R_H) and molecular weight (MW) of several molecules considered in this work.....	36
Table 2.5: Properties of the molecules shown in Figure 2.15.	39
Table 3.1: Physico-chemical data on limonene including the molecular weight (MW) and the molecular structure.	42
Table 4.1: Parameterization of the data shown in Figure 4.4.	69
Table 4.2: Average and 95 % confidence intervals of the diffusion coefficients of R6G ($D(R6G)$) to the diffusion coefficient of the intrinsic fluorophores($D(SOM)$) in brown limonene SOM at three different water activities.....	76
Table 5.1: Diffusion coefficients of R6G in sucrose-water solutions and the intrinsic fluorophores in brown limonene SOM.....	78

Table 5.1: Selected parameters used in rhodamine 6G rFRAP experiments in sucrose water solutions. τ_{eq} is the characteristic diffusion time of water within sucrose-water droplet (see Eq. 2.1). t_{exp} is the time used for conditioning..... 97

Table 5.2: Fit parameters of the third order polynomial fit ($f(x) = A + Bx + Cx^2 + Dx^3$) in Figure 5.1. 98

Table 5.3: Parameters from the polynomial fit in Figure 2.14 with $f(x) = A + Bx + Cx^2 + Dx^3$ based on Price *et al.*³¹ 99

Table 5.4: Selected parameters used in rFRAP experiments with the intrinsic fluorophores in brown limonene SOM. τ_{eq} is the characteristic diffusion time of water within sucrose-water droplet (see Eq. 2.1). t_{exp} is the time used for conditioning. 100

Table 5.5: Values of diffusion coefficients, fluorescence intensities and calculated concentrations in citric acid water solution and sucrose water solution for 90% RH of R6G in brown limonene SOM. τ_{eq} is the characteristic diffusion time of water within sucrose water droplet (see Eq. 2.1). t_{exp} is the time used for conditioning. 101

Table 5.6: Values of diffusion coefficients, fluorescence intensities and calculated concentrations in citric acid water solution and sucrose water solution for 80% RH of R6G in brown limonene SOM. τ_{eq} is the characteristic diffusion time of water within sucrose water droplet (see Eq. 2.1). t_{exp} is the time used for conditioning. 103

Table 5.7: Values of diffusion coefficients, fluorescence intensities and calculated concentrations in citric acid water solution and sucrose water solution for 70% RH of R6G in

brown limonene SOM. τ_{eq} is the characteristic diffusion time of water within sucrose-water droplet (see Eq. 2.1). t_{exp} is the time used for conditioning. 104

List of Figures

Figure 1.1: Formation and removal processes and classification of atmospheric particles.	2
Figure 1.2: Schematic of the formation of atmospheric particles and their effects on the climate. Based on Renbaum-Wolff <i>et al.</i> (2013). ⁸	3
Figure 1.3: Radiative forcing of climate forcing species including their uncertainties. Reproduced with permission from Stocker <i>et al.</i> (2013). ¹⁰	4
Figure 1.4: Illustration of the influence of diffusion rates on heterogeneous reactions within atmospheric particles. Reproduced with permission from Lindsay Renbaum-Wolff <i>et al.</i> , “Viscosity of α -pinene secondary organic material and implications for particle growth and reactivity”, PNAS, 2013, 110 (20), 8014-8019; doi: 10.1073/pnas.1219548110.....	5
Figure 2.1: Schematic of the flow cell used to condition samples to the desired water activities.	14
Figure 2.2: Schematic of the glass jar used to condition samples of water activities below 0.6.	14
Figure 2.3: Schematic of the sample used in the FRAP experiments. Panel a) is a top view and Panel b) is a side view. The sample consists of sucrose, water and trace amounts of the fluorescent tracer dye, rhodamine 6G.	16
Figure 2.4: Schematic illustrating the photobleaching and diffusion process of fluorescent molecules. Shown is a side view of the sample cell at various times t during the rFRAP experiment. See text for further details.	18

Figure 2.5: Schematic of a fluorescent film (view from top) and its bleached area. A section of a fluorescent film is scanned in the x- and y-direction. A defined rectangular area (bleached area) of the length l_x and the width l_y is photobleached. 19

Figure 2.6: A fluorescent film consisting of a sucrose-water solution ($a_w=0.75$) and R6G viewed using a laser scanning microscope. Panel A) shows the fluorescent film prior to photobleaching. Panel B) to F) show the recovery of the fluorescence signal over time t . Panel B) was taken directly after the photobleaching process at time $0s$, whereas panel F) shows the fluorescent film after $700s$ after the photobleaching step. The orange rectangle represents the area that was chosen for photobleaching..... 24

Figure 2.7: Plots of fluorescent intensity as a function of x-position, integrated over all y-positions of an a_w of 0.75. Panel A is an image taken directly after photobleaching and panel B) to D) show the recovery of the fluorescence intensity due to diffusion. The red line is a fit using Equation 2.8. 25

Figure 2.8: Plot of wD, t, r as a function of time t for a film of a solution containing R6G, sucrose and water of $a_w=0.75$. Every blue circle represents a value of wD, t, r obtained from fits to the experimental data, such as shown in from Figure 2.7. The red line is a linear plot to the data. Since $wD, t, r = r^2 + 4Dt$, the diffusion coefficient could be calculated from the slope of the line. The first $50s$ have been excluded from the analysis because of reversible photobleaching. 26

Figure 2.9: Cross section through a fluorescent film at $a_w=0.38$ after photobleaching. The photobleached areas have a size of $5 \times 5 \mu\text{m}$ (a) and $20 \times 20 \mu\text{m}$ (b). The fluorescent films were about $70 \mu\text{m}$ thick. 27

Figure 2.10: Fluorescence intensity as a function of the concentration of R6G in sucrose-water solutions, for concentrations in a 50 wt % sucrose-water solution. 28

Figure 2.11: Concentration of R6G in mM as a function of fluorescence intensity. The red line is a nonlinear fit to the data using an exponential function. 29

Figure 2.12: Illustration of the choice of droplets used for the experiment on reversible photobleaching. Panel a) shows the droplet which is to be photobleached (red circle) and the reference droplet (blue dashed circle) prior to photobleaching and panel b) shows both droplets after photobleaching. 31

Figure 2.13: The fluorescence intensity-versus-time for two droplets used to test for reversible photobleaching. A sucrose-water droplet containing R6G of $a_w=0.6$ was photobleached over its total area, so that its fluorescence intensity decreased by 18%. While the recovery of the photobleached droplet (blue triangles) was monitored a reference droplet (green crosses) not being photobleached was also monitored. For the analysis of the recovery, the fluorescence intensity was averaged across the complete droplet. 32

Figure 2.14: Shown are the diffusion coefficients of R6G in sucrose water solution in comparison to diffusion coefficient values calculated from viscosities from Quintas *et al.* (2006; blue triangles)⁴⁶, Migliori *et al.* (2007; blue crosses)⁴⁷, Telis *et al.* (2007 ; blue circles)⁴⁸ and Power *et al.* (2013 ; blue rectangles)^{15e} using the Stokes-Einstein equation and the R_H measured by Müller

et al. (2008)²⁴. The error bars for the diffusion coefficients of R6G represent 95% confidence limit, while the red star itself represent the average value of the diffusion coefficients measured. The black solid line represents a 4th order polynomial which was fit to the literature values. The dashed line represents the 95% prediction limit that was fit to the calculated diffusion coefficients..... 35

Figure 2.15: Shown are the diffusion coefficients of fluorescein, calcein (data used from Y. Chenyakin³²), water (data used from Price *et al.*³¹) and R6G in sucrose water solutions. The error bars in x-direction are 95% confidence intervals. 37

Figure 2.16: $D_{\text{measured}}/D_{\text{predicted}}$ as a function of $R_{\text{diffusing}}/R_{\text{matrix}}$. Panel A corresponds to $a_w=0.6$ and Panel B $a_w=0.38$. D_{measured} is the measured diffusion coefficient and $D_{\text{predicted}}$ is the predicted diffusion coefficient. $R_{\text{diffusing}}$ is the hydrodynamic radius of the diffusing species and R_{matrix} is the hydrodynamic radius of the matrix molecule (sucrose) (Ribeiro *et al.* (2006)²⁵. The data for calcein and fluorescein was taken from Chenyakin *et al.* (2016)^{16b}, the data for sucrose was taken from Price *et al.* (2016)⁵². In order to calculate $D_{\text{predicted}}$ using the Stokes-Einstein equation, a parameterization for the viscosity of sucrose water solution was used (see Appendix A). The error bars for all of the data points were calculated conservatively using the largest error possible for D_{measured} as well as $D_{\text{predicted}}$ and the total error was determined using a Gaussian error propagation..... 40

Figure 3.1: Simplified suggested reaction mechanism for the formation of larger organic molecules, which have the potential to be light absorbing in the UV- and the visible light range, from limonene (Nguyen *et al.* (2013)).⁵⁸ 42

Figure 3.2: Preparation of the SOM samples from the reaction of limonene with O₃. The orange circles represent SOM particles. 45

Figure 3.3: Images recorded during an rFRAP experiment with brown limonene SOM at three different water activities: 0.38, 0.6 and 0.9. The orange rectangles depict the area that is to be photobleached. Indicated in the figures are the times (t) after photobleaching. 48

Figure 3.4: Fluorescence intensities integrated over the bleach width in the y-direction as a function of x-position (in pixels) for selected brown limonene SOM films at a_w = 0.38, 0.6 and 0.9. The blue dots represent the intensity measurements and the red line is a fit to the data using Equation 2.8..... 50

Figure 3.5: Plot of $wD, t, r = r^2 + 4Dt$ as a function of time. The blue circles represent the data which was obtained from figures such as Figure 3.4. The red line is a linear fit to the data. The diffusion coefficients were obtained from the slopes and are $D = 0.0007792/4 = 0.0001948 \mu\text{m}^2/\text{s} = 1.95 \cdot 10^{-12} \text{ cm}^2/\text{s}$ for a_w=0.0.38, $D = 0.04189/4 = 0.0105 \mu\text{m}^2/\text{s} = 1.05 \cdot 10^{-10} \text{ cm}^2/\text{s}$ for a_w=0.6 and $D = 3.753/4 = 0.938 \mu\text{m}^2/\text{s} = 9.38 \cdot 10^{-9} \text{ cm}^2/\text{s}$ for a_w=0.9. 51

Figure 3.6: Diffusion coefficients of intrinsic fluorophores in brown Limonene SOM (black squares). The y-error bars were calculated from the 95% confidence limit. The grey solid line is a linear fit to the data and the grey dotted line the 95% prediction limit of the fit. The blue vertical bar depicts the highest and the lowest limit of calculated diffusion coefficients of brown limonene SOM (reacted with NH₃) based on viscosity measurements from Hinks *et al.* (2016). The secondary y-axis shows the mixing time, which is the time that would be needed for intrinsic fluorophores to mix within a 200 nm brown limonene particle. 57

Figure 4.1: Schematic illustrating the introduction of R6G into pure brown limonene SOM particles. First, the dye is nebulized onto a glass slide (panel a). Then, the dye is removed from half of the glass slide (panel b). The nebulized glass slide containing R6G is placed on top of a glass slide containing brown limonene SOM droplets and the two glass slides are sandwiched together (panel c). The resulting sample has both SOM films with R6G and without R6G (panel d). 62

Figure 4.2: Schematic illustrating the subtraction of fluorescence intensities of images of pure brown limonene SOM from images of brown limonene SOM films containing R6G. Panel a) shows the image of a fluorescent film consisting of R6G in brown limonene SOM at $t=0$ s, panel b) shows the image of a fluorescent film consisting of pure brown limonene SOM and panel c) shows an image that was produced by subtracting the fluorescent intensity of pure brown limonene SOM from the fluorescence intensity of a brown limonene SOM film containing R6G. Panels e) to g) show the corresponding profiles to the images of panels a) to c). 65

Figure 4.3: Integrated intensity as a function of the concentration of R6G in various media: citric acid in water (55 wt %), sucrose in water (50 wt %) and pure water. Experiments were carried out with a laser power of $4.08 \mu\text{W}$. The open and solid symbols depict measurements performed on two different days to confirm reproducibility of the measurements. For citric acid and sucrose water solutions measurements were performed on two different days and for R6G in water only one measurement was performed. The error bars represent one standard deviation (1σ) obtained from three different measurements. 68

Figure 4.4: Concentration of R6G (mM) as a function of integrated intensity in various media, citric acid in water (55 wt %), sucrose in water (50 wt %) and pure water. The solid lines are plots describing the trend of the data. The open and the solid symbols depict measurements performed on two different days to confirm reproducibility of the measurements. This plot is based on the data from Figure 4.3. 69

Figure 4.5: Fluorescence intensities as a function of distance in the x direction (in pixels) for selected films of R6G in brown limonene SOM at $a_w = 0.7, 0.8$ and 0.9 . The blue dots represent the intensity data and the red curve is a fit to the data using Eq. 2.8. Before the fit was applied, the fluorescence intensity data was normalized to an image taken prior to photobleaching. ... 71

Figure 4.6: Plot of $wD, t, r = r^2 + 4Dt$ as a function of time. The blue open circles represent experimental data, which was obtained from figures such as those in Figure 4.5. The red line is a linear fit to the data. The diffusion coefficients were obtained from the slopes and are. The diffusion coefficients are $D = 0.0583 \mu\text{m}^2/\text{s} = 5.83 \cdot 10^{-10} \text{cm}^2/\text{s}$, $0.1182 \mu\text{m}^2/\text{s} = 1.18 \cdot 10^{-9} \text{cm}^2/\text{s}$ and $0.8292 \mu\text{m}^2/\text{s} = 8.29 \cdot 10^{-9} \text{cm}^2/\text{s}$ for $a_w = 0.7, 0.8$ and 0.9 , respectively..... 72

Figure 4.7: Comparison of diffusion coefficients of the intrinsic fluorophores in brown limonene SOM measured for this chapter (to determine the hydrodynamic radius of the intrinsic fluorophores (green rectangles)) with diffusion coefficients of the intrinsic fluorophores measured in Chapter 3: (black rectangles). The symbols are average values and the error bars depict the 95% confidence limit. 74

Figure 4.8: Comparison of diffusion coefficients of R6G in brown limonene SOM (blue rectangles) with diffusion coefficients of the intrinsic fluorophores in brown limonene SOM

(green rectangles) determined in this chapter for the radius calculations. The symbols are the average values and the error bars give the 95% confidence limit. 75

Figure 5.1: Parameterization of the viscosity as a function of water activity for sucrose water solutions using viscosity data from several sources. 98

List of Symbols

a_w	water activity
c	concentration [μM , mM]
c_1	concentration prior to photobleaching
c_2	concentration after photobleaching
c_N	normalized concentration
D_p	particle diameter [\AA]
D	diffusion coefficient [cm^2/s]
D_{water}	diffusion coefficient of water [cm^2/s]
D_{measured}	measured diffusion coefficients [cm^2/s]
$D_{\text{predicted}}$	diffusion coefficients predicted using the Stokes-Einstein equation [cm^2/s]
$D(R6G)$	diffusion coefficient of Rhodamine 6G [cm^2/s]
$D(SOM)$	diffusion coefficient of the fluorescent organic molecule in brown limonene SOM [cm^2/s]
ϵ	extinction coefficient
η	dynamic viscosity [Pa s]
$\text{erf}(x)$	error function
F	fluorescence intensity
F_0	fluorescence intensity prior to photobleaching
F_λ	fluorescence intensity of a material at a certain excitation wavelength
F_N	fluorescence intensity normalized to F_0

I_0	intensity of incoming light
I	intensity of outgoing light
\vec{J}	flux of particles
K_0	effective bleach depth
k'	rate constant
k_B	Boltzmann-constant
l_x, l_y	length of the region of interest in x and y direction
MW	molecular weight [g/mol]
NA	numerical aperture
p_{H_2O}	water vapour pressure in the atmosphere
$p_{H_2O,sat}$	saturated water vapour pressure
μ	velocity of a spherical particle (as part of the Stokes law)
r	lateral resolution
$R_{diffusing}$	hydrodynamic radius of the diffusing molecules [Å]
R_{matrix}	hydrodynamic radius of the matrix molecules [Å]
R_H	hydrodynamic radius [Å]
RH	relative humidity [%]
sccm	standard cubic centimetres per minute
T	temperature [K or °C]
T_g	glass temperature [K or °C]
T^θ	reference temperature of 298.15 K

t	time [s, ms]
Y	transmittance prior to photobleaching
w	concentration of sucrose in water
$w(D, t, r)$	replaces the function $r^2 + 4Dt$
wt %	weight percent of sucrose in water
z	distance in z-direction

List of Acronyms

BC	black carbon
BrC	brown carbon
CCN	cloud condensation nuclei
CLSM	confocal laser scanning microscope
CW	continuous wavelength
FPR	fluorescence photobleaching recovery
FRAP	fluorescence recovery after photobleaching
IN	Ice nuclei
IR	infrared light range
LSM	laser scanning microscope
R6G	rhodamine 6G
rFRAP	rectangular fluorescence recovery after photobleaching
SOA	secondary organic aerosol
SOM	secondary organic material
UV	ultraviolet light range
VOC	volatile organic material

Acknowledgements

To complete this Master's thesis successfully would not have been possible without the great support of my supervisor, my family, my friends and my lab mates!

I would like to thank, first and foremost, my supervisor, Professor Dr. Allan Bertram. Thank you for your guidance through this complex project and for your advice whenever I did not see a solution to the plentiful challenges that this research project was offering. Yes, Ryan is right; the level of dedication, kindness and understanding that you show all of us is deeply appreciated and helps us grow as scientists.

A big thank you also goes to Dr. Saied Kamal, whose vast mathematical knowledge, his contagious enthusiasm for science and his support during scientific challenges have helped this project to move on. Thank you, Saied!

I would also like to thank the past and current Bertram group members who provided a friendly supportive and encouraging atmosphere. Thank you, Ryan M., James, Vickie, Meng, Erin, Adrian, Yuri, Allie, Cédric, Stephen, Mijung, Kaitlin, Ryan A., Jingwei, Michael, Pit, Christina, Ugo and Yuan! In particular, I would like to thank Ryan M. for his open ear and his suggestions whenever I got stuck, James for teaching me the very finicky bead mobility technique, Vickie for the helpful conversations and Yuri for introducing me into his project and teaching me the basics of the FRAP method. Thank you, Erin, Adrian and Meng for being brave and persistent hiking and lab companions and for being thorough proof-readers.

Also important for the progress of this thesis was Mallory Hinks' work who was preparing the brown limonene SOM samples in her lab in UC Irvine, Los Angeles, California, USA. Thank you, Mallory, for the fast preparation!

I will not forget to thank the members of the Mechanical shop who were unbelievably quick in finishing my requests and I would like to thank Pat from Chemistry Requisition and John from Chemistry Acquisition for their organizational skills.

I am especially grateful for my family and my friends, who have supported me during the past two years during dark (in the laser lab) and successful hours of research. Thank you for the special hiking, biking, climbing adventures, Rob, Sam, Gordon, Rike, Matthias, Jean-Simon, Clemens, Jonas, Livia and Nadia – the joy and laughter with you helped every day! Thank you everyone from the UBC Salsa Rueda group and the UBC gymnastics group, dancing and tumbling with you was a lot of fun! Thank you, Imke, for always having an open ear when needed! Mama and Papa, thank you for setting a great example and for giving me the love, support, encouragement and advice to achieve my goals! Kaja and Aina, thank you for all the good moments and for supporting your big sister with the dream to live in Canada.

Last, I wish to acknowledge that the research and work presented in this thesis was carried out in the UBC chemistry department which is located on the traditional, ancestral, and unceded territory of the Musqueam people.

To my parents, Bettina and Siegfried, and to my sisters, Aina and Kaja

Chapter 1: Introduction

1.1 Atmospheric Particles

1.1.1 Formation, Composition and Sizes

Atmospheric aerosols are particles that are suspended in the Earth's atmosphere. These particles can either be emitted directly to the atmosphere (primary particles) or can be formed in the atmosphere by gas-to-particle conversion (secondary particles) (Figure 1.1).¹

The sources of atmospheric particles can be either natural or anthropogenic. Anthropogenic sources include combustion of fossil fuels and industrial processes, while natural sources include volcanoes, plants, deserts and the ocean.² Due to their different sources atmospheric particles can consist of a range of components including organics, metal oxides and inorganic species such as sulfates, nitrates, and ammonium.²⁻³

Atmospheric particles can be divided based on their size into fine particles ($\leq 1 \mu\text{m}$ in diameter) and coarse particles (1-10 μm).² Coarse particles are mostly formed by mechanical impact of wind on the Earth's surface which causes dust, sea spray and vegetation debris to be emitted into the atmosphere. Fine particles, on the other hand, are formed by condensation of gases (Figure 1.1).²

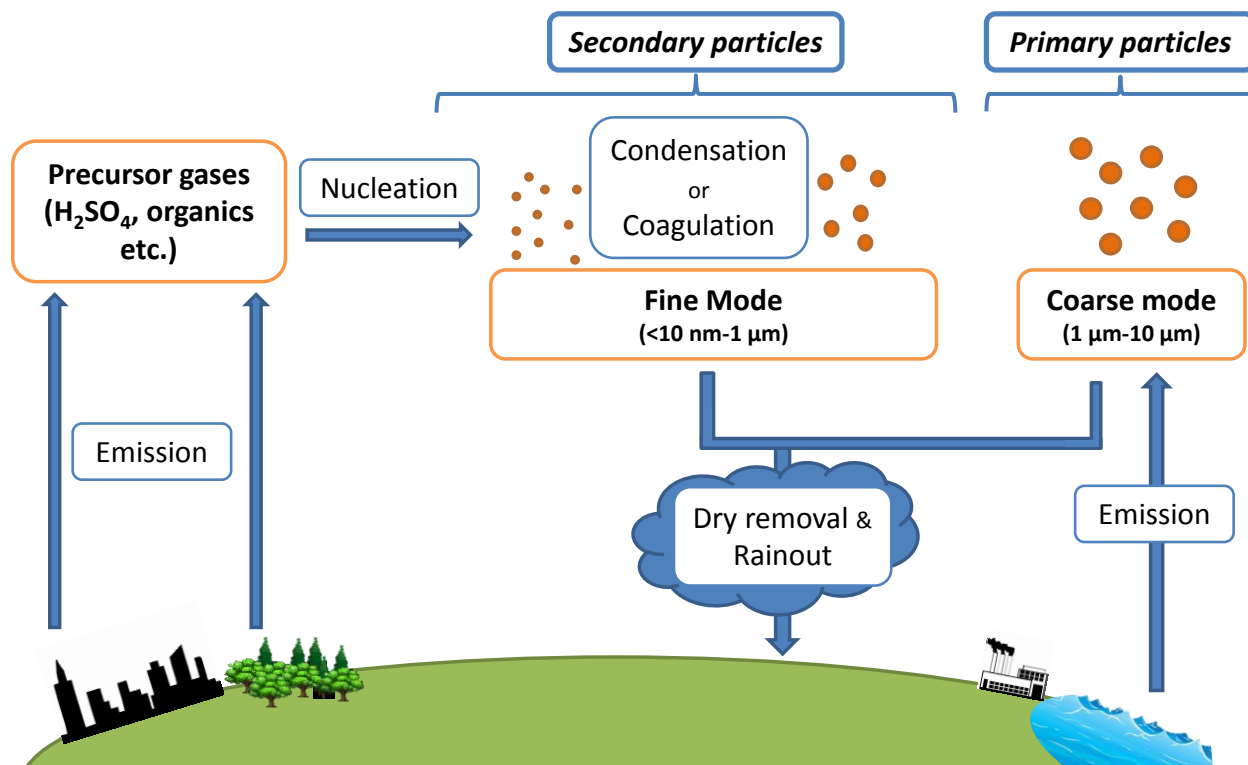


Figure 1.1: Formation and removal processes and classification of atmospheric particles.

1.1.2 Effects of Atmospheric Particles on Humans and Climate

Atmospheric particles have two major effects on this planet. First, they can affect public health. For example, atmospheric particles produced by fossil fuel combustion have been shown to increase chances of inflammation or even cancer.⁴ As another example, during harvesting season, when the concentrations of fungal spores and biologic particles are increased, farm workers reported coughing and breathlessness.⁵ Also, a negative effect on the lung function of children during an increase in fine particles, especially the organic fraction, was observed.⁶ Furthermore, studies with cells exposed to secondary organic aerosols (SOA) suggest that SOA can cause premature cell death.⁷

Second, atmospheric particles can affect climate (Figure 1.2). Atmospheric particles can directly affect climate by scattering and absorbing sunlight. An indirect effect is also possible, where atmospheric particles act as cloud condensation nuclei (CCN) or as ice nuclei (IN). If the atmospheric particles act as CCN or IN, they can induce cloud formation, and the clouds can then scatter light.²

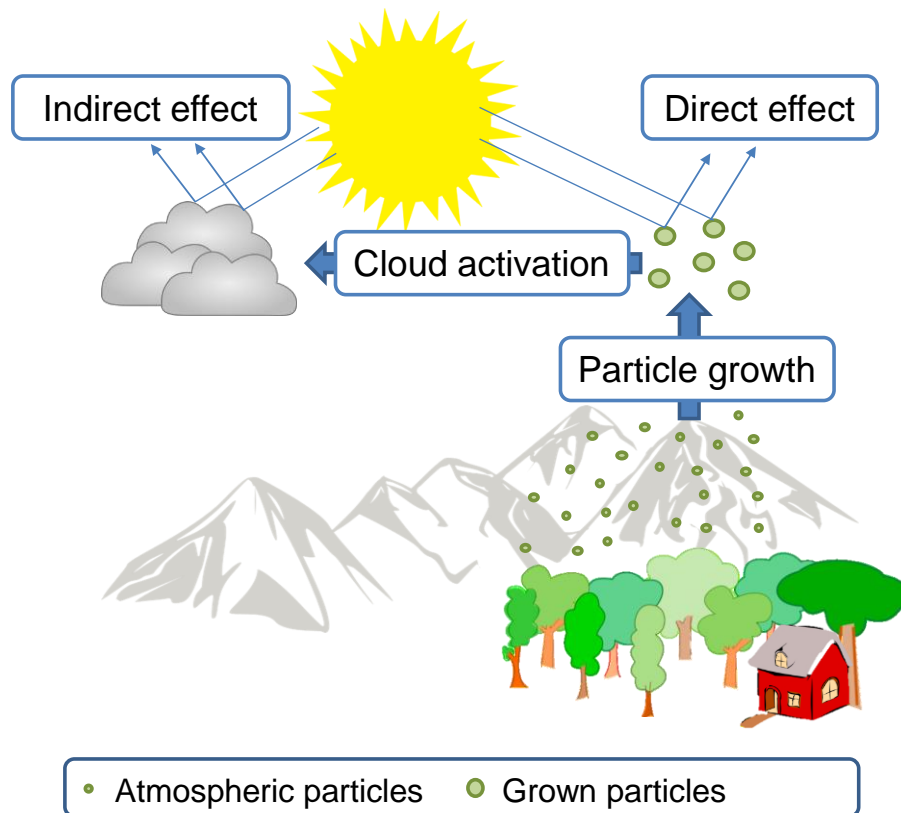


Figure 1.2: Schematic of the formation of atmospheric particles and their effects on the climate. Based on Renbaum-Wolff *et al.* (2013).⁸

There are many factors particles influencing the climate, including the concentrations of gases and atmospheric particles. To quantify the influence of atmospheric components (e.g. greenhouse gases and atmospheric particles) on the climate, a parameter called “radiative forc-

ing” has been introduced by the Intergovernmental Panel on Climate Change (IPCC, 1990).⁹ Radiative forcing is a measure of the effect that a factor (such as atmospheric particles) has on the radiative energy budget of the Earth-atmospheric system. Radiative forcing is normally reported at the top of the troposphere in units of W/m^2 . The values that are calculated can be positive or negative: positive values indicate a warming effect and negative values indicate a cooling effect of the contributing component.

The radiative forcing of greenhouse gases is known with very high confidence, while the radiative forcing of atmospheric aerosols has a high uncertainty (see Figure 1.3).¹⁰ The uncertainties in the radiative forcing of aerosols from aerosol-radiation (i.e. direct effect) and aerosol-cloud interactions (i.e. indirect effect) are as high as 100%. To be able to assess the impact of atmospheric aerosols on the climate with a higher level of confidence, more research is needed.

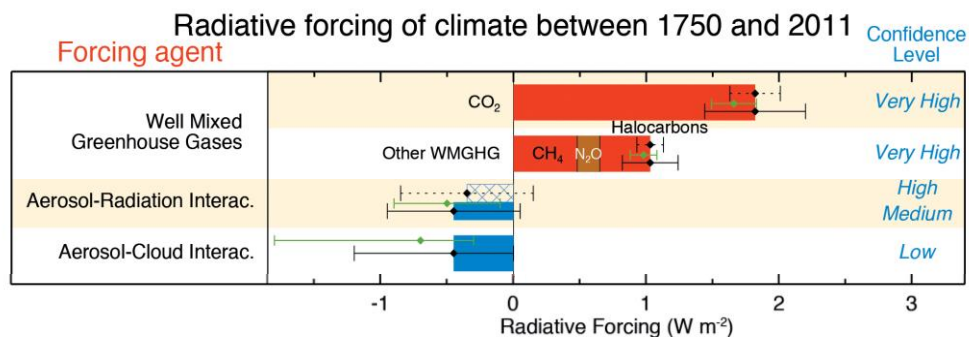


Figure 1.3: Radiative forcing of climate forcing species including their uncertainties. Reproduced with permission from Stocker *et al.* (2013).¹⁰

1.2 The Importance of Molecular Motion Within Atmospheric Particles

In the atmosphere, particles can undergo heterogeneous reactions with atmospheric gas-phase oxidants, such as ozone (O₃). The timescale of these reactions depends on the mobili-

ty of molecules within the atmospheric particles (Figure 1.4). Fast diffusion and low viscosity promote reactions throughout the entire volume of the particles. Slow diffusion and high viscosities favour reactions confined to the surface of the particles (Figure 1.4).⁸

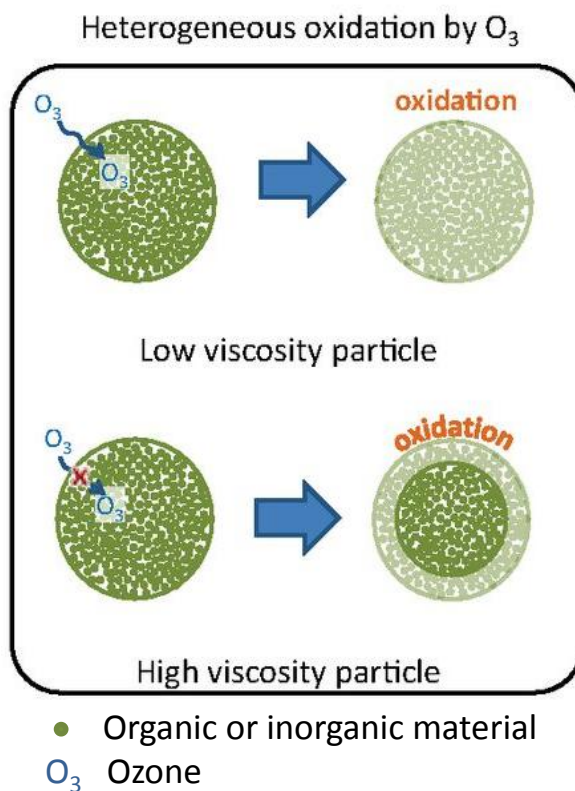


Figure 1.4: Illustration of the influence of diffusion rates on heterogeneous reactions within atmospheric particles. Reproduced with permission from Lindsay Renbaum-Wolff *et al.*, “Viscosity of α -pinene secondary organic material and implications for particle growth and reactivity”, *PNAS*, 2013, 110 (20), 8014-8019; doi: 10.1073/pnas.1219548110.

Molecular motion within atmospheric particles also influences the growth rate of these particles. Fast diffusion and low viscosities lead to fast growth rates of atmospheric particles, while slow diffusion and high viscosities lead to slow growth rates. Hence, predictions of size

and mass of atmospheric particles in atmospheric models are sensitive to molecular motion within atmospheric particles, with important implications for climate and air quality.

1.3 Theories of Molecular Motion

The heat induced, random movement of molecules is also known as Brownian motion. Brownian motion was first discovered in 1827 by the Scottish botanist Robert Brown.¹¹ Almost 80 years later in 1905, Einstein derived a mathematic expression to describe Brownian motion:^{2, 12}

$$\langle x^2 \rangle = 2 \cdot D \cdot t, \quad 1.1$$

where D is the diffusion coefficient and $\langle x^2 \rangle$ is the mean squared displacement, which is the distance, that a molecule moves on average within a certain time interval t . The Stokes-Einstein equation relates the diffusion coefficient, D , to the viscosity of the medium, η , and to the hydrodynamic radius of the diffusing molecule, R_H :

$$D = \frac{k_B T}{6\pi\eta R_H}, \quad 1.2$$

where k_B is the Boltzmann constant and T is the temperature. The Stokes-Einstein equation has been derived for laminar flow conditions, a spherical shape of the diffusion species¹² and for the case where the diffusing species is significantly larger than the molecules of the medium that the species is diffusing through. The latter condition guarantees that the diffusing species cannot slip between the molecules of the medium.¹³

1.4 Overview of this Thesis

As discussed above, molecular diffusion of molecules within atmospheric particles can influence their growth rate and reactivity with important implications for predicting the radiative forcing of atmospheric particles and air quality.¹⁴ Nevertheless, the scientific understanding of molecular diffusion within atmospheric particles remains poor.

In the past, diffusion coefficients of organic molecules within atmospheric particles have been estimated using viscosity measurements and the Stokes-Einstein equation.^{8, 15} However, the Stokes-Einstein equation is based on assumptions (section 1.3) which may not be applicable to atmospheric particles.¹⁶

In Chapter 2:, the validity of the Stokes-Einstein equation was tested by directly measuring diffusion coefficients of organic molecules in simple proxies of atmospheric particles with known viscosities (consisting of binary mixtures of sucrose and water) and by comparing the measured diffusion coefficients with Stokes-Einstein calculated diffusion coefficients. Diffusion coefficients were measured between 38% and 80% relative humidity (RH), since the relative humidity can change in the atmosphere.¹⁷

Measuring diffusion coefficients as a function of relative humidity is important because 1) as the RH changes in the atmosphere the water content of atmospheric particles changes to maintain equilibrium with the gas phase water vapour, and 2) diffusion coefficients within atmospheric particles are expected to be sensitive to water content. Relative humidity is defined by the following equation:

$$RH = \frac{p_{H_2O}}{p_{H_2O,sat}} \cdot 100, \quad 1.3$$

where p_{H_2O} is water vapour pressure in the atmosphere and $p_{H_2O,sat}$ is the saturation water vapour pressure at a certain temperature.² In the atmosphere, the relative humidity varies between 20 to 100 %.¹⁷ Many literature studies reported diffusion coefficients as a function of relative humidity or as a function of water activity, a_w , where $RH = 100 \cdot a_w$.

In Chapter 3:, diffusion coefficients of fluorescent organic molecules in brown limonene secondary organic material (SOM) were measured over a range of relative humidities from 38% to 90%. Brown limonene SOM is an important type of atmospheric particles,¹⁸ and there have only been a few measurements of diffusion coefficients in limited types of SOM^{15d} and none in brown limonene SOM. Up to now, it has been assumed in climate models that diffusion coefficients of organic molecules in SOM are large (similar to the diffusion coefficients of organic molecules in water), which may not be true under certain conditions such as low RH.^{15a, 19}

In Chapter 4:, the average hydrodynamic radius of fluorescent organic molecules in brown limonene SOM was determined. The chemical structure and size of these organic molecules were not known prior to this study.

Chapter 2: Diffusion Coefficients of Rhodamine 6G in Sucrose Water Solutions, a Proxy for Atmospheric Particles

2.1 Introduction

Secondary organic material (SOM) originates from volatile organic compounds (VOCs) which are emitted by anthropogenic sources (e.g. cars) or natural sources (e.g. trees). VOCs, such as limonene, α -pinene and toluene, amongst other hydrocarbons, are oxidized in the atmosphere by a complex series of reactions to form SOM.^{15a, 20} A fraction of this SOM can then condense to form SOM particles. SOM makes up 30-70% of the mass concentrations of atmospheric particles depending on the region of the atmosphere. SOM particles can influence climate either directly by absorbing or scattering sunlight or indirectly by acting as CCN or IN. Air quality and health can also be influenced by atmospheric particles.^{7, 21} See Section 1.1.2 for further details.

As discussed in Section 1.2, diffusion rates of organic molecules in atmospheric particles, such as SOM particles, influence particle growth rates and reactions rates. As a result, diffusion rates of organics in SOM have become an active area of research.²²

In the past, researchers assumed that the diffusion coefficients of organic molecules in SOM are large (similar to the diffusion coefficients of organic molecules in pure water). More recently, diffusion coefficients of organic molecules in SOM have been estimated by measuring viscosities in SOM particles and then calculating diffusion coefficients using the Stokes-Einstein and the measured viscosities.^{15a} For example, Song *et al.* (2015) used this approach to estimate diffusion coefficients of organic molecules in SOM derived from the ozonolysis of α -pinene.^{15d}

Hinks *et al.* (2016) also used this approach to determine diffusion coefficients of organic molecules in SOM produced from the ozonolysis of limonene.²³ However, the Stokes-Einstein equation is based on assumptions that might not be appropriate for atmospheric particles (section 1.4).

There have only been a few previous studies that have tested the validity of the Stokes-Einstein equation for predicting diffusion coefficients of organics in matrices consisting of organics and water (Note, both organics and water are important for SOM, since SOM is hygroscopic and will take up water in the atmosphere as relative humidity changes). Champion *et al.* (1997) found that the Stokes-Einstein equation underpredicts diffusion coefficients of the organic dye fluorescein in sucrose water solutions at viscosities above 7.9×10^4 Pa s ($T_g/T \geq 0.9$, where T_g is the glass transition temperature of the binary mixture of sucrose and water and T is the measured temperature).^{16c} Corti *et al.* (2008) found that the Stokes-Einstein equation gives valid results up to viscosities of 1.2 Pa s ($T_g/T \geq 0.7$) for the diffusion of fluorescein in sucrose water solutions, but shows a break down at higher viscosity values.^{16d} Longinotti and Corti (2007) found a breakdown of the Stokes-Einstein equation for the diffusion of ferrocene-methanol in sucrose water solutions at viscosities higher than 47.4 Pa s ($T_g/T \geq 0.8$).^{16e}

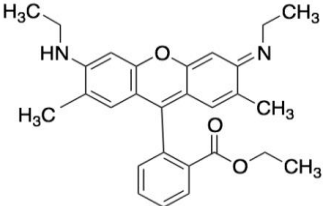
To add to the limited number of studies testing the Stokes-Einstein equation for predicting diffusion of organics in organic and water mixtures, the diffusion coefficients of the organic tracer molecule rhodamine 6G (Table 2.1) were measured at various atmospherically relevant RHs in mixtures of sucrose and water. The aim of the current study is to determine, if the Stokes-Einstein equation gives accurate results at atmospherically relevant RHs. Rhoda-

mine 6G (R6G) was chosen as a fluorophore for this study, since the hydrodynamic radius of R6G (5.89 \AA)²⁴ is similar to the radius of the matrix molecules (the radius of sucrose is 4.7 \AA).²⁵ In addition, R6G can be studied using the microscope system available in the department of chemistry at the University of British Columbia (Zeiss Axio Observer LSM 5 10 MP laser scanning microscope with a 543 nm laser). Sucrose-water mixtures have been chosen as matrix molecules, because 1) sucrose has an oxygen-to-carbon (O:C) ratio of 0.92, which is similar to the O:C ratio of SOM found in atmospheric particles²⁶, 2) viscosities of sucrose-water mixtures, information that is needed to test the Stokes-Einstein relation, are known over a wide range of water activities and 3) sucrose-water mixtures show similar viscosities to some types of SOM at room temperature (compare viscosity values of sucrose-water mixtures measured by Power *et al.* (2013) with the viscosities of toluene SOA measured by Song *et al.* (2016) and α -pinene viscosities measured by Grayson *et al.* (2016)).^{15e, 27}

This work is part of a manuscript that investigated the diffusion coefficients of fluorescein, R6G and calcein in sucrose-water mixtures:

Chenyakin, Y., Ullmann, D. A., Evoy, E., Renbaum-Wolff, L., Kamal, S., and Bertram, A. K.: Diffusion coefficients of organic molecules in sucrose–water solutions and comparison with Stokes–Einstein predictions, *Atmos. Chem. Phys.*, 17, 2423–2435, doi:10.5194/acp-17-2423-2017, 2017.

Table 2.1: Information on rhodamine 6G (R6G) including the molecular weight (MW), the chemical structure and the hydrodynamic radius.

Name	MW (g/mol)	Chemical Structure	Hydrodynamic Radius R_H (Å)
rhodamine 6G	479.01	 <p>The chemical structure of rhodamine 6G is a xanthene dye. It features a central xanthene ring system. The 6-position of the xanthene ring is substituted with a phenyl ring, which is further substituted with an ethyl ester group (-COOCH₂CH₃). The 3 and 7 positions of the xanthene ring are substituted with diethylamino groups (-N(CH₂CH₃)₂). The 2-position is substituted with a methyl group (-CH₃).</p>	5.89 (Müller et al., 2008) ²⁴

2.2 Experimental

Diffusion coefficients of R6G in mixtures of sucrose and water were determined using a technique called rectangular area fluorescence recovery after photobleaching (rFRAP). Below, the method of producing samples of sucrose, water and trace amounts of R6G needed for the rFRAP experiments is described (section 2.2.1). Then, the procedure of the rFRAP experiments is described in detail (section 2.3).

2.2.1 Sample Preparation

For the rFRAP experiments thin films (45-100 μm thick) containing homogeneous mixtures of sucrose (Sigma Aldrich, $\geq 99.5\%$), water and trace amounts of R6G (Acros Organics, 99%) were needed. The concentration of R6G in thin films was 0.51 mM. This concentration was chosen, so that the concentrations did not influence the viscosity of the sucrose-water mixture and the fluorescence signal was large enough to detect in the experiments. The water ac-

tivities (a_w) in the thin films ranged from 0.8 to 0.38; at these water activities, the sucrose-water solutions were supersaturated with respect to sucrose.

The method of preparing supersaturated solutions with respect to sucrose is as follows: first, a solution of 60 wt % sucrose in water with a concentration of 0.51 mM R6G was prepared gravimetrically and filtered using a 0.45 μm filter (Merck Millipore) followed by a 0.02 μm filter (WhatmanTM) to reduce dust particles in the solution which could enhance nucleation of crystalline sucrose.²⁸ Next, a droplet of the solution was pipetted onto a hydrophobic glass slide (Hampton Research), and in order to condition the droplets to a certain water activity, the glass slide containing the droplet was placed in a flow cell or in a glass jar with controlled relative humidity and hence water activity. The flow cell was used to achieve water activities from 0.6 to 0.8 and the glass jar was used to achieve water activities from 0.38 to 0.6. The flow cell used for conditioning droplets is shown in Figure 2.1 and the glass jar used for conditioning droplets is shown in Figure 2.2.

The a_w in the flow cell was controlled by using nitrogen gas (Ultrapure, Praxair) that was humidified by directing the gas through a bubbler within a temperature-controlled water bath. Subsequently, the humidified nitrogen gas was directed across the sample with a constant flow of 2500 sccm. To monitor the a_w of the humidified nitrogen gas, a dew point hygrometer combined with a chilled mirror sensor (General Eastern Model D2) and a handheld hygrometer (Omega RH85) were used. During the conditioning experiments the temperature of the sample was measured directly in the flow cell using a thermocouple thermometer (HH200A Omega).

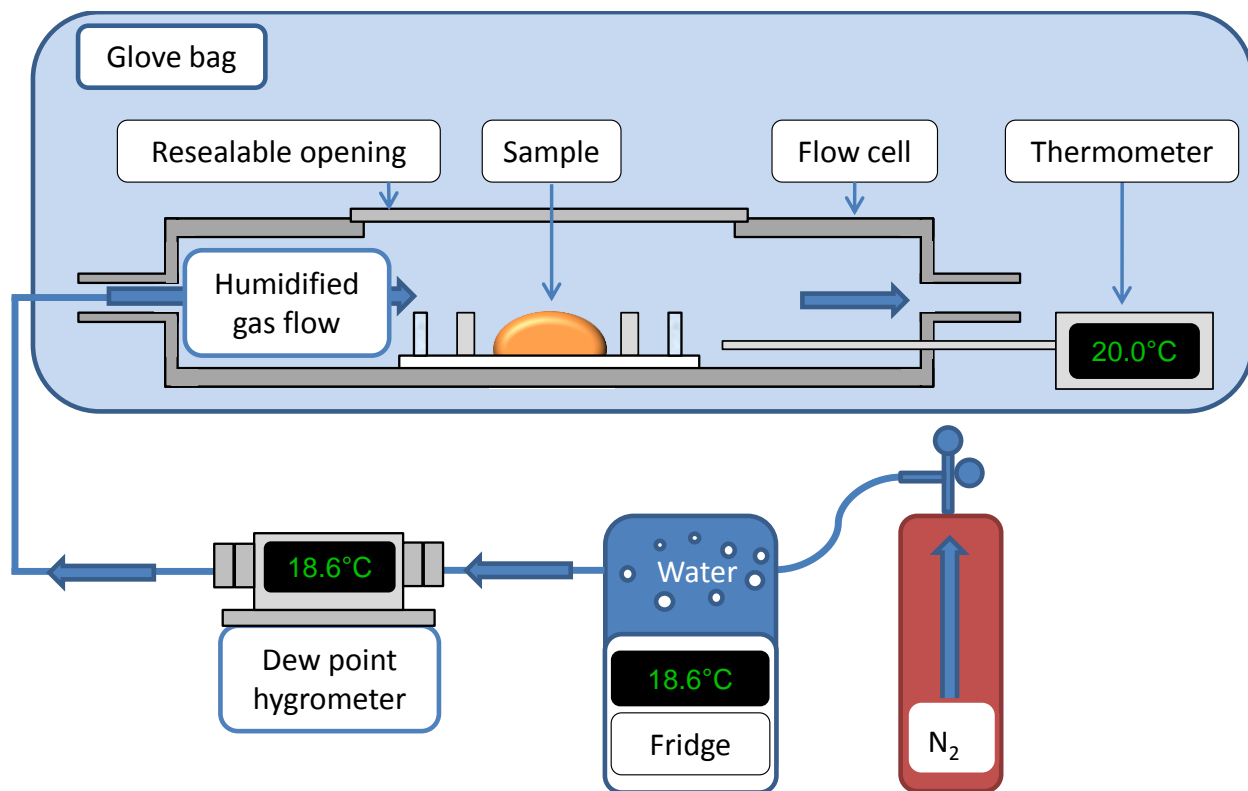


Figure 2.1: Schematic of the flow cell used to condition samples to the desired water activities.

Prior to performing experiments, the hygrometer in combination with the chilled mirror sensor was calibrated. For this, the deliquescence relative humidity of ammonium sulphate particles was determined and the experimental value was compared to the literature. The uncertainty of the a_w was 0.025 at $a_w=0.803$ after calibration.

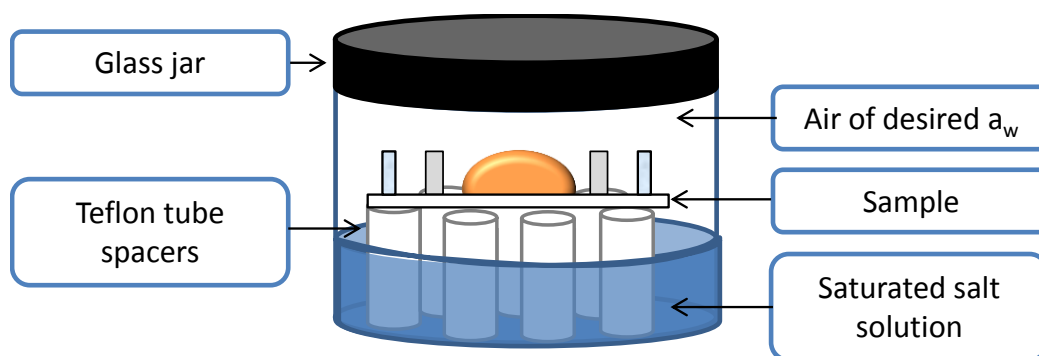


Figure 2.2: Schematic of the glass jar used to condition samples of water activities below 0.6.

In cases where sealed glass jars were used to condition the droplets to a known a_w , the a_w in the jars were controlled using a saturated inorganic salt solution of a certain a_w (see Table 2.2).²⁹ The sample droplet was placed on a glass slide and the glass slide was then placed above the inorganic salt solution by using spacers made of Teflon tubes which were placed in the inorganic salt solution and were long enough to keep the sample above the salt solution (Figure 2.2).

Table 2.2: Saturated salt solutions used for conditioning and storing samples at specific water activities in sealed glass jars.

Water activity (+/- 0.025) at 20°C	Salt	Reference
0.80	ammonium sulfate	Greenspan ²⁹
0.70	potassium iodide	Greenspan ²⁹
0.60	sodium bromide	Greenspan ²⁹
0.50	calcium nitrate tetrahydrate (at 25°C)	Winston and Bates ³⁰
0.38	sodium iodide	Greenspan ²⁹

The time needed for the droplets to condition to the water activity in the flow cell was estimated based on the following equation^{15f}:

$$\tau_{eq} = \frac{r^2}{D_{water} \cdot \pi^2} \quad 2.1$$

Where τ_{eq} is the characteristic diffusion time of water within sucrose-water droplet, r is the radius of the sucrose-water droplet and D_{water} is the diffusion coefficient of water in sucrose-water solutions. D_{water} was obtained from Price *et al.* (2014)³¹:

$$\log D_{water} = a + ba_w + ca_w^2 + da_w^3, \quad 2.2$$

where a_w is the water activity, D_{water} is the diffusion coefficient of water, a , b , c and d are constants with the following values: $a = -20.89$, $b = 25.92$, $c = -26.97$ and $d = 13.25$.

A minimum time of $3 \cdot \tau_{eq}$ was used to condition the droplets, which has been shown to be a sufficient time period for the samples to equilibrate.³²

Once the droplet of sample was conditioned to a certain a_w , a second hydrophobic glass slide was placed on top and the droplet was sandwiched between the two slides to make a thin film with thickness 45-120 μm where the thickness was controlled using aluminum spacers (Figure 2.3). Whether samples were conditioned in glass jars over saturated salt solutions or within a flow cell, the sandwiching process was done within a Glove BagTM where the air had the same a_w as was used to condition the sample. To ensure that the water activity of the samples did not change over time, the glass slides were sealed with vacuum grease and were stored over an inorganic salt solution of the corresponding water activity.

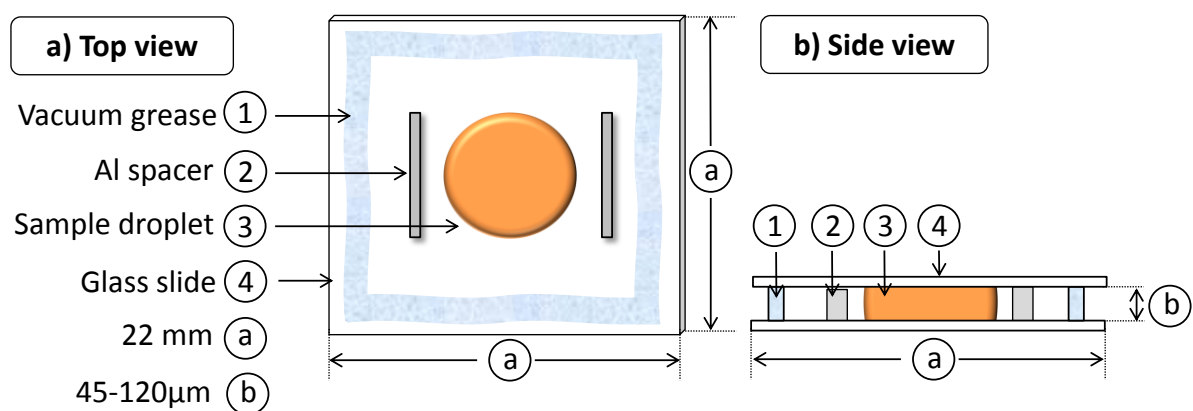


Figure 2.3: Schematic of the sample used in the FRAP experiments. Panel a) is a top view and Panel b) is a side view. The sample consists of sucrose, water and trace amounts of the fluorescent tracer dye, rhodamine 6G.

2.3 Introduction to Fluorescence Recovery After Photobleaching (FRAP)

Fluorescence recovery after photobleaching (FRAP) has been used for nearly forty years³³ to analyze the mobility of molecules in various components such as cytoplasm of cells³⁴, cell nuclei³⁵ and biopolymers³⁶. The FRAP method is based on its predecessor, fluorescence photobleaching recovery (FPR)³⁷, and has undergone improvements because of the development of confocal microscopes and new types of lasers.³⁸

In this work, we use a variation of the FRAP technique called rectangular area fluorescence recovery after photobleaching (rFRAP).^{37, 39} The rFRAP measurement technique is based upon the diffusion of fluorescent organic tracer molecules through a medium, which is illustrated in Figure 2.4 showing a side view of the sample cell. The green circles depict fluorescent tracer molecules, the black circles depict tracer molecules that have been photobleached (i.e. irreversibly lost their ability to fluoresce) and the orange rectangle represents the area that has been chosen for photobleaching. Panel A) shows a homogeneously fluorescent film prior to photobleaching. Panel B) shows the same film just after photobleaching with a high intensity laser beam. Panel C) to F) show the recovery of the fluorescence within the photobleached rectangle over time t after photobleaching. Diffusion coefficients can be determined from the time dependence of this fluorescence recovery (see section 2.3.2 for further details).

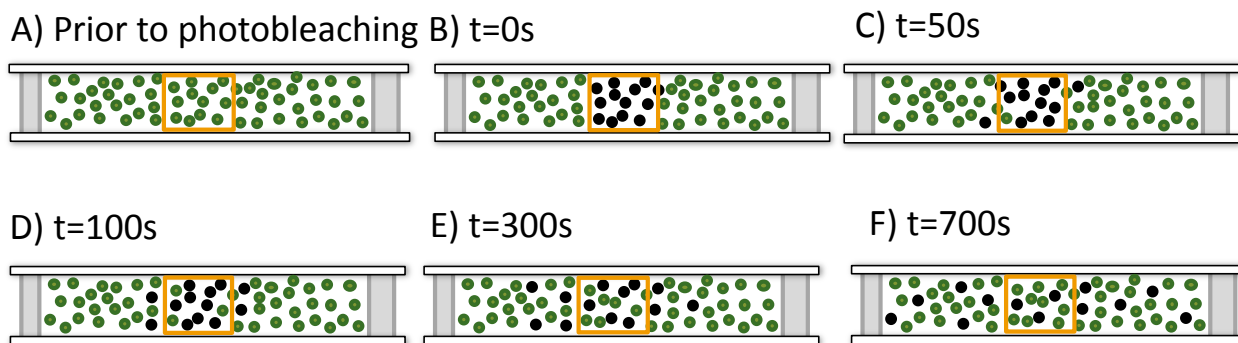


Figure 2.4: Schematic illustrating the photobleaching and diffusion process of fluorescent molecules. Shown is a side view of the sample cell at various times t during the rFRAP experiment. See text for further details.

2.3.1 FRAP Measurements

The FRAP measurements were conducted on a Zeiss Axio Observer LSM 5 10 MP laser scanning microscope with the low numerical aperture 10x 0.3 NA objective (Zeiss EC-Plan Neofluar 10x/0.3) to ensure near uniform photobleaching in the z -direction. One-dimensional scanning of a speed of 8 was performed, which translates to a pixel dwell of $2.56 \mu\text{s}$ and an image scan time of 1.57 s. The images were acquired with 512×512 pixels with a pinhole set to $80 \mu\text{m}$. For scanning and photobleaching, a Helium-Neon laser (543 nm) with a maximum power of 1.2 mW was used. For photobleaching a laser power of $330 \mu\text{W}$ was used and for scanning a laser power of $4.08 \mu\text{W}$ was used. The experiments were performed using the Zen 2008 software and photobleaching was performed in the “Zoom-In” bleach mode. For photobleaching, a time was chosen such that the fluorescence intensity within the bleached area was decreased by between 10 and 32 %. Previous work has shown that bleach depths smaller than 50 % give accurate diffusion values.⁴⁰

The geometry chosen for photobleaching in the experiments was a rectangle with length (l_x) and width (l_y) (Figure 2.5). The sizes of the rectangles chosen depended on the diffusion times with smaller areas for longer diffusion times. The image sizes in relation to the bleach size were chosen such that the entire bleach profile could be imaged even for long recovery times. For samples at $a_w=0.75$ and 0.8 , bleached areas of $36\ \mu\text{m}$ by $36\ \mu\text{m}$ and image sizes of $199.61\ \mu\text{m}$ by $199.61\ \mu\text{m}$ were chosen. For samples at $a_w=0.6$, bleached areas of 10 by $10\ \mu\text{m}$ and image sizes of $99.8\ \mu\text{m}$ by $99.8\ \mu\text{m}$ were used and for $a_w=0.52$ and 0.38 , bleached areas of 5 by $5\ \mu\text{m}$ and image sizes of $59.88\ \mu\text{m}$ by $59.88\ \mu\text{m}$ were used.

A minimum of three samples was prepared for each a_w and three measurements per sample were obtained.

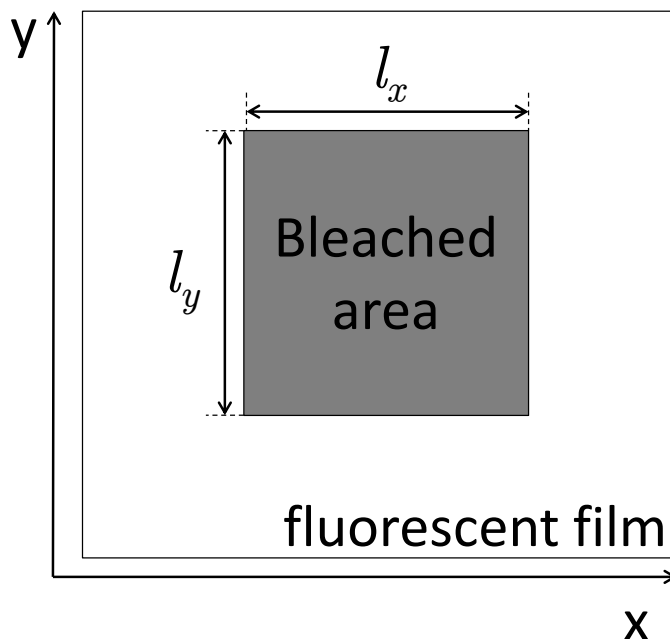


Figure 2.5: Schematic of a fluorescent film (view from top) and its bleached area. A section of a fluorescent film is scanned in the x- and y-direction. A defined rectangular area (bleached area) of the length l_x and the width l_y is photobleached.

2.3.2 Analysis of the FRAP Data

Fick's first law of diffusion describes the relationship between the net flux \vec{J} of particles that occurs due to a change in concentration with a change in distance ($\frac{\partial c}{\partial z}$):

$$\vec{J} = -D \cdot \frac{\partial c}{\partial z}, \quad 2.3$$

where D is the diffusion constant or diffusion coefficient.⁴¹ Fick's second law of diffusion describes the relationship between the change in concentration with a change in time to the second derivative of the concentration with respect to distance:

$$\frac{\partial c}{\partial t} = D \cdot \frac{\partial^2 c}{\partial z^2}, \quad 2.4$$

where D is location-independent.⁴² Fick's second law describes how the concentration profile changes as the particles start diffusing from higher towards lower concentrations in order to balance concentration differences.

To describe diffusion of fluorescent molecules in an rFRAP experiment, Deschout *et al.*⁴⁰ developed a mathematical model based on Fick's first and second laws.

Deschout *et al.*⁴⁰ made assumptions which were partially based on Axelrod *et al.*³⁷:

- a. The bleaching process is a first-order reaction and irreversible.^{37, 40}
- b. The time that is chosen for photobleaching is short, such that, no diffusion of fluorescent molecules in or out of the bleached area takes place during photobleaching.^{37, 40}
- c. The photobleached area is rectangular.^{37, 40}

- d. Photobleaching should be limited to a maximum of 50% of the fluorophores in the samples.⁴⁰
- e. A two dimensional diffusion is assumed with molecules diffusing only in the x- and y-plane and the sample being photobleached uniformly in z-direction which is a reasonable assumption for 45-120 μm thick films and using a regular CLSM with a low numerical aperture lens.⁴⁰

Using all of the assumptions above Deschout *et al.* derived a mathematic expression for two dimensional single photon rFRAP based on Fick's second law of diffusion (see section 1.3):

$$\frac{F(x, y, t)}{F_0} = 1 - \frac{K_0}{4} \left[\operatorname{erf} \left(\frac{x + \frac{l_x}{2}}{\sqrt{r^2 + 4Dt}} \right) - \operatorname{erf} \left(\frac{x - \frac{l_x}{2}}{\sqrt{r^2 + 4Dt}} \right) \right] \times \left[\operatorname{erf} \left(\frac{y + \frac{l_y}{2}}{\sqrt{r^2 + 4Dt}} \right) - \operatorname{erf} \left(\frac{y - \frac{l_y}{2}}{\sqrt{r^2 + 4Dt}} \right) \right], \quad 2.5$$

where F is the fluorescence intensity at coordinate (x, y) and time t . F is normalized to the fluorescence intensity prior to photobleaching, $F_0(x, y)$. K_0 is the effective bleach depth, which describes the decrease of the fluorescence intensity within the photobleached area. l_x and l_y are the lengths of the photobleached area. r is the lateral resolution of the microscope and D is the diffusion coefficient. The error function is defined as:

$$\operatorname{erf}(z) = \frac{2}{\sqrt{\pi}} \cdot \int_0^z e^{-x^2} dx. \quad 2.6$$

In this work, a one-dimensional model for the analysis of the recovery of the fluorescence intensity was used. For samples of a_w of 0.80 to 0.52, the fluorescence images recorded

after photobleaching were integrated over the entire width of image in the y-direction. For this case, Eq. 2.5 was simplified by integrating the intensities over all y positions:

$$\frac{F(x, t)}{F_0} = 1 - \frac{K_0}{4} \left[\operatorname{erf} \left(\frac{x + \frac{l_x}{2}}{\sqrt{r^2 + 4Dt}} \right) - \operatorname{erf} \left(\frac{x - \frac{l_x}{2}}{\sqrt{r^2 + 4Dt}} \right) \right] \times \left(\int_{-\infty}^{+\infty} \left[\operatorname{erf} \left(\frac{y + \frac{l_y}{2}}{\sqrt{r^2 + 4Dt}} \right) - \operatorname{erf} \left(\frac{y - \frac{l_y}{2}}{\sqrt{r^2 + 4Dt}} \right) \right] dy \right), \quad 2.7$$

which resulted in the following expression:

$$\frac{F(x, t)}{F_0} = 1 - \frac{K_0}{4} \left[\operatorname{erf} \left(\frac{x + \frac{l_x}{2}}{\sqrt{r^2 + 4Dt}} \right) - \operatorname{erf} \left(\frac{x - \frac{l_x}{2}}{\sqrt{r^2 + 4Dt}} \right) \right] \times 2l_y, \quad 2.8$$

For samples of $a_w=0.38$, the fluorescence images recorded after photobleaching were integrated only over the width of the bleach area $\left(-\frac{l_y}{2} \text{ to } +\frac{l_y}{2}\right)$ in order to increase the signal-to-noise ratio, which resulted in the following equation:

$$\frac{F(x, t)}{F_0} = 1 - \frac{K_0}{4} \left[\operatorname{erf} \left(\frac{x + \frac{l_x}{2}}{\sqrt{r^2 + 4Dt}} \right) - \operatorname{erf} \left(\frac{x - \frac{l_x}{2}}{\sqrt{r^2 + 4Dt}} \right) \right] \times \left(\int_{-\frac{l_y}{2}}^{+\frac{l_y}{2}} \left[\operatorname{erf} \left(\frac{y + \frac{l_y}{2}}{\sqrt{r^2 + 4Dt}} \right) - \operatorname{erf} \left(\frac{y - \frac{l_y}{2}}{\sqrt{r^2 + 4Dt}} \right) \right] dy \right), \quad 2.9$$

Equations 2.8 and 2.9 were implemented into a Matlab script which was used to analyze the images of the recovery process. In the following sections, the expression $r^2 + 4Dt$ will be replaced by $w(D, t, r)$.

Shown in Figure 2.6 is an example of images recorded during a typical rFRAP experiment for the diffusion of R6G in a sucrose-water mixture. Steps involved analyzing these types of images are listed below:

- a. The images after photobleaching were normalized to an image recorded prior to photobleaching or a region in the image not affected by photobleaching using the open source programme ImageJ⁴³. Images of films with $0.52 \leq a_w \leq 0.8$ were normalized to a prebleach image. Images of films at $a_w = 0.38$ were normalized using a region in the image outside of the photobleaching region and not affected by diffusion. The latter method of normalization was used for films at $a_w = 0.38$, since gradual photobleaching of the entire image occurred during these measurement due to long experimental time.
- b. In a subsequent step, the images were downsized from 512x512 pixels to 128x128 pixels by averaging in order to reduce noise. Then, the data was reduced from two dimensions to one dimension by integrating the intensities over all y -positions for the case of samples $a_w \geq 0.52$ or integrating the intensities for y -positions ranging from $-\frac{l_y}{2}$ to $+\frac{l_y}{2}$ for the case of $a_w = 0.38$. See Figure 2.7 as an example.
- c. The normalized data in 1-dimensional form was fit to Eq.2.8 or 2.9 using a Matlab script (The Mathworks, Natick, MA, USA) with K_0 as well as the background left as free parameters for the analysis. Examples of fits are shown in Figure 2.7. From this step $w(D, t, r)$ was determined for each time at which an image was recorded.

- d. $w(D, t, r)$ was plotted as a function of t and a straight line was fit to the data (Figure 2.8). Since $w(D, t, r) = (r^2 + 4Dt)$, the diffusion coefficient, D , could be calculated from the slope of the line.

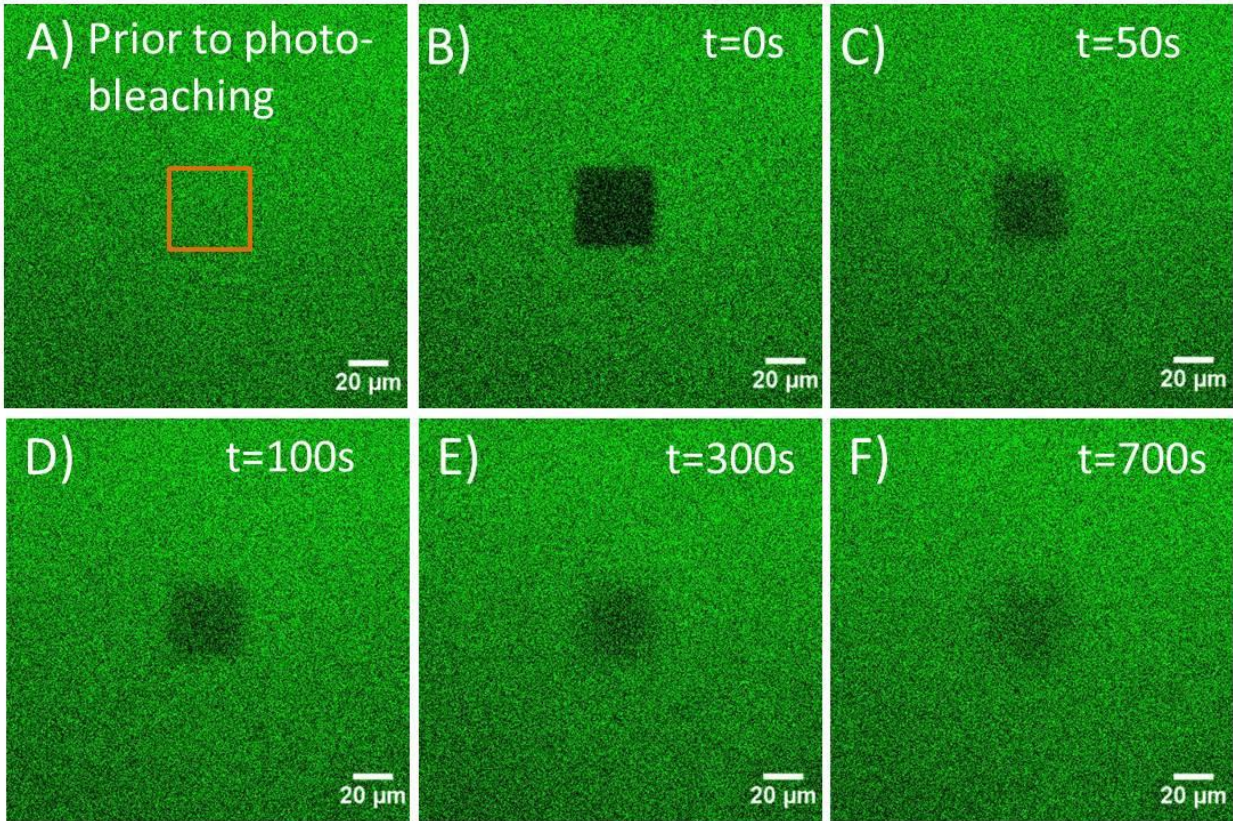


Figure 2.6: A fluorescent film consisting of a sucrose-water solution ($a_w=0.75$) and R6G viewed using a laser scanning microscope. Panel A) shows the fluorescent film prior to photobleaching. Panel B) to F) show the recovery of the fluorescence signal over time t . Panel B) was taken directly after the photobleaching process at time 0s, whereas panel F) shows the fluorescent film after 700s after the photobleaching step. The orange rectangle represents the area that was chosen for photobleaching.

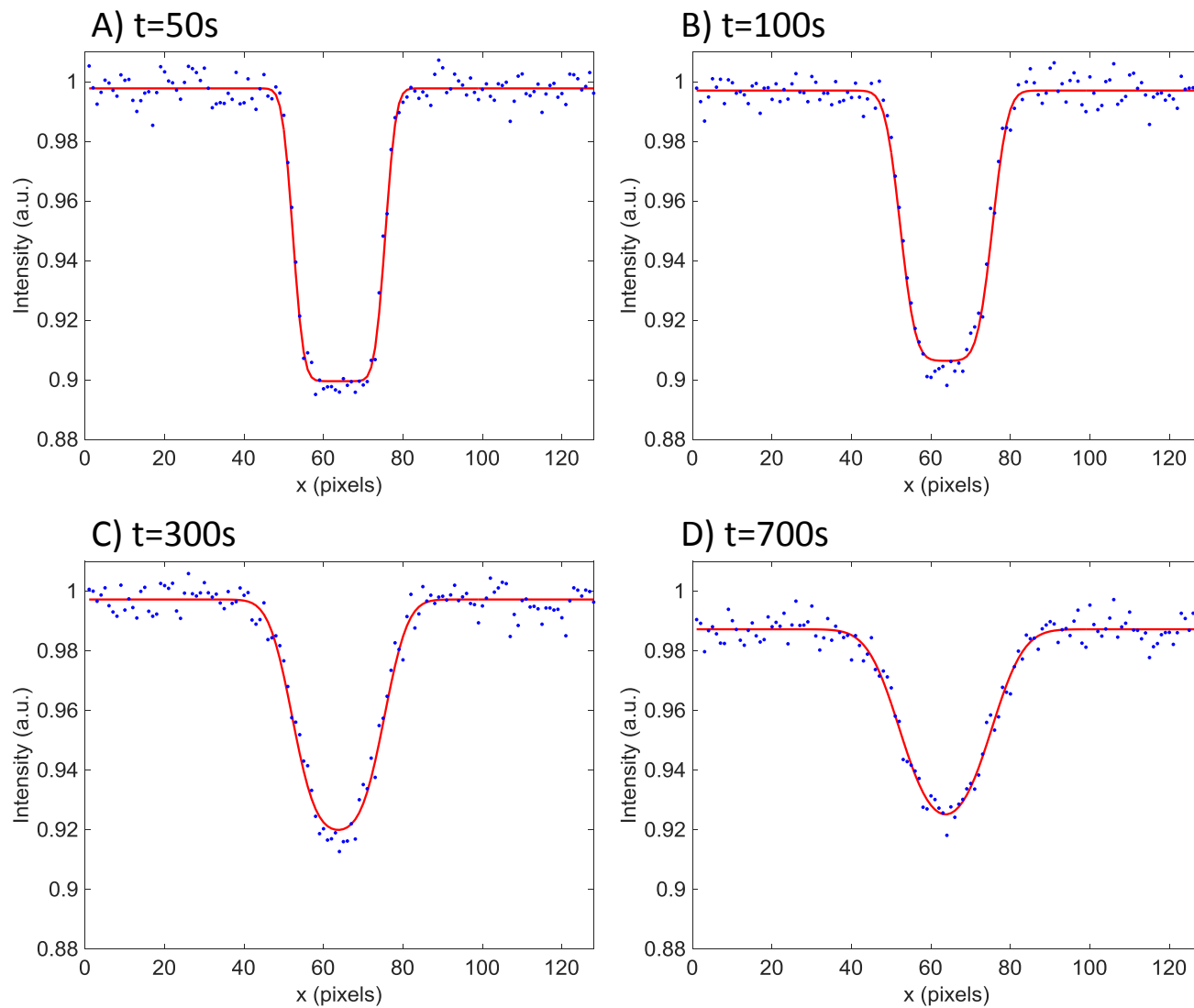


Figure 2.7: Plots of fluorescent intensity as a function of x-position, integrated over all y-positions of an a_w of 0.75. Panel A is an image taken directly after photobleaching and panel B) to D) show the recovery of the fluorescence intensity due to diffusion. The red line is a fit using Equation 2.8.

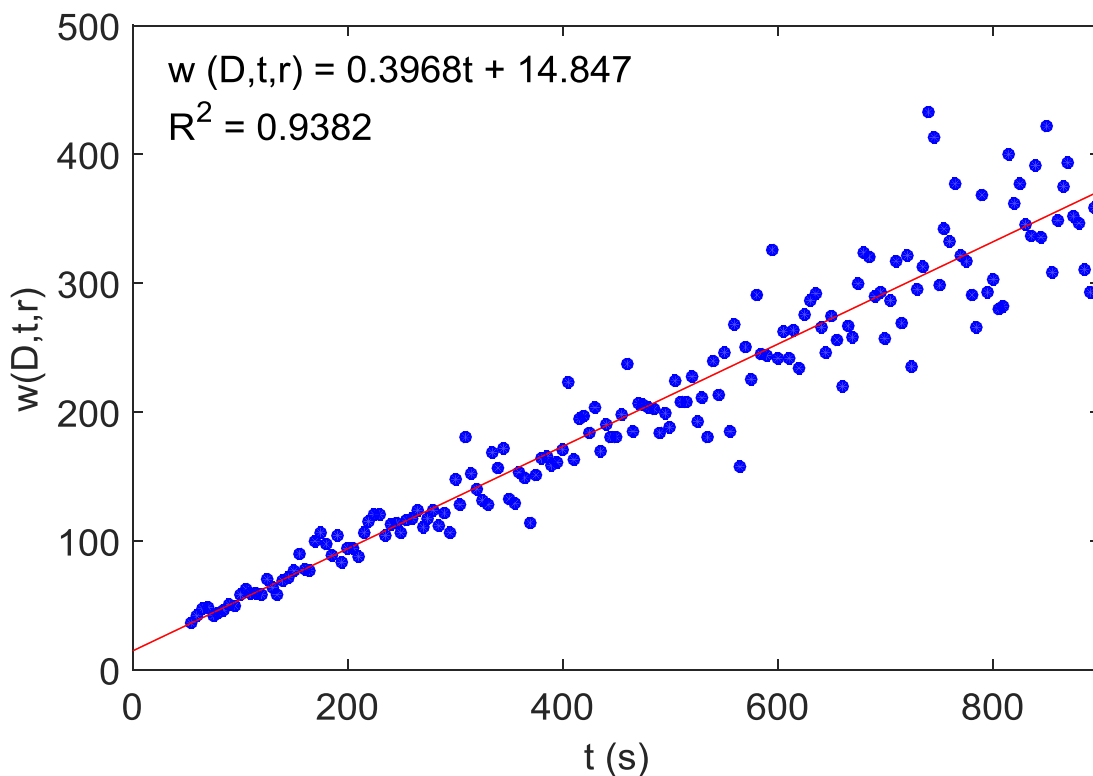


Figure 2.8: Plot of $w(D, t, r)$ as a function of time t for a film of a solution containing R6G, sucrose and water of $a_w=0.75$. Every blue circle represents a value of $w(D, t, r)$ obtained from fits to the experimental data, such as shown in from Figure 2.7. The red line is a linear plot to the data. Since $w(D, t, r) = (r^2 + 4Dt)$, the diffusion coefficient could be calculated from the slope of the line. The first 50s have been excluded from the analysis because of reversible photobleaching.

2.3.3 Cylindrical Geometry of the Photobleaching Region

Prior to determining diffusion coefficients with the rFRAP technique, the geometry of the photobleached region in z-direction was determined. The films chosen had a thickness between 45 and 120 μm and were prepared at an $a_w=0.38$ to ensure that the photobleached area does not recover significantly while taking a stack of images in z-direction (z-stack). Photo-

bleaching areas of 5 by 5, 10 by 10 and 20 by 20 μm were used. The photobleaching was near cylindrically shaped in z-direction for all the film thicknesses tested as expected (Figure 2.9).

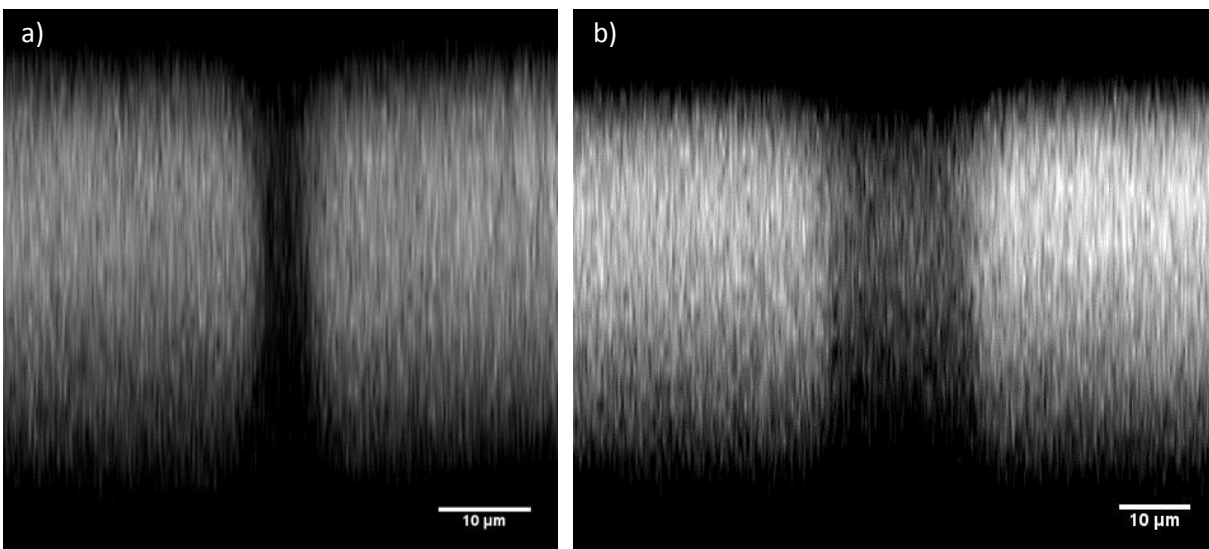


Figure 2.9: Cross section through a fluorescent film at $a_w=0.38$ after photobleaching. The photobleached areas have a size of $5 \times 5 \mu\text{m}$ (a) and $20 \times 20 \mu\text{m}$ (b). The fluorescent films were about $70 \mu\text{m}$ thick.

2.3.4 Corrections for Nonlinearity of the Fluorescence Intensity as a Function of Concentration of R6G

In FRAP experiments, the relationship between the fluorescence intensity and the concentration of R6G needs to be known. To determine this relationship, samples consisting of 50 wt % sucrose-water solution and different concentrations of R6G were prepared and the relationship between fluorescence intensity and concentration of R6G was determined. Shown in Figure 2.10 are the results from these measurements. Each data point consists of an average of three values obtained by measuring the fluorescence intensity of three droplets of the same concentration. Error bars represent the standard deviation (1σ) of the fluorescence intensities.

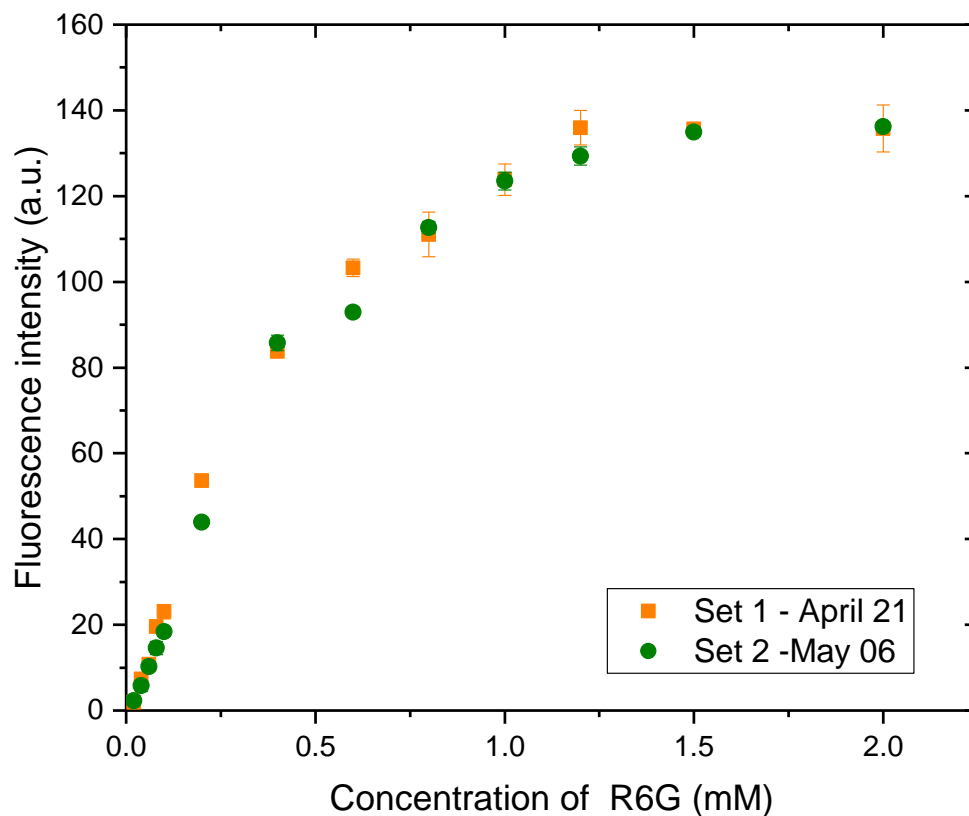


Figure 2.10: Fluorescence intensity as a function of the concentration of R6G in sucrose-water solutions, for concentrations in a 50 wt % sucrose-water solution.

As mentioned above, the concentration of R6G used in the rFRAP experiments was 0.51 mM. Since the fluorescence intensity does not show a linear relationship to the concentration above 0.1 mM, the non-linearity of the fluorescence intensity with the concentration needs to be accounted for in the analysis of the FRAP data.

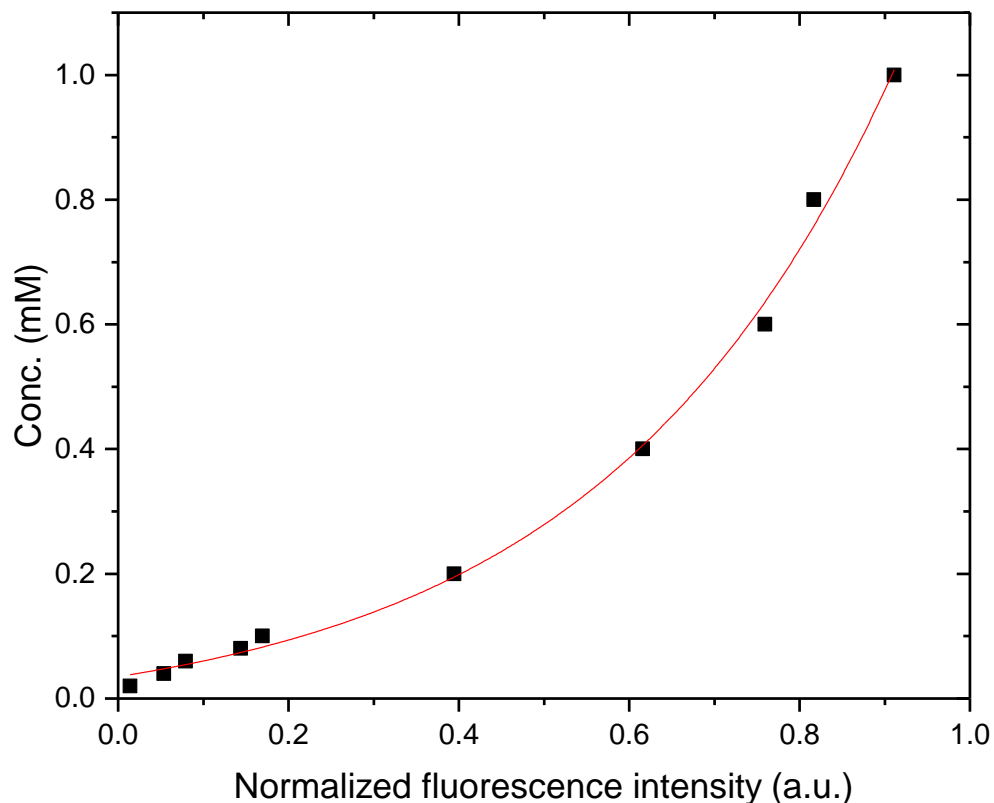


Figure 2.11: Concentration of R6G in mM as a function of fluorescence intensity. The red line is a nonlinear fit to the data using an exponential function.

An exponential function was fit to the data in Figure 2.11 (red line). The obtained relationship (shown in Table 2.3) was used to convert fluorescence intensity into concentration in the rFRAP analysis. The difference between diffusion coefficients calculated assuming a linear relation between concentration and fluorescence intensity compared to using an exponential function (Table 2.3) was relatively small (within the uncertainty of the measurements). Nevertheless, the exponential function was used to convert fluorescence intensity to concentration for completeness in the data reported here.

Table 2.3: Best fit parameters for concentration vs. normalized fluorescence intensity data in Figure 2.11.

$c = c_0 + A \cdot e^{(B \cdot x)}$, where c is the concentration and x is the normalized fluorescence intensity. The R^2 value indicated the quality of the fit.

Variable	c_0	A	B	R^2
Value	-0.0398	0.0748	2.8974	0.9955

2.3.5 Corrections for Reversible Photobleaching

It has been observed in former studies that some types of photobleached organic dyes can recover within the first few seconds (referred to as “reversible photobleaching”). This reversible photobleaching can be due to photoswitching or recovery of the triplet state.⁴⁴ Additional experiments were performed to test, if reversible photobleaching occurs with R6G as a tracer dye.

To test for reversible photobleaching, small droplets (10-50 μm radius) of the 10 wt % sucrose-water solution containing R6G were nebulized onto a glass slide and were conditioned at a water activity of $a_w=0.6$. For the experiments, two droplets were chosen of a similar size: one droplet was photobleached across the entire area of the droplet and the second droplet was used as a reference droplet to ensure that the droplets were not photobleached while monitoring (Figure 2.12). For photobleaching, bleaching depths of 16%, 30% and 55% were used.

Since the complete droplet had been photobleached uniformly, a recovery of fluorescence intensity due to diffusion of fluorescent molecules could be excluded. Also, the reference droplet helped to determine, if changes to the image happened (i.e. change in distance or

change in illumination) so that a change in fluorescence due to illumination was not attributed to fluorescence recovery.

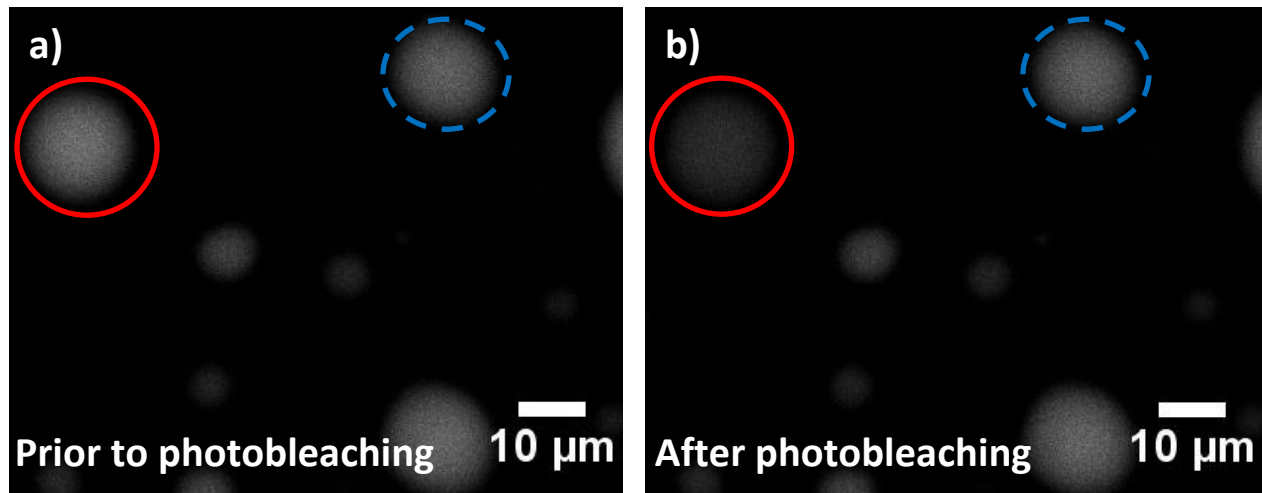


Figure 2.12: Illustration of the choice of droplets used for the experiment on reversible photobleaching. Panel a) shows the droplet which is to be photobleached (red circle) and the reference droplet (blue dashed circle) prior to photobleaching and panel b) shows both droplets after photobleaching.

An example of results from one of these tests is shown in Figure 2.13. The results show that reversible photobleaching occurs within the first 50s after photobleaching. However, no dependence on the bleaching depth was observed. To account for the reversible photobleaching in the data analysis, data recorded during the first 50s after photobleaching were excluded from the data analysis.

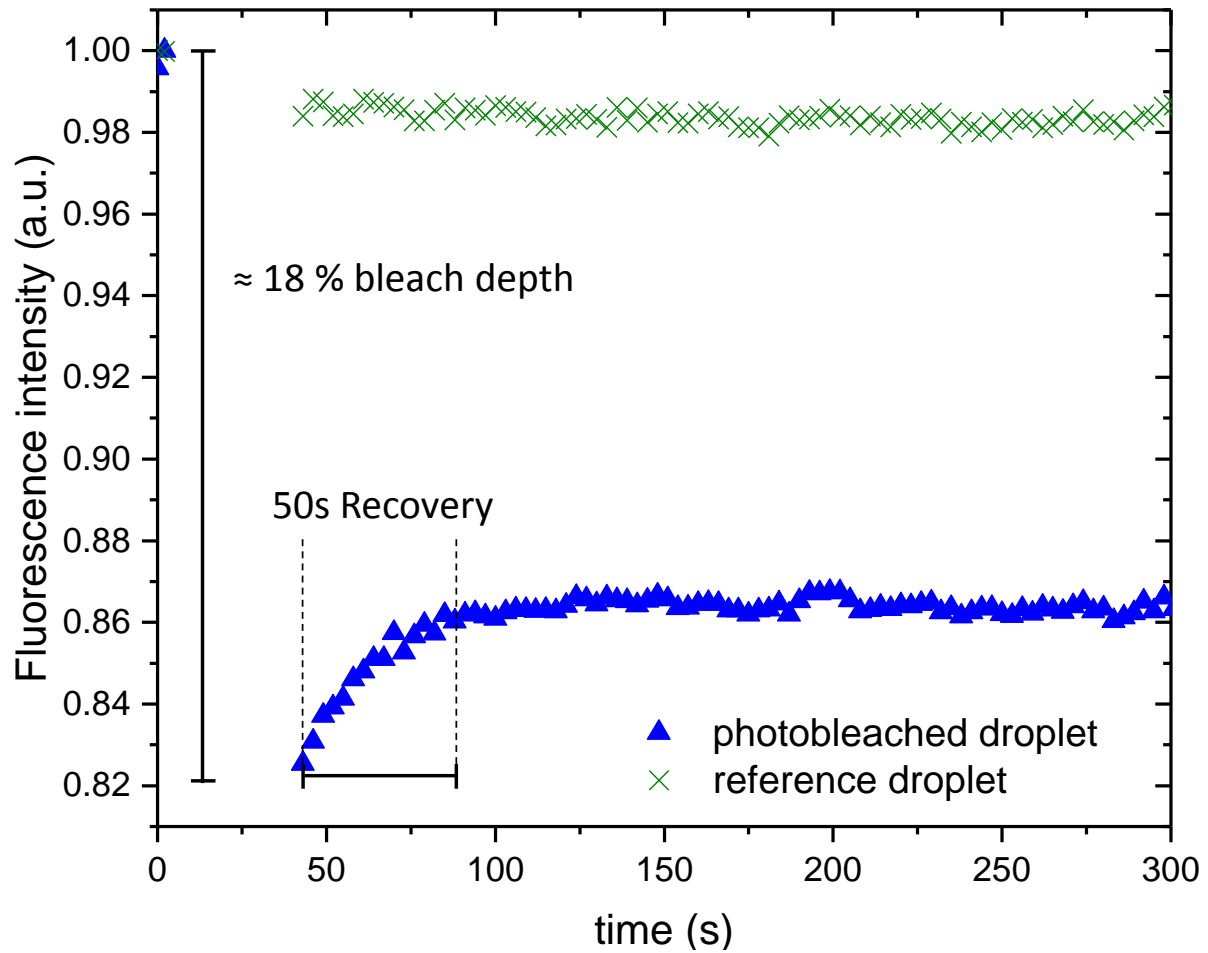


Figure 2.13: The fluorescence intensity-versus-time for two droplets used to test for reversible photobleaching. A sucrose-water droplet containing R6G of $a_w=0.6$ was photobleached over its total area, so that its fluorescence intensity decreased by 18%. While the recovery of the photobleached droplet (blue triangles) was monitored a reference droplet (green crosses) not being photobleached was also monitored. For the analysis of the recovery, the fluorescence intensity was averaged across the complete droplet.

2.4 Results and Discussion

2.4.1 Diffusion Coefficients of R6G in Sucrose Water Solutions

The diffusion coefficients in this work were measured across a wide range of water activities from 0.38 to 0.80. As expected, the diffusion coefficients decrease with decreasing a_w , since the viscosity of sucrose water solutions increase as the water activity increases.^{15e} For the water activities from 0.38 to 0.8, the diffusion coefficients ranged from $1.50 \cdot 10^{-14}$ to $4.73 \cdot 10^{-9}$ cm²/s. Since the time needed for recovery of the fluorescence signal for $a_w < 0.38$ was on the order of months, diffusion coefficients were not measured at $a_w < 0.38$.

2.4.2 Breakdown of the Stokes-Einstein Equation

In Figure 2.14, the measured diffusion coefficients of R6G are displayed as a function of water activity. A secondary and tertiary x-axis have been included in Figure 2.14 is the mass fraction of sucrose and T_g/T , where T_g is the glass transition temperature and T is the temperature of the matrix (which is sucrose and water in this case). This information has been included in Figure 2.14, since literature studies conducted in the past report diffusion coefficient values as a function of mass fraction of sucrose or as a function of T_g/T . The glass transition temperature was calculated using Champion *et al.* (1997) and the relationship between the water activity and the mass fraction of sucrose was determined using Zobrist *et al.* (2011).⁴⁵

In Figure 2.14, the measured diffusion coefficients of R6G were compared to diffusion coefficients calculated using the Stokes-Einstein equation, the hydrodynamic radius (R_H) of 5.89 Å measured by Müller *et al.* (2008)²⁴ and various viscosity values. Also included are a 4th

order polynomial fit and 95% confidence limit to the calculated diffusion coefficient values. The measured diffusion coefficients of R6G in sucrose water solutions show good agreement with the values calculated with the Stokes-Einstein equation for values above a_w of 0.5. However, at an a_w of 0.38 the diffusion coefficient of R6G deviates from the calculated value by a factor of between 2 and 50.

An a_w of 0.38 would correspond to a T_g/T value of 0.94 (Figure 2.14). In the past, a breakdown of the Stokes-Einstein equation has been observed for fluorescein at T_g/T of 0.86 and 0.65 in sucrose water solutions by Champion *et al.* (1997)^{16c} and Corti *et al.* (2008)^{16d}, respectively. The measurements in this work are in agreement with the T_g/T value measured by Champion *et al.* (1997) but deviate from Corti *et al.* (2008).

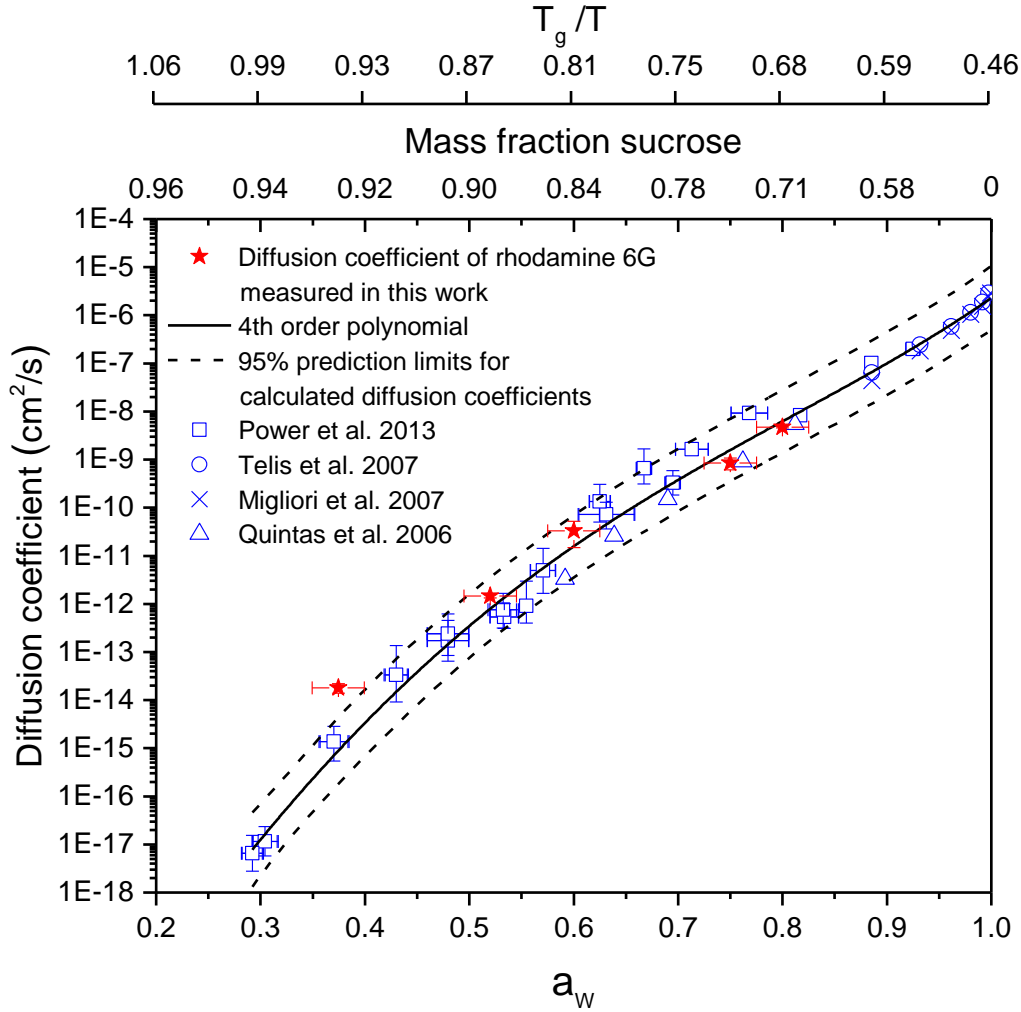


Figure 2.14: Shown are the diffusion coefficients of R6G in sucrose water solution in comparison to diffusion coefficient values calculated from viscosities from Quintas *et al.* (2006; blue triangles)⁴⁶, Migliori *et al.* (2007; blue crosses)⁴⁷, Telis *et al.* (2007; blue circles)⁴⁸ and Power *et al.* (2013; blue rectangles)^{15e} using the Stokes-Einstein equation and the R_H measured by Müller *et al.* (2008)²⁴. The error bars for the diffusion coefficients of R6G represent 95% confidence limit, while the red star itself represent the average value of the diffusion coefficients measured. The black solid line represents a 4th order polynomial which was fit to the literature values. The dashed line represents the 95% prediction limit that was fit to the calculated diffusion coefficients.

2.4.3 Comparison with Diffusion Coefficients of Other Molecules in Sucrose Water Solutions

In Figure 2.15, diffusion coefficients of R6G in sucrose water solutions are compared with diffusion coefficients of other molecules in the same solution. The data for the diffusion coefficients of fluorescein and calcein was taken from Y. Chenyakin³². The diffusion coefficients of water were calculated using a polynomial fit from Price *et al.* (2014) (Appendix A.3).

Since calcein is larger and fluorescein is smaller than R6G (Table 2.4), one would expect the diffusion coefficient of R6G to be in between the diffusion coefficients of calcein and fluorescein at a given a_w . However, the uncertainties in the measurements of this work are too large to conclude this. Water has the smallest hydrodynamic radius of all molecules analyzed and shows significantly larger values for diffusion coefficients compared to the other molecules analyzed.

Table 2.4: Hydrodynamic radius (R_H) and molecular weight (MW) of several molecules considered in this work.

Diffusing molecule	R_H (Å)	MW (g/mol)
fluorescein	5.02 (Mustafa <i>et al.</i> (1993) ⁴⁹)	376
rhodamine 6G	5.89 (Müller <i>et al.</i> (2008) ²⁴)	479
calcein	7.4 (Tamba <i>et al.</i> (2010) ⁵⁰)	622
water	1.41 (Pang (2014) ⁵¹) ^a	18

^a The reported radius is the Van-der-Waals radius instead of the hydrodynamic radius.

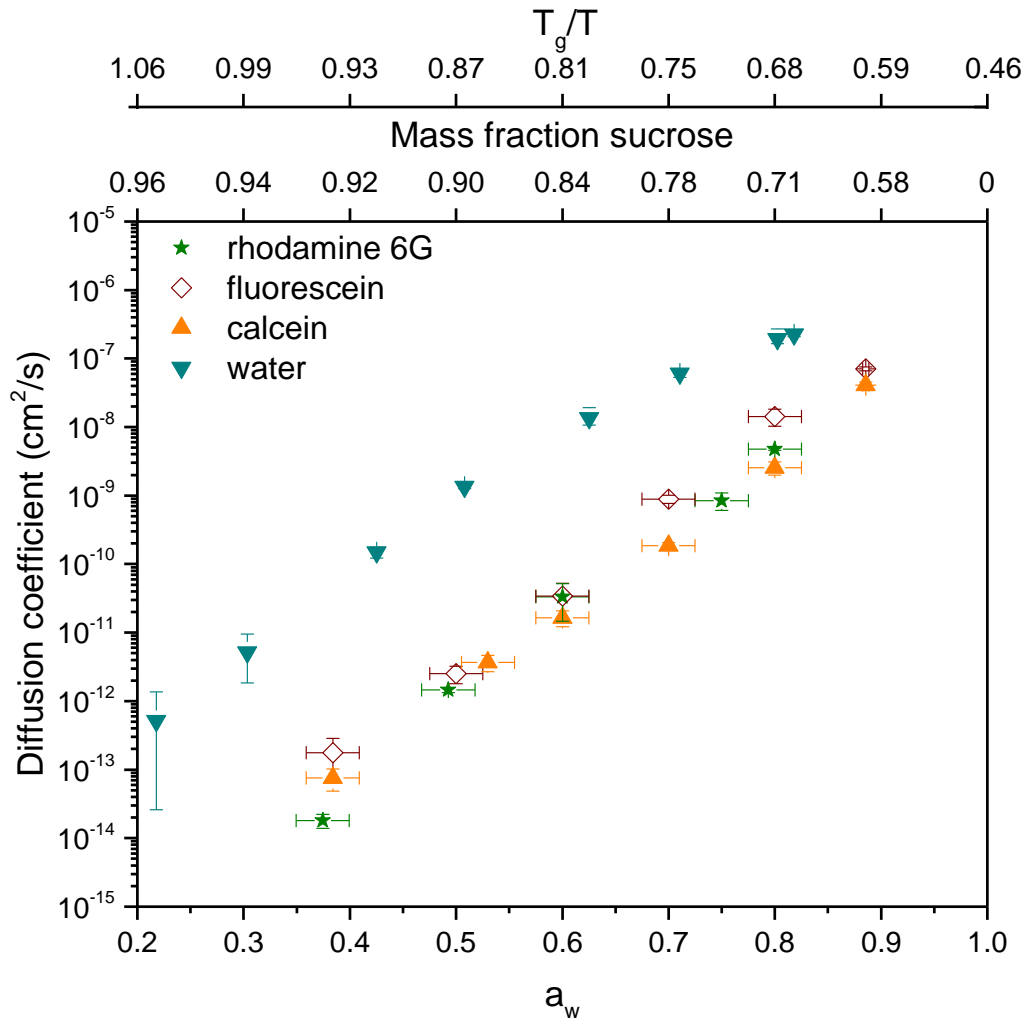


Figure 2.15: Shown are the diffusion coefficients of fluorescein, calcein (data used from Y. Chenyakin³²), water (data used from Price *et al.*³¹) and R6G in sucrose water solutions. The error bars in x-direction are 95% confidence intervals.

2.4.4 Breakdown of the Stokes-Einstein Equation for Molecules of Different Hydrodynamic Radii

As illustrated in Figure 2.16, diffusion coefficients have been measured for other large dyes and water in sucrose water solutions (Table 2.5). In addition, diffusion coefficients have

been measured for sucrose in sucrose water solutions. In this work, the measured diffusion coefficients were used to generate Figure 2.16. Shown in Figure 2.16, is the ratio of the measured diffusion coefficients, D_{measured} , to the Stokes-Einstein predicted diffusion coefficients, $D_{\text{predicted}}$, as a function of the ratio of the radius of the diffusing molecule, $R_{\text{diffusing}}$, (i.e. calcein etc.) to the radius of the matrix, R_{matrix} , (hydrodynamic radius of sucrose = 4.7 \AA^{25}). The results for fluorescein and calcein in Figure 2.16 are based on measured diffusion values by Chenyakin *et al.*^{16b}. The results for water and sucrose are based on Price *et al.* (2014)³¹ and Price *et al.* (2016)⁵², respectively.

In Figure 2.16, a $D_{\text{measured}}/D_{\text{predicted}}$ -value that equals 1, indicates agreement between the Stokes-Einstein equation and measured diffusion coefficient values. Values below and above 1 indicate an over- and an underprediction.

For larger molecules with $R_{\text{diffusing}}/R_{\text{matrix}}$ -values of 1.00 to 1.57, such as sucrose, fluorescein, rhodamine 6G and calcein, the Stokes-Einstein equation holds at $a_w=0.6$. However, for molecules as small as water and a $R_{\text{diffusing}}/R_{\text{matrix}}$ -value of 0.3, the Stokes-Einstein equation breaks down at $a_w=0.6$ and underpredicts the diffusion coefficient by up to 2.5 orders of magnitude.

At $a_w=0.38$, the Stokes-Einstein equation breaks down for larger molecules as well as for water. For calcein, the Stokes-Einstein equation underpredicts the diffusion coefficients in sucrose water solutions by a factor of 7 to a factor of 150. For R6G, the values are underpredicted by a factor of 2 to a factor of 50 and for fluorescein the diffusion coefficients are underpredict-

ed by a factor of 8 to a factor of 500. Sucrose shows an underprediction of a factor of 20 to a factor of 90. Water shows an underprediction of up to 4.5 orders of magnitude.

Table 2.5: Properties of the molecules shown in Figure 2.16.

Molecule	R_H (Å)	MW (g/mol)	$R_{diffusing}/R_{matrix}$
water	1.41 (Pang (2014) ⁵¹)	18	0.30
sucrose	4.7 (Ribeiro <i>et al.</i> (2006) ²⁵)	342	1.00
fluorescein	5.02 (Mustafa <i>et al.</i> (1993) ⁴⁹)	376	1.07
rhodamine 6G	5.89 (Müller <i>et al.</i> (2008) ²⁴)	479	1.25
calcein	7.4 (Tamba <i>et al.</i> (2010) ⁵⁰)	622	1.57

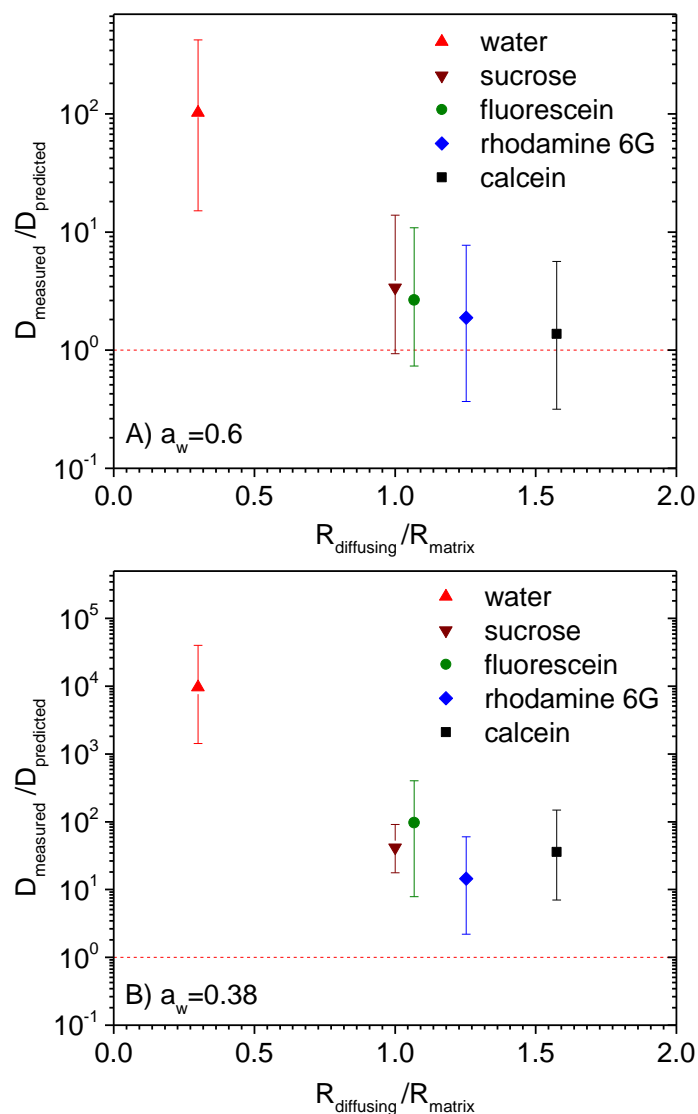


Figure 2.16: $D_{\text{measured}}/D_{\text{predicted}}$ as a function of $R_{\text{diffusing}}/R_{\text{matrix}}$. Panel A corresponds to $a_w=0.6$ and Panel B $a_w=0.38$.

D_{measured} is the measured diffusion coefficient and $D_{\text{predicted}}$ is the predicted diffusion coefficient. $R_{\text{diffusing}}$ is the hydrodynamic radius of the diffusing species and R_{matrix} is the hydrodynamic radius of the matrix molecule (sucrose) (Ribeiro *et al.* (2006)²⁵. The data for calcein and fluorescein was taken from Chenyakin *et al.* (2016)^{16b}, the data for sucrose was taken from Price *et al.* (2016)⁵². In order to calculate $D_{\text{predicted}}$ using the Stokes-Einstein equation, a parameterization for the viscosity of sucrose water solution was used (see Appendix A). The error bars for all of the data points were calculated conservatively using the largest error possible for D_{measured} as well as $D_{\text{predicted}}$ and the total error was determined using a Gaussian error propagation.

Chapter 3: Diffusion Coefficients and Mixing Times of Fluorescent Organic Molecules in Brown Limonene Secondary Organic Material

3.1 Introduction

Brown carbon in atmospheric particles, referred to as BrC, is yellow to brown coloured and absorbs in the near ultra violet (300-400 nm) and the visible range.¹⁸ BrC is divided into primary and secondary BrC depending on its mechanism of formation in the atmosphere. Primary BrC is directly emitted to the atmosphere during combustion processes, such as forest fires and biomass burning⁵³, or it can be directly emitted to the atmosphere from soils, fungi or plants^{18, 54}. Secondary BrC, on the other hand, is produced by a complex series of gas-phase reactions followed by condensation of reaction products in the atmosphere.

A few terpenes, such as limonene (Table 3.1), can form secondary BrC and 16 % of the global emissions of monoterpenes consist of limonene.^{20, 55} Once in the atmosphere, limonene can react with OH, NO₃ and ozone to form secondary organic material (SOM), a fraction of which can condense to form particles.⁵⁶

After the limonene SOM particles are formed, they can react with ammonia, to form brown limonene SOM particles, which show enhanced fluorescence and absorption.⁵⁷ Once formed, brown limonene SOM particles may play a role in climate and visibility by directly absorbing solar radiation.

At this point, the identity of the compounds that cause the enhanced fluorescence and absorption in both BrC and brown limonene SOM are uncertain.⁵⁵ Even though the molecular structures of the fluorescent and absorbing substances in BrC and brown limonene SOM are

uncertain, some molecular structures for the formation of possible UV- and visible light absorbing molecules have been suggested by Nguyen *et al.* (Figure 3.1).⁵⁸

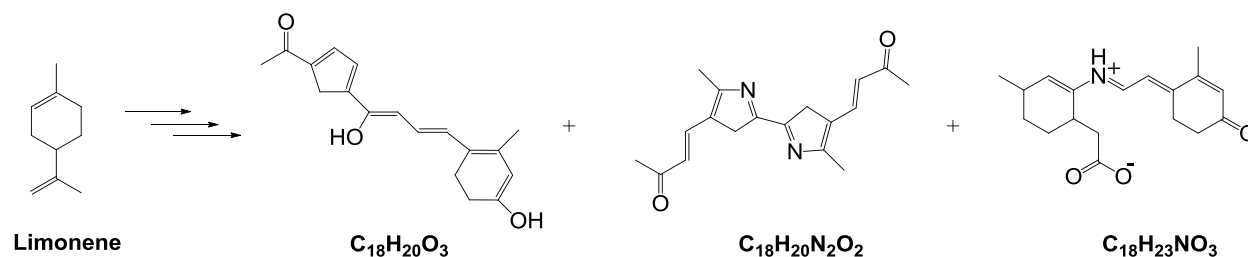


Figure 3.1: Simplified suggested reaction mechanism for the formation of larger organic molecules, which have the potential to be light absorbing in the UV- and the visible light range, from limonene (Nguyen *et al.* (2013)).⁵⁸

Table 3.1: Physico-chemical data on limonene including the molecular weight (MW) and the molecular structure.

Compound	Molecular formula	Molecular structure	MW (g/mol)
Limonene	$\text{C}_{10}\text{H}_{16}$		136.24

When predicting the formation and evaporation of SOM, including brown limonene SOM particles, it is often assumed that diffusion rates of organics are fast (i.e. similar to the diffusion rates of organics within water).^{8, 15a, 19a-c} However, measurements have shown recently that diffusion rates of organics within SOM particles may be much slower than initially thought under certain conditions (such as low relative humidities).^{22a, 59} If these diffusion rates are significantly slower than originally thought, then past predictions of SOM particles and their atmospheric implications may be inaccurate and chemical transport models will need to be modified.

To determine diffusion rates of organics in SOM, researchers have previously measured viscosities of SOM particles and then calculated diffusion rates of organics within the SOM using the viscosities and the Stokes-Einstein equation.^{8, 15d, 23} However, as shown in Chapter 2, this approach can underpredict diffusion rates due to the breakdown of the Stokes-Einstein equation at high viscosities.

There have only been a few direct measurements of diffusion rates within SOM, and most of these studies have been limited to dry conditions.^{59a, 60} Within the atmosphere, however, RH varies typically from 20 to 100% (and hence a_w varies from 0.2 to 1). This variability of RH and water activity can change diffusion rates of organics significantly, since water acts as a plasticizer and as the water activity in SOM increases, the diffusion rates of organics should also increase.^{15e}

In the current study, diffusion coefficients of organic fluorescent molecules within brown limonene SOM are measured over a wide range of water activities using rFRAP. Brown limonene SOM was chosen as a matrix for this study, since it is thought to be an important type of SOM particle in the atmosphere (because of its high abundance and its ability to absorb light) and since it already contains fluorescent organic molecules (i.e. intrinsic organic fluorophores) that can be used in the rFRAP experiments. This avoids the need to add a fluorescent organic tracer molecule for the rFRAP measurements. From the diffusion rates, mixing times of organic molecules within SOM particles due to molecular diffusion are calculated and the implications are discussed.

3.2 Experimental

3.2.1 Generation and Collection of Brown Limonene SOM

Particles containing limonene secondary organic material were generated in a 20 L flow tube by dark ozonolysis of limonene by M. Hinks at UC Irvine, California, USA. Pure liquid limonene (Sigma-Aldrich, 97%) was injected and volatilized under a flow of dry air resulting in a typical mixing ratio of 70 ppm in the flow tube. Ozone was produced externally by photolysis of O₂ (Airgas, Ultra High Purity) and then added to the flow tube resulting in a mixing ratio of 10 ppm of ozone. Within the flow tube, the reaction of gas-phase limonene with ozone led to a concentration of 1,000 µg/m³ of limonene SOM particles in the air. Upon exiting the flow tube, the SOM particles then passed through a charcoal denuder to eliminate excess ozone and gas-phase organics. The SOM particles were collected on a hydrophobic slide (Hampton Research) continuously for 45 min using a Sioutas impactor equipped with a single stage (stage D -0.25 µm cut point at 9 SLM collection flow rate) (Figure 3.2).

Brown limonene SOM particles were generated by placing the hydrophobic slide containing the limonene SOM particles within a small, glass petri dish, which was inserted within a larger covered petri dish containing a solution of 0.1 M ammonium sulfate (EMD, >99 %). Over a period of three days, ammonia vapour from the solution (300 ppb NH₃ estimated using the Extended AIM Aerosol Thermodynamics Model II)⁶¹ reacted with the fresh limonene SOM forming a visible brown colour.

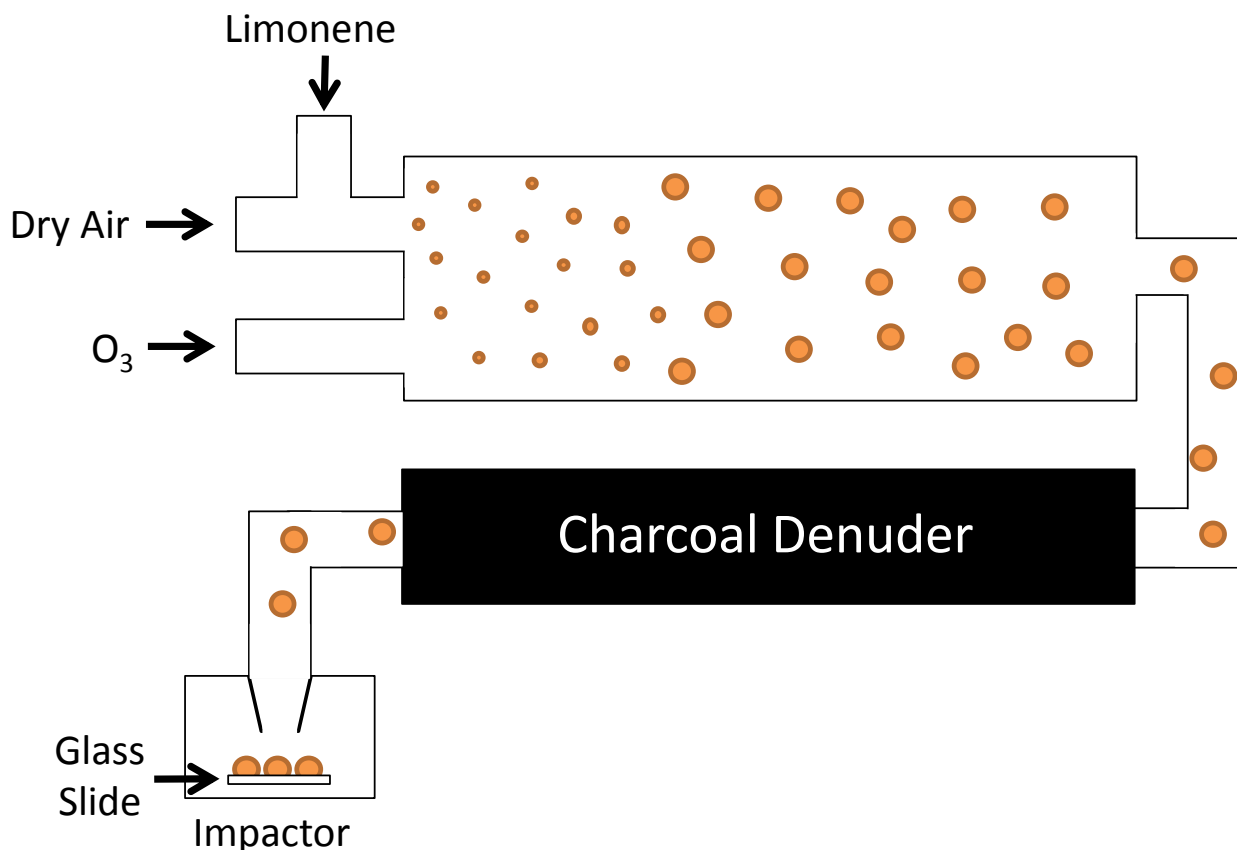


Figure 3.2: Preparation of the SOM samples from the reaction of limonene with O₃. The orange circles represent SOM particles.

3.2.2 Preparation of Thin Films of Brown Limonene SOM at Water Activities Ranging from 0.38 to 0.9

The brown limonene SOM samples were received on hydrophobic glass slides (Hampton Research, Canada) from UC Irvine, California, USA. Three to six small droplets (radius of 100 μm to 225 μm) of the sample were transferred from the sample to a second hydrophobic glass slide using the tip of a needle (BD Precision Glide™ Needle, 0.9 mm x 40 mm). The brown limonene SOM droplets were conditioned at the desired water activity using the setup described in sec-

tion 2.2.1. To calculate the conditioning times of the brown limonene droplets with the surrounding water vapour, it was assumed that the diffusion rate of water within brown limonene SOM was equal to the diffusion rate of water in sucrose-water mixtures at the same water activity. This assumption most likely overestimates the time needed for conditioning, since the viscosity of sucrose-water mixtures is higher than the viscosity of brown limonene SOM at the same water activity.⁸ For each a_w , a minimum of three glass slides containing four to six droplets of brown limonene SOM were prepared. Once the droplets were conditioned to a known water activity, a second glass slide was placed on top of the droplet, and the droplet was sandwiched between the two slides as discussed in section 2.2.1, forming a thin film (thickness = 30-90 μm) of the brown limonene SOM. The diffusion coefficients were measured three times per glass slide for each thin film prepared.

3.2.3 Measurements of Diffusion Coefficients Using rFRAP

Diffusion coefficients of the intrinsic fluorophores within the brown limonene SOM were measured with rFRAP. The same microscope, Zeiss Axio Observer LSM 5 10 MP laser scanning microscope, and similar scanning settings as described in section 2.3 were used. The scanning laser power was varied between 21.3 to 42.6 μW depending on the fluorescence of the sample. In order to achieve a bleach depth of about 30%, the laser power for photobleaching was varied between 93 and 297 μW depending on the sample.

For the experiments, a rectangular geometry was chosen with the sizes of the rectangle depending on the diffusion times with smaller areas for longer diffusion times. The image sizes

were chosen in relation to the bleach size such that the diffusing front in the experiments remained within the image even for long recovery times. For samples at $a_w \geq 0.8$ photobleaching areas of $20 \mu\text{m}$ by $20 \mu\text{m}$ and image sizes of $199.61 \mu\text{m}$ by $199.61 \mu\text{m}$ were chosen. For samples conditioned to $0.5 \leq a_w \leq 0.7$, photobleaching areas of 10 by $10 \mu\text{m}$ and image sizes of $99.8 \mu\text{m}$ by $99.8 \mu\text{m}$ were used, and for $a_w = 0.38$ photobleaching areas of 10 by $10 \mu\text{m}$ and image sizes of $99.8 \mu\text{m}$ by 99.8 or 59.88 by $59.88 \mu\text{m}$ were used.

Shown in Figure 3.3 are examples of images recorded during a FRAP experiment with brown limonene SOM films with water activities of 0.38 , 0.6 and 0.9 . At a low water activity of 0.38 , the recovery times are on the order of hours, while at high water activities of 0.9 the recoveries are on the time scale of seconds.

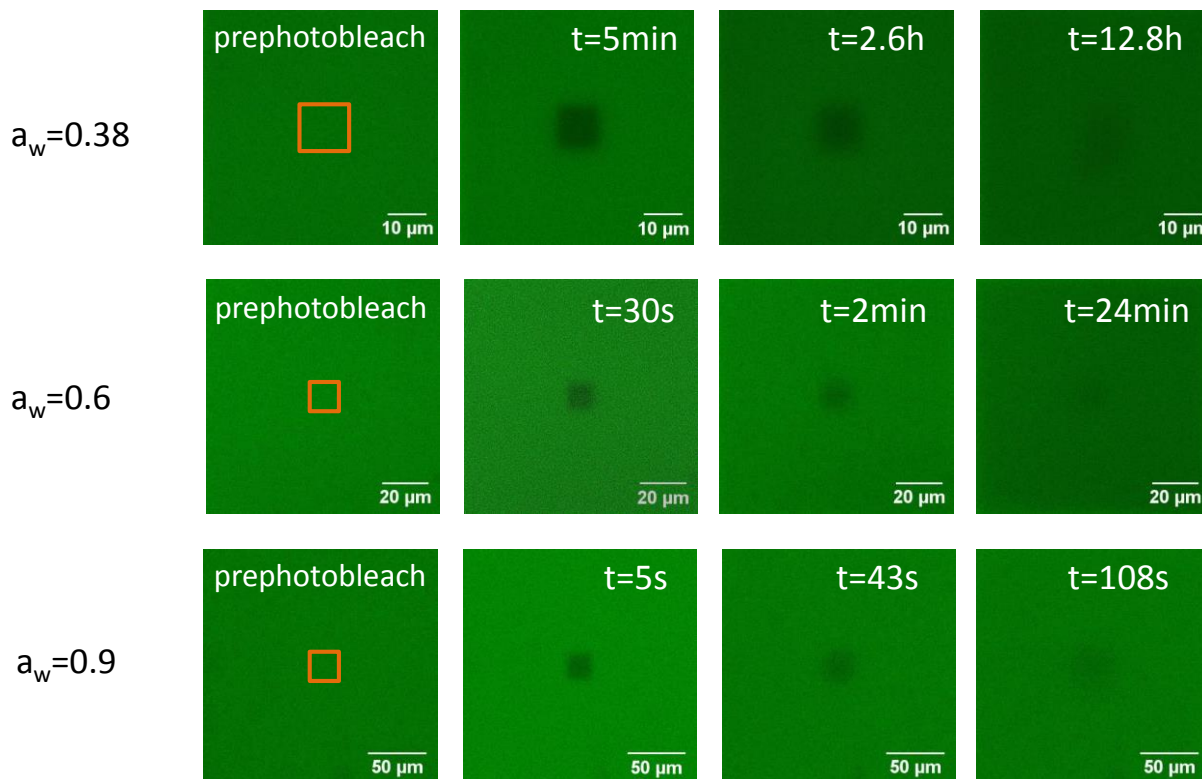


Figure 3.3: Images recorded during an rFRAP experiment with brown limonene SOM at three different water activities: 0.38, 0.6 and 0.9. The orange rectangles depict the area that is to be photobleached. Indicated in the figures are the times (t) after photobleaching.

3.2.4 Analysis of the Images from the rFRAP Recovery Experiments

The analysis of images from the rFRAP experiments with brown limonene SOM films was conducted as described in section 2.3. When analyzing the images as a function of time after photobleaching, the images were normalized to the image recorded prior to photobleaching. Images were not analyzed using a region within the image itself, as described in section 2.3, since in some cases there were no large regions within the images unaffected by diffusion.

Figure 3.4 shows examples of fluorescence intensities integrated over the width of the bleach area according to Eq. 2.9 as a function of distance along the x-dimension in the image.

Also included are fits to the data using Eq. 2.9. Figure 3.5 shows plots of $w(D,t,r)$ as a function of time extracted from plots such as Figure 3.4 for the brown limonene experiments. In Figure 3.5, the first five seconds were excluded from the data analysis, since experiments similar to section 2.3.5 showed that reversible photobleaching was occurring during the first five seconds after photobleaching. Note, that in these plots the maximum intensity even far away from the photobleached region decreases with time after photobleaching. This is, because the scanning laser used to monitor the fluorescence with time after photobleaching is also causing some minor photobleaching. However, this does not affect the calculations of the diffusion coefficients, since the diffusion coefficient is only dependent on the bleach width, which is not affected by this gradual photobleaching.

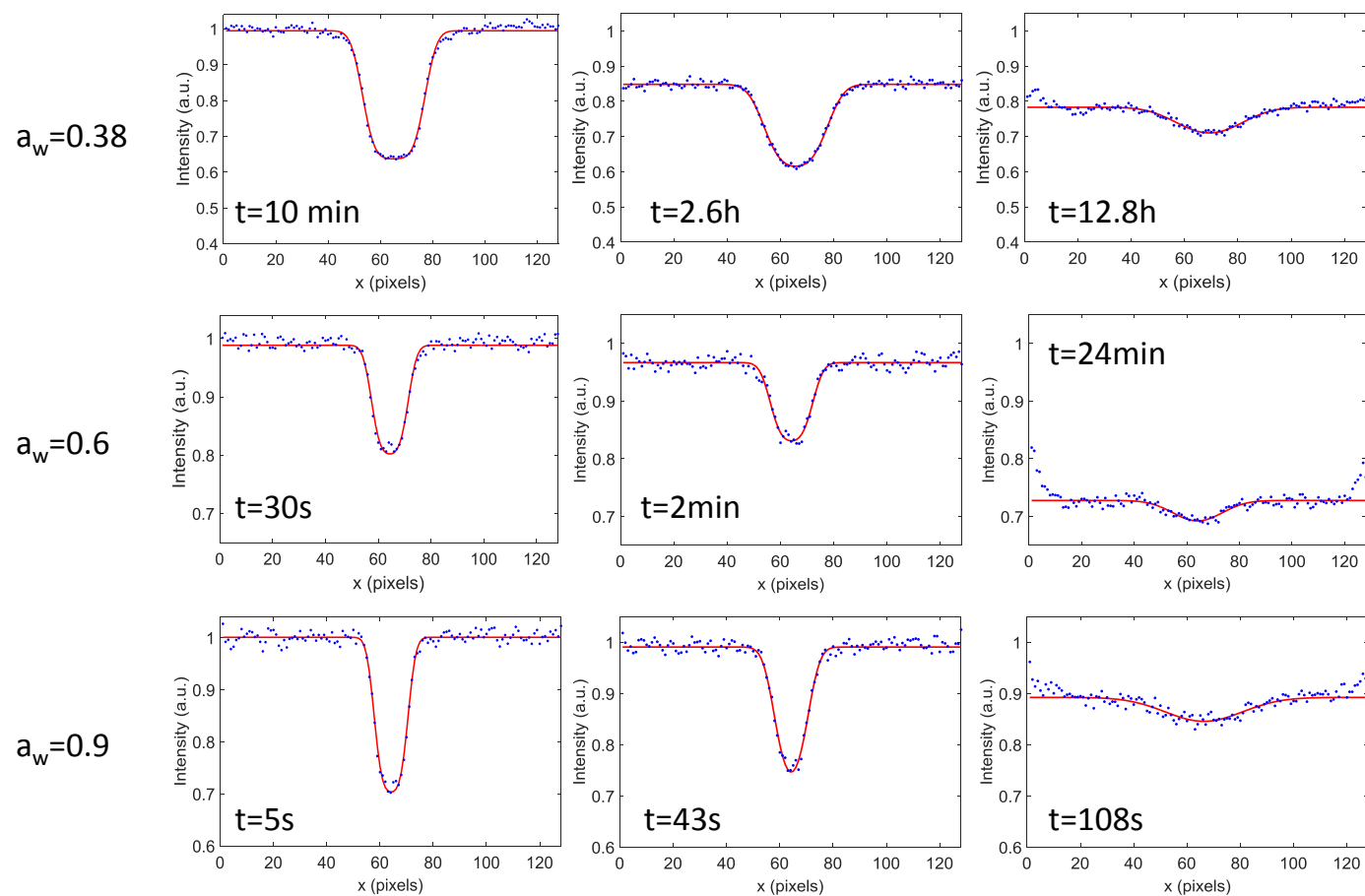


Figure 3.4: Fluorescence intensities integrated over the bleach width in the y-direction as a function of x-position (in pixels) for selected brown limonene SOM films at $a_w = 0.38, 0.6$ and 0.9 . The blue dots represent the intensity measurements and the red line is a fit to the data using Equation 2.8.

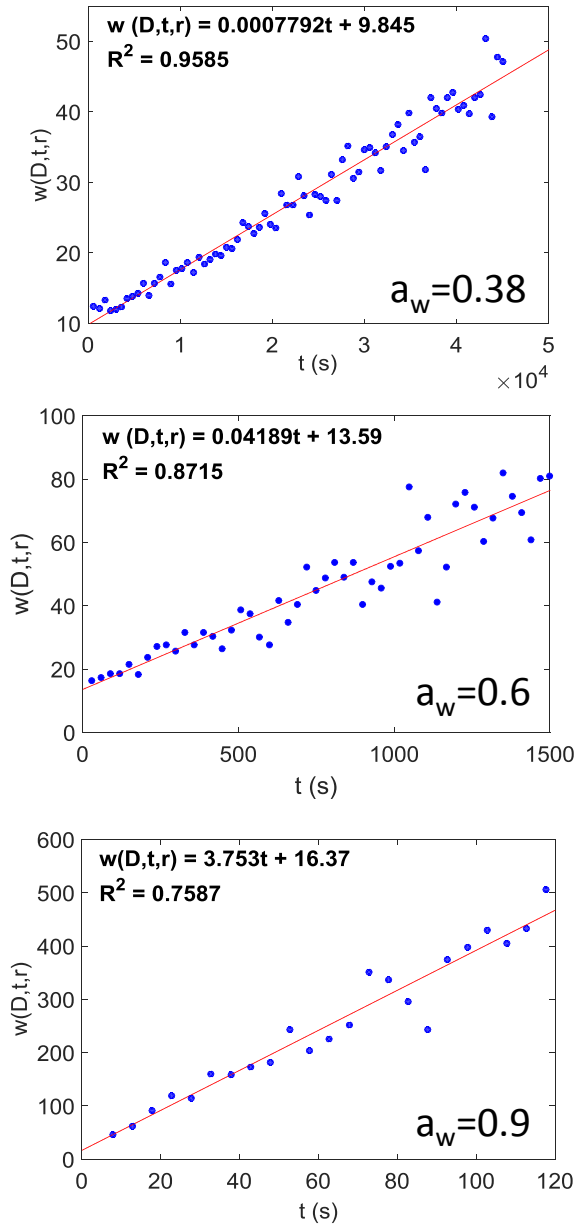


Figure 3.5: Plot of $w(D, t, r) = r^2 + 4Dt$ as a function of time. The blue circles represent the data which was obtained from figures such as Figure 3.4. The red line is a linear fit to the data. The diffusion coefficients were obtained from the slopes and are $D = 0.0007792/4 = 0.0001948 \mu\text{m}^2/\text{s} = 1.95 \cdot 10^{-12} \text{cm}^2/\text{s}$ for $a_w = 0.38$, $D = 0.04189/4 = 0.0105 \mu\text{m}^2/\text{s} = 1.05 \cdot 10^{-10} \text{cm}^2/\text{s}$ for $a_w = 0.6$ and $D = 3.753/4 = 0.938 \mu\text{m}^2/\text{s} = 9.38 \cdot 10^{-9} \text{cm}^2/\text{s}$ for $a_w = 0.9$.

3.2.5 Effect of Laser Power on Measured Diffusion Coefficients

In order to see if the laser intensities used for photobleaching influenced the measured diffusion coefficients, experimental diffusion coefficients were determined using two different laser intensities for photobleaching: a laser power of 139.9 μW was used for 20% bleach depth and a laser power of 330 μW for 50% bleach depth. The tests were performed on the same sample. The sample was conditioned to $a_w = 0.9$ and for each photobleaching test, a new area was chosen.

The tests at the different bleach depths gave diffusion coefficients which agree within the error margin. Using a laser power of 139.9 μW , a diffusion coefficient of $(2.5 \pm 0.5) \cdot 10^{-9} \text{ cm}^2/\text{s}$ was obtained and using a laser power of 330 μW a diffusion coefficient of $(2.8 \pm 0.1) \cdot 10^{-9} \text{ cm}^2/\text{s}$ was obtained (uncertainties correspond to confidence intervals). From these observations it was concluded that the laser power used during photobleaching does not significantly influence the measured diffusion coefficients in brown limonene SOM.

3.2.6 Corrections for Non-linearity of the Fluorescence Intensity as a Function of Concentration of the Intrinsic Fluorophores

As discussed in Section 2.3.4, in rFRAP experiments the relationship between the fluorescence intensity and the concentration of fluorophore needs to be known. In the previous chapter, this relationship was determined by measuring the fluorescence intensity as a function of fluorophore concentration in the films. However, this was not possible for the case of the intrinsic fluorophores in brown limonene SOM, because the concentration of the intrinsic fluor-

ophores could not be changed in the film and the concentration of the intrinsic fluorophores could not be measured. To overcome this limitation, a relationship between the normalized fluorescence signal and the normalized concentration was derived from first principles that could be used together with knowledge of the transmittance of the light through the brown limonene SOM samples to convert normalized fluorescence signal to normalized concentrations (details are below).

The fluorescence intensity F of a material depends on the intensity of the incoming light, I_0 , the intensity of the outgoing light, I , and the rate constant, k' , that takes the ability of a molecule to fluoresce into account:⁶²

$$F = k'(I_0 - I). \quad 3.1$$

In addition, the absorbance of a material with respect to the concentration of fluorescing molecules can be described by the Beer-Lambert law:

$$A = \epsilon cl = \log\left(\frac{I_0}{I}\right), \quad 3.2$$

where ϵ is the extinction coefficient, l is the distance the light has to travel through the fluorescent medium (which is the thickness of the thin film in this case) and c is the concentration.

Eq. 3.1 and Eq. 3.2 can be combined to give the following:

$$F = k'I_0(1 - 10^{-\epsilon lc}). \quad 3.3$$

In the experiments, ϵ , l , k' as well as I_0 are constant, but the photobleaching process changes the concentration c of the intrinsic fluorophores and hence the fluorescence intensity F chang-

es. The fluorescence intensity before photobleaching (prephotobleaching) can be described by the following expression:

$$F_1 = k'I_0(1 - 10^{-\epsilon lc_1}), \quad 3.4$$

where the subscript 1 represents pre-photobleaching conditions. The fluorescence intensity after photobleaching can be described by the following expression:

$$F_2 = k'I_0(1 - 10^{-\epsilon lc_2}), \quad 3.5$$

where the subscript 2 represents post-photobleaching conditions. A normalized fluorescence intensity, F_N , can be introduced with respect to the fluorescence intensity prior to photobleaching, F_1 :

$$F_N = \frac{F_2}{F_1} = \frac{k'I_0(1 - 10^{-\epsilon lc_2})}{k'I_0(1 - 10^{-\epsilon lc_1})} = \frac{1 - 10^{-\epsilon lc_2}}{1 - 10^{-\epsilon lc_1}}. \quad 3.6$$

The transmittance T_1 prior to the photobleaching process is:

$$T_1 = 10^{-\epsilon lc_1}, \quad 3.7$$

which can be measured with the same confocal laser scanning microscope that is used for the rFRAP experiments. Eq. 3.7 can be substituted into Eq. 3.6 to give the following:

$$F_N = \frac{1 - 10^{-\epsilon lc_2}}{1 - T_1}. \quad 3.8$$

Equation 3.8 can be solved for c_2 , which gives:

$$c_2 = -\frac{1}{\epsilon l} \cdot [\log(1 - F_N(1 - T_1))]. \quad 3.9$$

Since the factor ϵl is not a measured quantity and stays constant, it can be expressed in terms of the pre-bleached concentration, c_1 , using Eq.3.7:

$$\epsilon l = -\frac{c_1}{\log(T_1)}, \quad 3.10$$

Substituting Eq. 3.10 into Eq. 3.9 gives the following equation, where $c_N = \frac{c_2}{c_1}$ is the concentration after photobleaching normalized to the pre-photobleaching concentration:

$$c_N = \frac{\log[1 - (1 - T_1) \cdot F_N]}{\log(T_1)}. \quad 3.11$$

T_1 was measured using the same confocal microscope used for the rFRAP experiments and then the fluorescence intensity profile in the rFRAP experiments was transformed to normalized concentrations using Eq. 3.11 and the measured T_1 . The normalized concentrations were then used when calculating diffusion coefficients.

Similar to the diffusion coefficients of R6G in sucrose water solutions, the corrected and uncorrected diffusion coefficients of the fluorescent organic molecule in brown limonene SOM do not show significant differences (the difference was within the uncertainties of the measurements). Nevertheless, for completeness the corrected values were used in the following sections.

3.3 Results and Discussion

3.3.1 Diffusion Coefficients of Intrinsic Fluorophores within Brown Limonene SOM

Error! Reference source not found. shows the diffusion coefficients of intrinsic fluorophores in brown limonene SOM as a function of water activity.

The diffusion coefficients ranged from $8.32 \cdot 10^{-9} \text{ cm}^2/\text{s}$ to $3.82 \times 10^{-12} \text{ cm}^2/\text{s}$ as the water activity decreased from 0.9 to 0.38. The decrease in diffusion coefficients (3.5 orders of magnitude) as the water activity decreased was expected, since brown limonene SOM is hygroscopic and water is a plasticizer.⁶³

Also included in **Error! Reference source not found.** are estimates of diffusion coefficients based on measured viscosities of brown limonene SOM²³, the Stokes-Einstein relation and an assumed hydrodynamic radius of 7.34 Å for the intrinsic fluorophores (see next chapter). Although the two datasets do not overlap in terms of water activity, if diffusion coefficients are extrapolated to $a_w=0.3$ using a linear fit, good agreement is observed between the two data sets at this water activity. This suggests that the Stokes-Einstein predicted diffusion coefficients are consistent with the measured diffusion coefficients at values of $1.50 \cdot 10^{-14}$ cm²/s, which is consistent with the results in the previous chapter.

Often it is assumed in chemical transport models when predicting the formation of SOM particles that the mixing time of organics by molecular diffusion within SOM particles is <1 hour. To determine the validity of this assumption, mixing times of organic molecules by molecular diffusion within SOM particles were calculated in **Error! Reference source not found.** using the measured diffusion coefficients and the following equation:^{15f}

$$\tau_{mixing} = \frac{D_p^2}{4\pi^2 D}, \quad 3.12$$

where D_p is the diameter of the atmospheric particle and D the measured diffusion coefficient. For the calculation of the mixing time, a diameter of the atmospheric particle of 200 nm was assumed. The mixing time is the time, after which the concentration of the diffusing molecule in the atmospheric particle deviates by 1/e from the equilibrium concentration.⁸

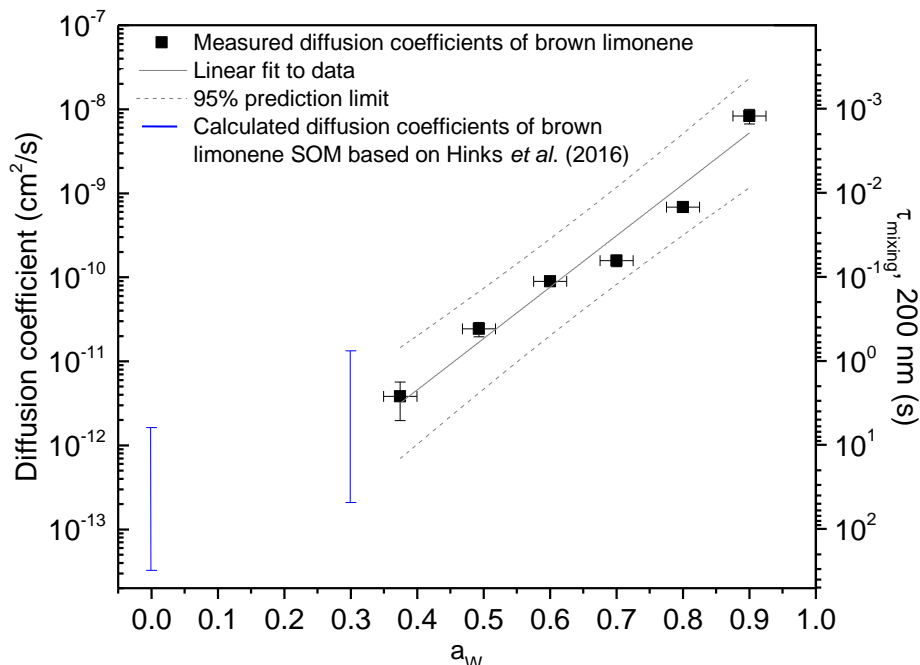


Figure 3.6: Diffusion coefficients of intrinsic fluorophores in brown Limonene SOM (black squares). The y-error bars were calculated from the 95% confidence limit. The grey solid line is a linear fit to the data and the grey dotted line the 95% prediction limit of the fit. The blue vertical bar depicts the highest and the lowest limit of calculated diffusion coefficients of brown limonene SOM (reacted with NH_3) based on viscosity measurements from Hinks *et al.* (2016). The secondary y-axis shows the mixing time, which is the time that would be needed for intrinsic fluorophores to mix within a 200 nm brown limonene particle.

Shown in **Error! Reference source not found.** are mixing times (secondary y-axis) calculated using Eq. 3.12. Mixing times ranged from 0.001 to 2.6s across water activities of 0.9 and 0.38. These small values illustrate that mixing times of large organics within brown limonene SOM are short ($\ll 1\text{hr}$) for most of the relative humidities found in the atmosphere. Hence the assumption of well mixed SOM particles in chemical transport models within 1 hr seems appropriate for brown limonene SOM. The results in this study apply to large organic molecules, since the fluorescent organic molecules studied here likely have molecular weights in the range of

285 up to 777 g/mol based on the mass spectrometry results and the mechanism proposed by Nguyen *et al.* (2013) for intrinsic fluorophores in brown limonene SOM particles.⁵⁸ For comparison some of the most abundant molecules identified in limonene SOM particles are limononaldehyde and ketolimononaldehyde, which have molecular weights of 168.23 and 170.20 g/mol, respectively.⁶⁴

Chapter 4: The Hydrodynamic Radius of Intrinsic Fluorophores in Brown Limonene SOM

4.1 Introduction

Brown limonene SOM is formed from the reaction of limonene with ozone followed by aging with ammonia gas. Brown limonene SOM absorbs in the near UV (300-400 nm) and the visible range and emits fluorescence over the range of 400 to 550 nm.⁶⁵

Nguyen *et al.* (2013) studied ketolimononaldehyde, which is a second-generation ozonolysis product of limonene.⁵⁸ The group reacted ketolimononaldehyde with ammonia and looked at the absorbance at wavelengths between 300 and 600 nm as well as performed an ESI/HRMS on the obtained products. The majority of products, that were detected, were monomers (C₉), dimers (C₁₈), trimers (C₂₇) and tetramers (C₃₆) of ketolimononaldehyde. The products shown in Figure 3.1 were chosen as examples for potentially light absorbing compounds and possible intrinsic fluorophores in brown limonene SOM because of their high double bond equivalencies (DBE; C₁₈H₂₀O₃ = DBE 9, C₁₈H₂₀N₂O₂ = DBE 10, C₁₈H₂₃NO₃ = DBE 8).⁵⁸

Another study on composition of light absorbing compounds and intrinsic fluorophores in brown limonene SOM was performed by Bones *et al.* (2010).⁵⁵ This study found that the absorbing species in SOM are minor components of SOM which show a maximum mass-to-charge ratio of 800. However, the definite structures of the light absorbing compounds and intrinsic fluorophores in brown limonene SOM have not been solved to date.

The goal of the current chapter is to determine the average radius of the intrinsic fluorophores in brown limonene SOM. This information provides additional constraints on the

mechanism for forming these molecules, which is needed for predicting the formation of brown limonene SOM in the atmosphere. To determine the average radius of the intrinsic fluorophores the diffusion rates of R6G in brown limonene SOM were measured and compared to the diffusion rates of the intrinsic fluorophores within brown limonene SOM. Since the radius of R6G is known, the radius of the intrinsic fluorophores can be calculated using the relative diffusion rates and the Stokes-Einstein equation. Experiments were carried out at water activities of 0.7, 0.8 and 0.9. At these water activities, diffusion rates are fast and since the fluorescent organic molecules studied in this work are large, the Stokes-Einstein equation should be applicable.

4.2 Experimental

4.2.1 Preparation of Brown Limonene SOM Samples at Water Activities of 0.7, 0.8 and 0.9

Brown limonene SOM was generated in a 20L flow tube by dark ozonolysis of limonene by M. Hinks at UC Irvine, California, USA according to section 3.2.1. Brown limonene SOM was received on a glass slide (Hampton Research) from which droplets were transferred to a second glass slide using the tip of a needle (BD Precision Glide™ Needle, 0.9 mm x 40 mm). The brown limonene SOM droplets were conditioned at the desired water activity using the setup described in section 2.2.1. To calculate conditioning times, it was again assumed that the diffusion rate of water within brown limonene SOM was equal to the diffusion rate of water in sucrose-water mixtures at the same water activity as explained in section 3.2.2.

4.2.2 Introduction of R6G into Brown Limonene SOM Samples

For the introduction of the R6G dye into brown limonene SOM droplets, the following procedure was used:

First, R6G was dissolved in acetone to give a saturated solution (0.022 g R6G in 50 mL acetone). The solution was then nebulized onto a glass slide (Hampton Research) (Figure 4.1, panel a). In order to ensure an even distribution of R6G, the glass slide was moved in a circular motion through the stream of nebulized acetone/R6G. In the next step, R6G was removed using acetone from half of the glass slide (Figure 4.1, panel b). For the introduction of R6G, the glass slide with the R6G was placed carefully on top of the glass slide with the six brown limonene SOM droplets (Figure 4.1, panel c) and the two slides were sandwiched together forming six thin films of brown limonene SOM, three films with R6G introduced and three films without R6G (Figure 4.1, panel D). The three films without R6G were used to subtract the fluorescence intensity of the intrinsic fluorophores from fluorescence intensity of the samples containing R6G as well as to measure the diffusion coefficients of the intrinsic fluorophores. See below for further details.

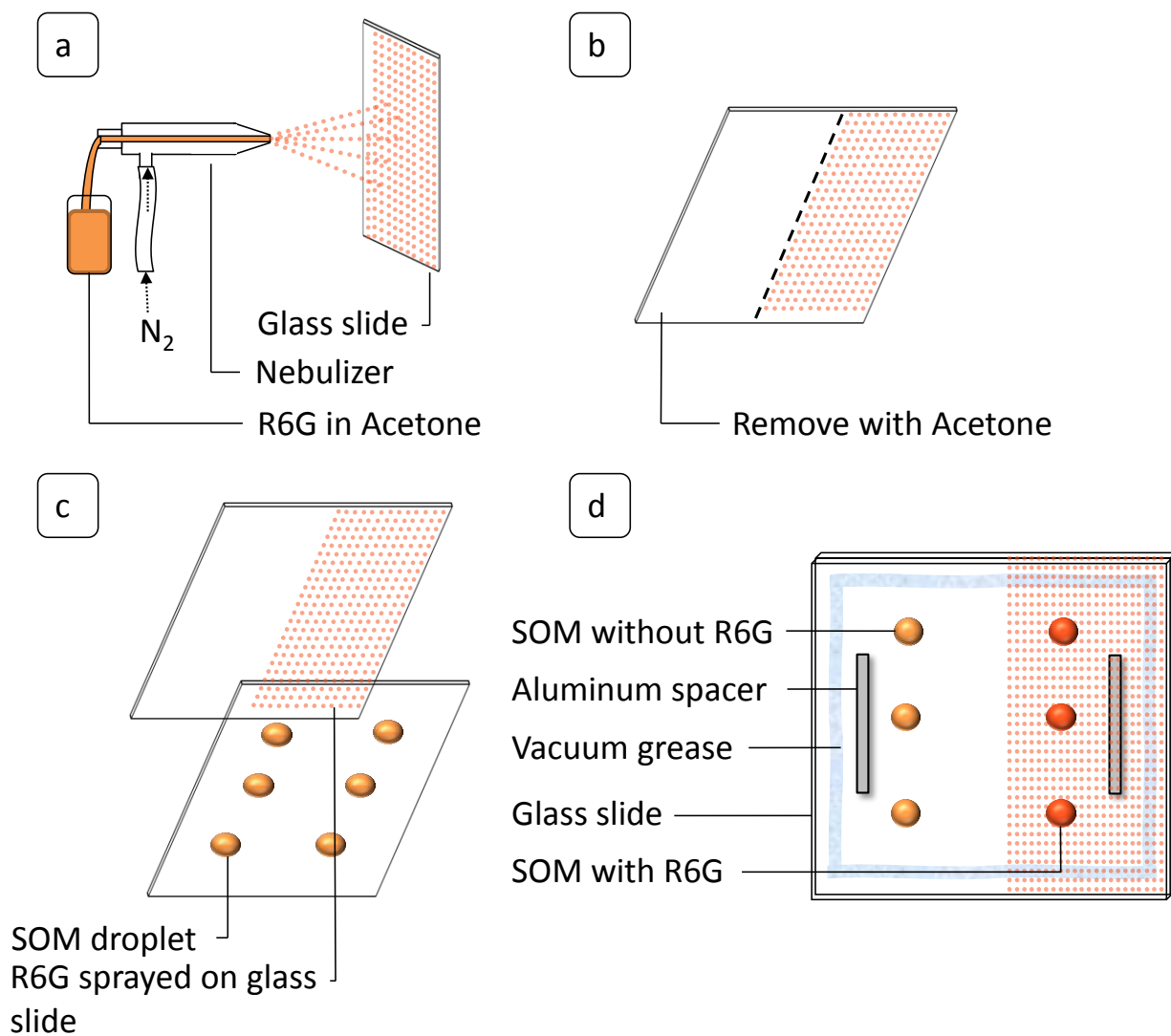


Figure 4.1: Schematic illustrating the introduction of R6G into pure brown limonene SOM particles. First, the dye is nebulized onto a glass slide (panel a). Then, the dye is removed from half of the glass slide (panel b). The nebulized glass slide containing R6G is placed on top of a glass slide containing brown limonene SOM droplets and the two glass slides are sandwiched together (panel c). The resulting sample has both SOM films with R6G and without R6G (panel d).

4.2.3 rFRAP Experiments: Measurements of Diffusion Coefficients of R6G and the Intrinsic Fluorophores in Brown Limonene SOM

Diffusion coefficients of R6G and the intrinsic fluorophores in brown limonene SOM were determined using rFRAP. The three films without R6G added were used to determine the diffusion coefficients of the intrinsic fluorophores. The three films with R6G added were used to determine the diffusion coefficients of R6G. Although the diffusion coefficients of the intrinsic fluorophores were determined in the previous chapter, they were measured again here to ensure consistent preparation between the two types of films to eliminate uncertainties when determining the hydrodynamic radius of the intrinsic fluorophores.

For photobleaching all the thin films containing R6G, a laser power of 330 μW was used and for scanning 4.08 μW or 6.29 μW were used. For photobleaching the thin films containing only the intrinsic fluorophores, a laser power of 170.5 μW was used and for scanning a laser power of 21.3 μW was used. The geometry chosen for the experiments was a rectangle with varying length (x) and width (y). The sizes of the rectangles were chosen depending on the diffusion times with smaller areas for longer diffusion times. The image sizes in relation to the bleach size were chosen such that the diffusing front remained within the monitored area. For samples at $a_w=0.9$ areas of 36 μm by 36 μm and 20 by 20 μm and image sizes of 199.61 μm by 199.61 μm were chosen. For samples conditioned to $a_w=0.8$, areas of 20 by 20 μm and 10x10 μm and image sizes of 99.8 μm by 99.8 μm were used and for $a_w=0.7$ bleach areas of 10x10 μm and image sizes of 99.8 μm by 99.8 μm were used.

A minimum of three samples was prepared for each a_w and three measurements per sample were obtained. The three values of the diffusion coefficients for R6G, which were extracted for one sample, were averaged.

4.2.4 Analysis of rFRAP Images Recorded for the Samples Containing R6G

The brown limonene SOM samples containing R6G contained two types of fluorophores (R6G and the intrinsic fluorophores). To determine only the diffusion coefficient of the R6G, the rFRAP methodology had to be modified from previous chapters.

As illustrated in Figure 4.2, images corresponding to films containing only the intrinsic fluorophores were subtracted from images corresponding to films containing R6G and the intrinsic fluorophores prior to extracting diffusion coefficients for R6G. The subtraction was performed for all images prior to normalizing and downsizing. At a laser power of $4.08 \mu\text{W}$ the fluorescence intensity of the intrinsic fluorophores was relatively low (Figure 4.2, panel b). Hence, the subtraction process did not strongly affect the intensity profile as shown panel c in Figure 4.2. After the subtraction the new intensity profile was analyzed according to section 2.3.2.

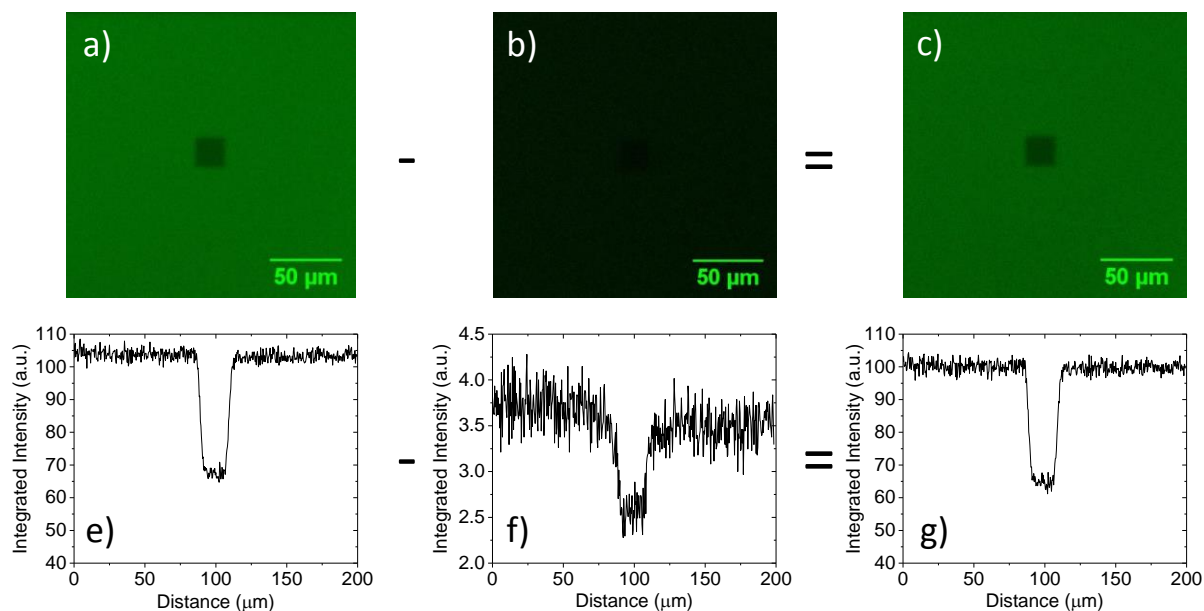


Figure 4.2: Schematic illustrating the subtraction of fluorescence intensities of images of pure brown limonene SOM from images of brown limonene SOM films containing R6G. Panel a) shows the image of a fluorescent film consisting of R6G in brown limonene SOM at $t=0$ s, panel b) shows the image of a fluorescent film consisting of pure brown limonene SOM and panel c) shows an image that was produced by subtracting the fluorescent intensity of pure brown limonene SOM from the fluorescence intensity of a brown limonene SOM film containing R6G. Panels e) to g) show the corresponding profiles to the images of panels a) to c).

In order to determine if the subtraction had a large effect on the calculated diffusion coefficients, diffusion coefficients were calculated using images that have been subtracted and ones that have not been subtracted. The difference in diffusion coefficients between the two cases ranged from 2 to 57%, which is within the uncertainty of our measurements. Nevertheless, for completeness, in the results section only the results from images that had the fluorescence from the intrinsic fluorophores subtracted were reported.

4.2.5 Correction for Reversible Photobleaching

In Chapter 2.3.5, it was shown that reversible photobleaching occurs for R6G in sucrose within the first 50s after photobleaching. For the brown limonene SOM experiments, diffusion coefficients were determined using two methods: using all data collected after photobleaching and using only data recorded 50s after photobleaching. The difference in diffusion coefficients determined using both techniques ranged from 1 to 11%, which is within the uncertainty of the measurements. In the results section, we only include data recorded 50s after photobleaching to ensure reversible photobleaching was not an issue in our experiments.

4.2.6 Corrections for Non-linearity of Fluorescence Intensity as a Function of Concentration of R6G

The concentration of R6G in brown limonene SOM was estimated from the fluorescence intensity of those films. Since brown limonene SOM are a complex mixture of various chemical compounds, the fluorescence intensity behaviour of R6G in three different media, which might be used to approximate the fluorescence behaviour of R6G in SOM, was studied. The media chosen were water, sucrose water solution (50 wt %) and citric acid water solution (55 wt %).

Figure 4.3 shows a plot of the integrated fluorescence intensity as a function of concentration for these three different media. The fluorescence intensity varies significantly with the type of media. R6G shows the highest fluorescence intensity in citric acid water solution probably related to the pH. Using the 4th order polynomial fits depicted in Figure 4.4 and the fluorescence intensities of R6G in brown limonene SOM films, the concentrations of R6G in brown

limonene SOM were estimated. The concentrations varied between a minimum of 0.084 mM, using a calculation based on the values for citric acid, or 0.080 mM, when calculated for sucrose, up to 0.543 mM, calculated for citric acid, or 1.165 mM, when calculated for sucrose (Appendix C). However, most concentrations were between 0.1 and 0.3 mM, which is within the linear region for the fluorescence intensity. Thus, it was possible to use the fluorescence intensity data without any further corrections.

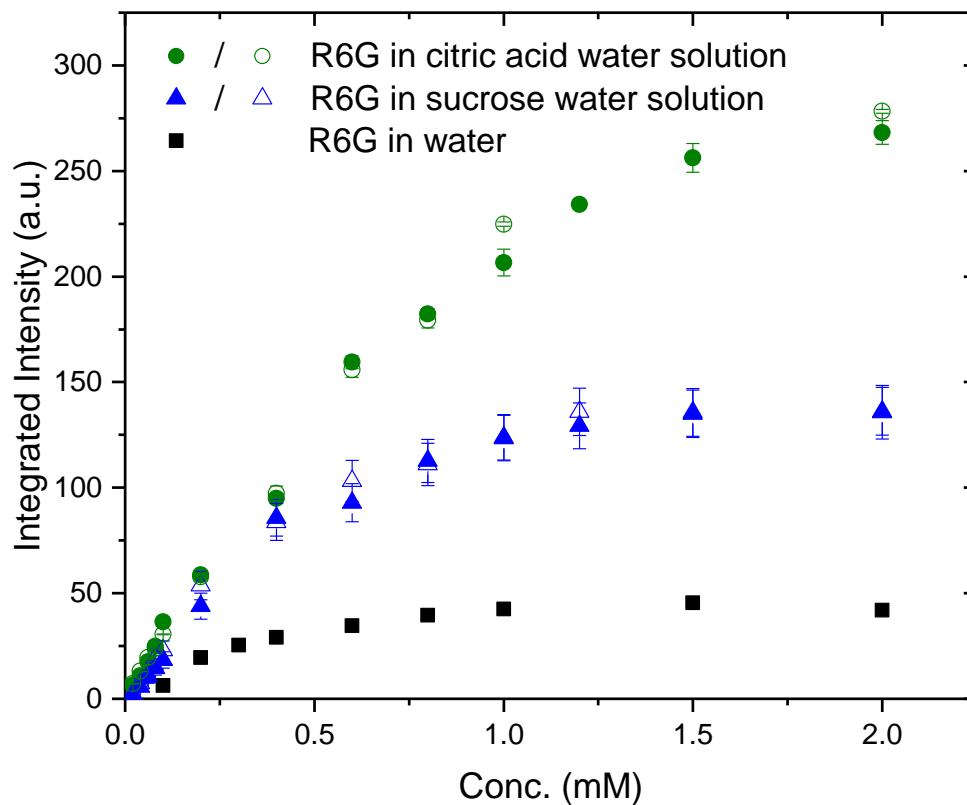


Figure 4.3: Integrated intensity as a function of the concentration of R6G in various media: citric acid in water (55 wt %), sucrose in water (50 wt %) and pure water. Experiments were carried out with a laser power of 4.08 μ W. The open and solid symbols depict measurements performed on two different days to confirm reproducibility of the measurements. For citric acid and sucrose water solutions measurements were performed on two different days and for R6G in water only one measurement was performed. The error bars represent one standard deviation (1σ) obtained from three different measurements.

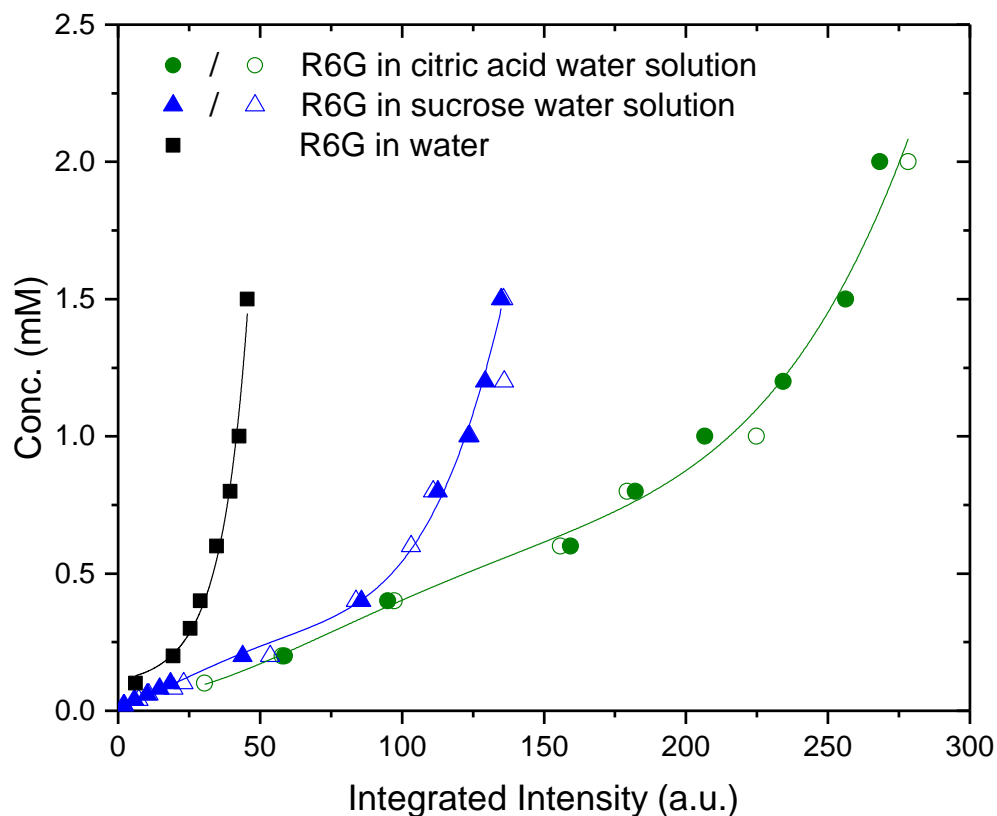


Figure 4.4: Concentration of R6G (mM) as a function of integrated intensity in various media, citric acid in water (55 wt %), sucrose in water (50 wt %) and pure water. The solid lines are plots describing the trend of the data. The open and the solid symbols depict measurements performed on two different days to confirm reproducibility of the measurements. This plot is based on the data from Figure 4.3.

Table 4.1: Parameterization of the data shown in Figure 4.4.

Medium	Function
Citric acid in water (Green circles)	$f(x) = (4.52 \cdot 10^{-2}) - (3.65 \cdot 10^{-4}) \cdot x + (8.24 \cdot 10^{-5}) \cdot x^2$ $- (-5.61 \cdot 10^{-7}) \cdot x^3 + (1.31 \cdot 10^{-9}) \cdot x^4$
Sucrose in water (blue triangles)	$f(x) = (2.13 \cdot 10^{-2}) + (2.60 \cdot 10^{-2}) \cdot x + (1.06 \cdot 10^{-4}) \cdot x^2$ $- (2.10 \cdot 10^{-6}) \cdot x^3 + (1.31 \cdot 10^{-8}) \cdot x^4$
Water (black rectangles)	$f(x) = \exp(-2.17 + (1.17 \cdot 10^{-2}) \cdot x + 9.66 \cdot x^2)$

4.3 Results and discussion

4.3.1 Example of Experimental Data

In Figure 4.5, fluorescence intensity (integrated over the bleach width in the y-direction) as a function of x-position is shown for water activities of 0.7, 0.8 and 0.9. The red line represents a fit to the data using Eq. 2.8. Figure 4.5 illustrates that Eq. 2.8 fits well to the experimental data. Figure 4.8 shows examples of plots of $w(D,t,r)$ as a function of time, which are extracted from plots such as Figure 4.5. Figure 4.6 illustrates that plots of $w(D,t,r)$ as a function of t , are described well by a linear function, as expected.

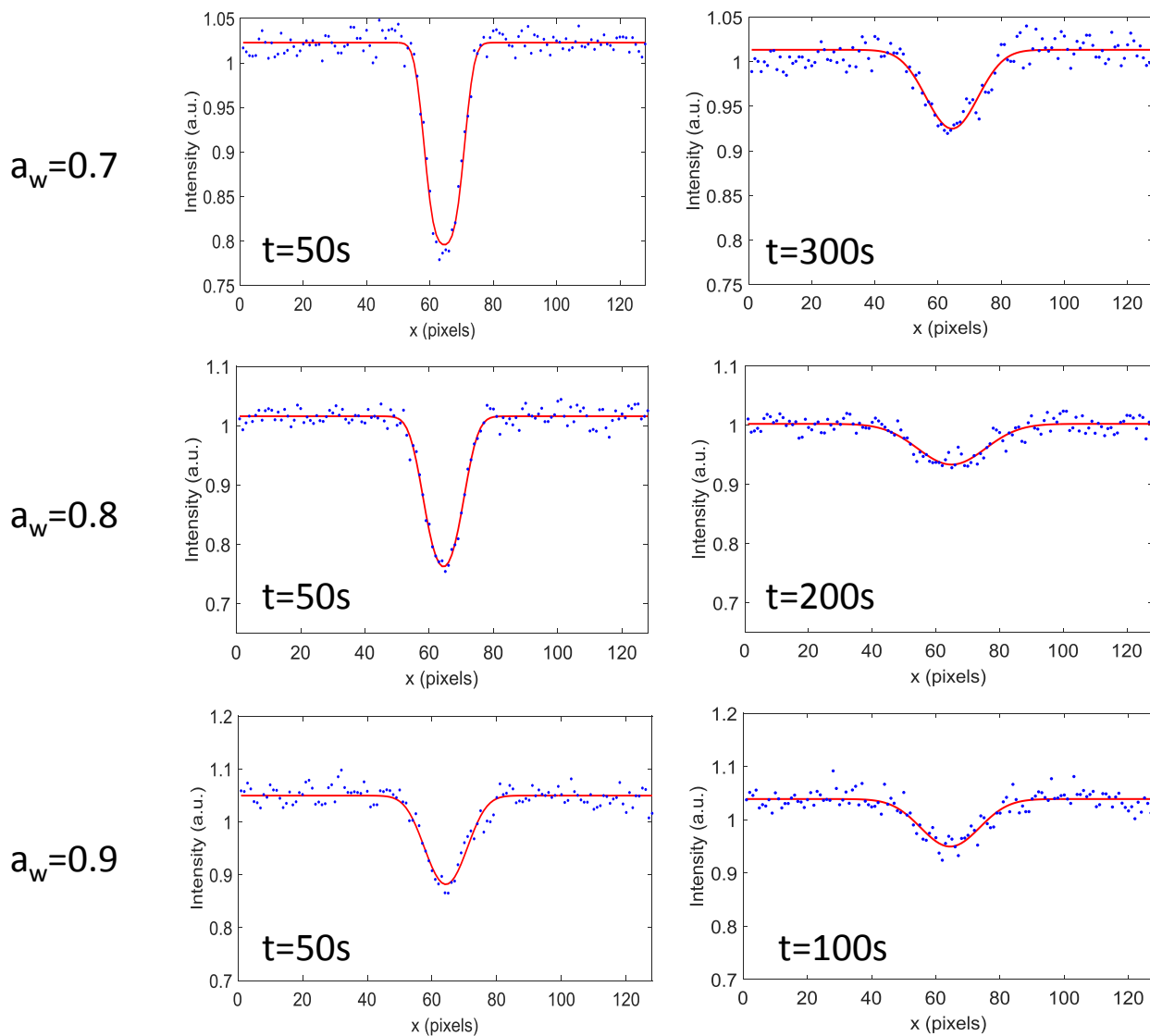
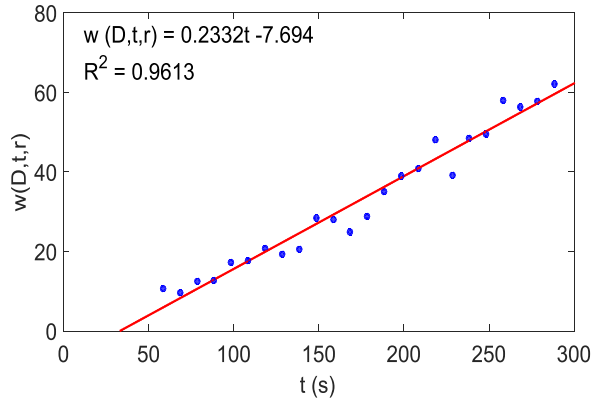
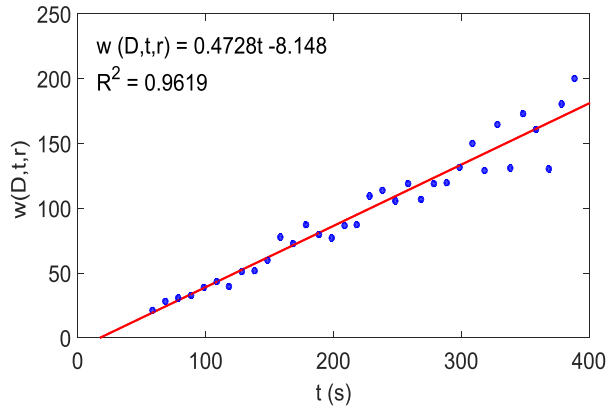


Figure 4.5: Fluorescence intensities as a function of distance in the x direction (in pixels) for selected films of R6G in brown limonene SOM at $a_w = 0.7, 0.8$ and 0.9 . The blue dots represent the intensity data and the red curve is a fit to the data using Eq. 2.8. Before the fit was applied, the fluorescence intensity data was normalized to an image taken prior to photobleaching.

$a_w=0.7$



$a_w=0.8$



$a_w=0.9$

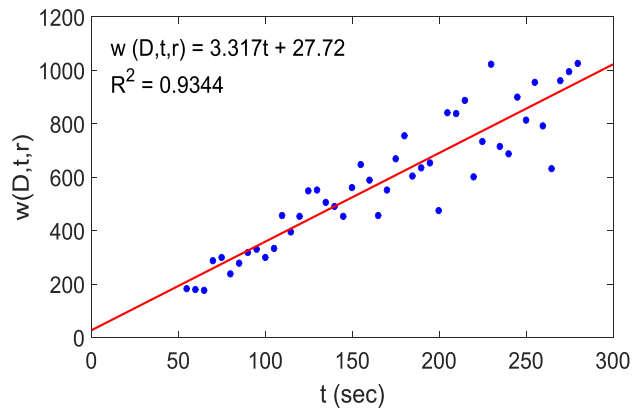


Figure 4.6: Plot of $w(D, t, r) = r^2 + 4Dt$ as a function of time. The blue open circles represent experimental data, which was obtained from figures such as those in Figure 4.5. The red line is a linear fit to the data. The diffusion coefficients were obtained from the slopes and are. The diffusion coefficients are $D = 0.0583 \mu\text{m}^2/\text{s} = 5.83 \cdot 10^{-10} \text{cm}^2/\text{s}$, $0.1182 \mu\text{m}^2/\text{s} = 1.18 \cdot 10^{-9} \text{cm}^2/\text{s}$ and $0.8292 \mu\text{m}^2/\text{s} = 8.29 \cdot 10^{-9} \text{cm}^2/\text{s}$ for $a_w = 0.7, 0.8$ and 0.9 , respectively.

4.3.2 Measured Diffusion Coefficients of the Intrinsic Fluorophores in Brown Limonene

SOM

Shown in Figure 4.7 are the diffusion coefficients of the intrinsic fluorophores in brown limonene SOM determined from work related to this chapter and compared with the diffusion coefficients of the intrinsic fluorophores measure independently in chapter 3. At water activities of 0.7 and 0.8, the measurements agree within the uncertainties of the measurements. At a water activity of 0.9, the measurements determined in this chapter are on average a factor of 3 higher than the values determined in the previous chapter. The difference between the two measurements may be related to the uncertainties in the water activities (± 0.025) as well as small differences in the composition of the SOM from batch to batch, although the latter seems unlikely since good agreement is observed at water activities of 0.7 and 0.8.

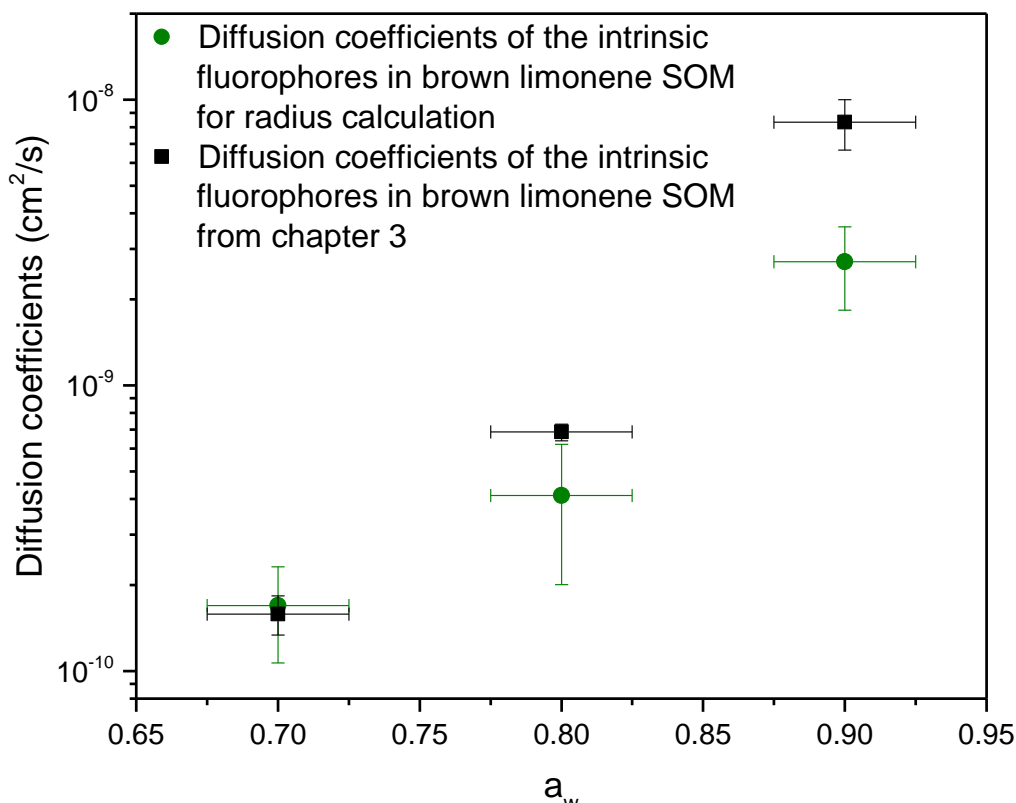


Figure 4.7: Comparison of diffusion coefficients of the intrinsic fluorophores in brown limonene SOM measured for this chapter (to determine the hydrodynamic radius of the intrinsic fluorophores (green rectangles)) with diffusion coefficients of the intrinsic fluorophores measured in Chapter 3: (black rectangles). The symbols are average values and the error bars depict the 95% confidence limit.

4.3.3 Measured Diffusion Coefficients of R6G in Brown Limonene SOM

Figure 4.8 shows the diffusion coefficients of R6G in brown limonene SOM in comparison to the diffusion coefficients of the intrinsic fluorophores in brown limonene SOM measured at identical water activities and in an identical same matrix. The diffusion coefficients of R6G in brown limonene SOM are on average smaller than the diffusion coefficients of the intrinsic fluorophores. This leads to the conclusion that the average radius of the intrinsic fluorophores must be larger than the hydrodynamic radius of R6G.

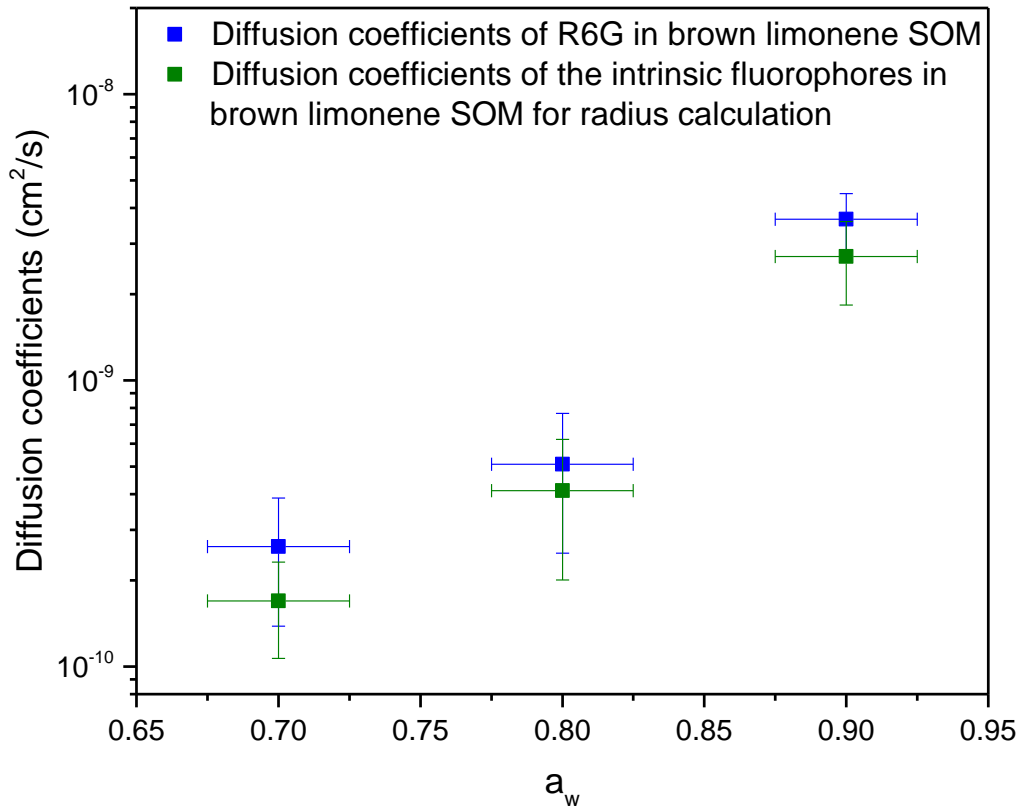


Figure 4.8: Comparison of diffusion coefficients of R6G in brown limonene SOM (blue rectangles) with diffusion coefficients of the intrinsic fluorophores in brown limonene SOM (green rectangles) determined in this chapter for the radius calculations. The symbols are the average values and the error bars give the 95% confidence limit.

4.3.4 Calculation of the Hydrodynamic Radius of Intrinsic Fluorophores in Brown Limonene SOM

For the calculation of the hydrodynamic radius of the intrinsic fluorophores in brown limonene SOM, the ratio of the diffusion coefficient of R6G in brown limonene SOM ($D(R6G)$) to the diffusion coefficient of intrinsic fluorophores in brown limonene ($D(SOM)$) was calculated for each activity. Table 4.2 shows the average ratio as well as the 95% confidence interval at the three different water activities. The ratio at each water activity agrees within the uncertainty of

the measurements (95% confidence interval), indicating that the ratio is not a strong function of the water activity.

Using the average value of the ratio for all water activities of 1.25 and a hydrodynamic radius of R6G of 5.89 Å (Müller *et al.*²⁴), the average hydrodynamic radius of the intrinsic fluorophores diffusing in brown limonene SOM equals (7.34 ±1.47) Å. The uncertainty in the number was calculated using 95% confidence limit of the average value for all water activities (Table 4.2).

Table 4.2: Average and 95 % confidence intervals of the diffusion coefficients of R6G (D(R6G)) to the diffusion coefficient of the intrinsic fluorophores(D(SOM)) in brown limonene SOM at three different water activities.

a_w	Average D(R6G)/D(SOM)	95 % confidence interval
0.9	1.37	±0.13
0.8	1.09	±0.30
0.7	1.28	±0.32
Average	1.25	±0.25

4.3.5 Comparison with Previous Suggestions of the Molecular Structures and Formulas for the Light Absorbing Compounds and Intrinsic Fluorophores in Brown Limonene SOM

As discussed in the introduction of this chapter, Nguyen *et al.* (2013) suggested the following molecular formulas for the light absorbing compounds and intrinsic fluorophores in brown limonene SOM: $C_{18}H_{20}O_3$, $C_{18}H_{20}N_2O_2$, and $C_{18}H_{23}NO_3$.⁵⁸ Here, the focus lies on the dimers suggested by Nguyen *et al.* (2013), since the structures of these molecules were provided by Nguyen *et al.* (2013). The structures of these molecules are shown in Figure 3.1. To calculate a lower limit

to the hydrodynamic radii of these molecules, a spherical geometry was assumed and a density of 1.3 g/cm^3 .⁶⁶ With these assumptions hydrodynamic radii of 4.51 Å, 4.48 Å and 4.42 Å, respectively, were calculated. To calculate an upper limit of the hydrodynamic radii for these molecules, the Van-der-Waals radii (using the molecular structures together with the bond angles and bond lengths) were calculated and it was assumed that the molecules diffused perpendicular to the plane containing the carbon backbone of the molecule. With these assumptions hydrodynamic radii of 6.3 Å, 7.6 Å and 5.5 Å, respectively, were obtained. These upper limits are consistent with the measured hydrodynamic radius. Hence, the molecules suggested by Nguyen *et al.* (2013) are consistent with the measured hydrodynamic radii of the intrinsic fluorophores studied here.⁵⁸

Chapter 5: Conclusion and Future Work

5.1 Measurement of Diffusion Coefficients in Proxies of Atmospheric Particles

In chapter 2 diffusion coefficients of R6G in sucrose water solutions were measured at water activities ranging from 0.38 to 0.8 using rFRAP. In chapter 3, diffusion coefficients of intrinsic fluorophores in brown limonene SOM were measured at water activities ranging from 0.38 to 0.9 using rFRAP. The range of diffusion coefficients measured is listed in Table 5.1.

For R6G in sucrose water solutions, a breakdown of the Stokes-Einstein equation was observed at water activities of 0.38 (3.3×10^6 Pa s and a T_g/T of 0.94) with a deviation from the measured diffusion coefficients by a factor of 2 to 50.

In chapter 3, diffusion coefficients of the intrinsic fluorophores in brown limonene SOM were measured for the first time. A dependence of diffusion coefficients on water activity was observed and mixing times were calculated based on the measured diffusion coefficients. Since the mixing times even at water activities as low as 0.38 did not exceed 2.6s, rapid mixing within brown limonene SOM can be assumed in atmospheric models.

These research findings will lead to improved models of air quality and climate.

Table 5.1: Diffusion coefficients of R6G in sucrose-water solutions and the intrinsic fluorophores in brown limonene SOM.

Fluorescent dye	Tested medium	Diffusion coefficient, $a_{w,high}$ (cm ² /s)	Diffusion coefficient, $a_{w,low}$ (cm ² /s)
Rhodamine 6G (R6G)	Sucrose-Water	$4.75 \cdot 10^{-9}$ at $a_w=0.8$	$1.5 \cdot 10^{-14}$ at $a_w=0.38$
Intrinsic fluorophores in brown limonene SOM	brown limonene SOM	$8.32 \cdot 10^{-9}$ at $a_w=0.9$	$3.82 \cdot 10^{-12}$ at $a_w=0.38$

5.2 Average Hydrodynamic Radius of the Intrinsic Fluorophores in Brown Limonene SOM

Chapter 4 focuses on the calculation of the average hydrodynamic radius of intrinsic fluorophores in brown limonene SOM. This was achieved by measuring the diffusion coefficients of R6G within brown limonene SOM and measuring the diffusion coefficients of the intrinsic fluorophores within brown limonene SOM at three different water activities, 0.7, 0.8 and 0.9. Assuming the Stokes-Einstein equation is valid under these conditions (high water activities and low viscosities) the hydrodynamic radius could be calculated using the known hydrodynamic radius of R6G. The average hydrodynamic radius of the intrinsic fluorophores was found to be 7.34 ± 1.47 Å.

5.3 Consideration of Future Work

In order to be able to calculate diffusion coefficients accurately from viscosities, even outside the validity range of the Stokes-Einstein equation more data would be needed at lower water activities ($a_w < 0.38$). Correction factors could be calculated for water activities where the Stokes-Einstein equation breaks down.

Since the ratio of the radius of the diffusing molecule in comparison to the matrix molecules is an important factor that determines when the Stokes-Einstein equation breaks down, measurements of diffusing molecules of sizes between $1.4 \text{ Å} < R_H < 5.02 \text{ Å}$ (a ratio of $R_{\text{diffusing}}/R_{\text{matrix}}$ between $1 < R_{\text{diffusing}}/R_{\text{matrix}} < 3.6$) and sizes between $7.4 \text{ Å} < R_H < 83.1 \text{ Å}$ (a ratio of $R_{\text{diffusing}}/R_{\text{matrix}}$ between $5.2 < R_{\text{diffusing}}/R_{\text{matrix}} < 60$) in sucrose-water solutions should be studied. This would cover size ranges that have not been studied in this work and would give a better picture

of the breakdown of the Stokes-Einstein equation. In this work, diffusing molecules of smaller radii have not been studied because of limitations in excitation wavelengths available for the study.

Another factor, important in the atmosphere other than the water activity, is the temperature. Temperatures found in the troposphere go down as low as -56°C (217 K).² The study presented in this work was performed at room temperature; however, a study of the change of the diffusion coefficients as a function of temperature at varying water activities would give insight into the temperature dependence of mixing times and reaction rates within and reaction rates of atmospheric particles. These studies could be done for sucrose water solutions and brown limonene SOM particles.

Because the composition of atmospheric particles is highly variable and subject to constant change, a study using different matrices with different functional groups would improve the understanding of diffusion in, for instance, polar media and media with different pHs.

Bibliography

1. Curtius, J. In *Nucleation of atmospheric particles*, EPJ Web of Conferences, EDP Sciences: 2009; pp 199-209.
2. Seinfeld, J. H.; Pandis, S. N., *Atmospheric chemistry and physics: from air pollution to climate change*. John Wiley & Sons: 2016.
3. Pöschl, U., Atmospheric Aerosols: Composition, Transformation, Climate and Health Effects. *Angewandte Chemie International Edition* 2005, *44* (46), 7520-7540.
4. (a) Tie, X.; Wu, D.; Brasseur, G., Lung cancer mortality and exposure to atmospheric aerosol particles in Guangzhou, China. *Atmospheric Environment* 2009, *43* (14), 2375-2377;(b) Donaldson, K.; Brown, D.; Clouter, A.; Duffin, R.; MacNee, W.; Renwick, L.; Tran, L.; Stone, V., The pulmonary toxicology of ultrafine particles. *Journal of aerosol medicine* 2002, *15* (2), 213-220;(c) Salvi, S.; Blomberg, A.; Rudell, B.; Kelly, F.; Sandström, T.; Holgate, S. T.; Frew, A., Acute Inflammatory Responses in the Airways and Peripheral Blood After Short-Term Exposure to Diesel Exhaust in Healthy Human Volunteers. *American Journal of Respiratory and Critical Care Medicine* 1999, *159* (3), 702-709.
5. Darke, C.; Knowelden, J.; Lacey, J.; Ward, A. M., Respiratory disease of workers harvesting grain. *Thorax* 1976, *31* (3), 294-302.
6. Hauck, H.; Berner, A.; Frischer, T.; Gomiscek, B.; Kundi, M.; Neuberger, M.; Puxbaum, H.; Preining, O., AUPHEP—Austrian Project on Health Effects of Particulates—general overview. *Atmospheric Environment* 2004, *38* (24), 3905-3915.

7. Baltensperger, U.; Dommen, J.; Alfarra, M. R.; Duplissy, J.; Gaeggeler, K.; Metzger, A.; Facchini, M. C.; Decesari, S.; Finessi, E.; Reinnig, C., Combined determination of the chemical composition and of health effects of secondary organic aerosols: the POLYSOA project. *Journal of aerosol medicine and pulmonary drug delivery* 2008, 21 (1), 145-154.
8. Renbaum-Wolff, L.; Grayson, J. W.; Bateman, A. P.; Kuwata, M.; Sellier, M.; Murray, B. J.; Shilling, J. E.; Martin, S. T.; Bertram, A. K., Viscosity of α -pinene secondary organic material and implications for particle growth and reactivity. *Proceedings of the National Academy of Sciences* 2013, 110 (20), 8014-8019.
9. Houghton, J. T., L.G. Meira Filho, B.A. Callander, N. Harris, A. Kattenberg, and K. Maskell (eds.) *IPCC, 1996: Climate Change 1995: The Science of Climate Change. Contribution of Working Group I to the Second Assessment Report of the Intergovernmental Panel on Climate Change*; Cambridge, United Kingdom and New York, NY, USA, 1996; p 572.
10. Stocker, T. F., D. Qin, G.-K. Plattner, M. Tignor, S. K. Allen, J. Boschung, A. Nauels, Y. Xia, V. Bex and P.M. Midgley (eds.), *Climate Change 2013: The Physical Science Basis. Contribution of Working Group I to the Fifth Assessment Report of the Intergovernmental Panel on Climate Change*. Cambridge University Press: Cambridge, United Kingdom and New York, NY, USA, 2013. <http://www.ipcc.ch/>.
11. Brown, R., XXVII. A brief account of microscopical observations made in the months of June, July and August 1827, on the particles contained in the pollen of plants; and on the general existence of active molecules in organic and inorganic bodies. *Philosophical Magazine Series 2* 1828, 4 (21), 161-173.

12. Einstein, A., Über die von der molekularkinetischen Theorie der Wärme geforderte Bewegung von in ruhenden Flüssigkeiten suspendierten Teilchen. *Annalen der Physik* 1905, 322 (8), 549-560.
13. (a) Edward, J. T., Molecular volumes and the Stokes-Einstein equation. *Journal of Chemical Education* 1970, 47 (4), 261;(b) Levine, I. N., *Physical Chemistry*. Sixth Edition ed.; McGraw-Hill Education: New York, NY, 2008.
14. Solomon, S., D. Qin, M. Manning, Z. Chen, M. Marquis, K.B. Averyt, M. Tignor and; (eds.), H. L. M., *IPCC Fourth Assessment Report: Climate Change 2007: The Physical Science Basis: Contribution of Working Group I to the Fourth Assessment Report of the Intergovernmental Panel on Climate Change*. Cambridge University Press: Cambridge, United Kingdom and New York, NY, USA, 2007; p 996.
15. (a) Hallquist, M.; Wenger, J. C.; Baltensperger, U.; Rudich, Y.; Simpson, D.; Claeys, M.; Dommen, J.; Donahue, N. M.; George, C.; Goldstein, A. H.; Hamilton, J. F.; Herrmann, H.; Hoffmann, T.; Iinuma, Y.; Jang, M.; Jenkin, M. E.; Jimenez, J. L.; Kiendler-Scharr, A.; Maenhaut, W.; McFiggans, G.; Mentel, T. F.; Monod, A.; Prévôt, A. S. H.; Seinfeld, J. H.; Surratt, J. D.; Szmigielski, R.; Wildt, J., The formation, properties and impact of secondary organic aerosol: current and emerging issues. *Atmos. Chem. Phys.* 2009, 9 (14), 5155-5236;(b) Booth, A. M.; Murphy, B.; Riipinen, I.; Percival, C. J.; Topping, D. O., Connecting Bulk Viscosity Measurements to Kinetic Limitations on Attaining Equilibrium for a Model Aerosol Composition. *Environmental Science & Technology* 2014, 48 (16), 9298-9305;(c) Pajunoja, A.; Malila, J.; Hao, L.; Joutsensaari, J.; Lehtinen, K. E. J.; Virtanen,

- A., Estimating the Viscosity Range of SOA Particles Based on Their Coalescence Time. *Aerosol Science and Technology* 2014, 48 (2), i-iv;(d) Song, M.; Liu, P. F.; Hanna, S. J.; Li, Y. J.; Martin, S. T.; Bertram, A. K., Relative humidity-dependent viscosities of isoprene-derived secondary organic material and atmospheric implications for isoprene-dominant forests. *Atmos. Chem. Phys.* 2015, 15 (9), 5145-5159;(e) Power, R. M.; Simpson, S. H.; Reid, J. P.; Hudson, A. J., The transition from liquid to solid-like behaviour in ultrahigh viscosity aerosol particles. *Chemical Science* 2013, 4 (6), 2597-2604;(f) Shiraiwa, M.; Ammann, M.; Koop, T.; Pöschl, U., Gas uptake and chemical aging of semisolid organic aerosol particles. *Proceedings of the National Academy of Sciences* 2011, 108 (27), 11003-11008.
16. (a) Price, H. C.; Mattsson, J.; Zhang, Y.; Bertram, A. K.; Davies, J. F.; Grayson, J. W.; Martin, S. T.; O'Sullivan, D.; Reid, J. P.; Rickards, A. M., Water diffusion in atmospherically relevant α -pinene secondary organic material. *Chemical Science* 2015, 6 (8), 4876-4883;(b) Chenyakin, Y.; Ullmann, D. A.; Evoy, E.; Renbaum-Wolff, L.; Kamal, S.; Bertram, A. K., Diffusion coefficients of organic molecules in sucrose-water solutions and comparison with Stokes-Einstein predictions. *Atmos. Chem. Phys. Discuss.* 2016, 2016, 1-29;(c) Champion, D.; Hervet, H.; Blond, G.; Le Meste, M.; Simatos, D., Translational Diffusion in Sucrose Solutions in the Vicinity of Their Glass Transition Temperature. *The Journal of Physical Chemistry B* 1997, 101 (50), 10674-10679;(d) Corti, H. R.; Frank, G. A.; Marconi, M. C., An Alternate Solution of Fluorescence Recovery Kinetics after Spot-Bleaching for Measuring Diffusion Coefficients. 2. Diffusion of Fluorescein in Aqueous

- Sucrose Solutions. *Journal of Solution Chemistry* 2008, 37 (11), 1593-1608;(e) Longinotti, M. P.; Corti, H. R., Diffusion of ferrocene methanol in super-cooled aqueous solutions using cylindrical microelectrodes. *Electrochemistry Communications* 2007, 9 (7), 1444-1450.
17. (a) Hamed, A.; Korhonen, H.; Sihto, S. L.; Joutsensaari, J.; Järvinen, H.; Petäjä, T.; Arnold, F.; Nieminen, T.; Kulmala, M.; Smith, J. N., The role of relative humidity in continental new particle formation. *Journal of Geophysical Research: Atmospheres* 2011, 116 (D3);(b) and, I. M. H.; Soden, B. J., WATER VAPOR FEEDBACK AND GLOBAL WARMING. *Annual Review of Energy and the Environment* 2000, 25 (1), 441-475;(c) Martin, S. T., Phase Transitions of Aqueous Atmospheric Particles. *Chemical Reviews* 2000, 100 (9), 3403-3454.
18. Laskin, A.; Laskin, J.; Nizkorodov, S. A., Chemistry of Atmospheric Brown Carbon. *Chemical Reviews* 2015, 115 (10), 4335-4382.
19. (a) Kamens, R.; Jang, M.; Chien, C.-J.; Leach, K., Aerosol formation from the reaction of α -pinene and ozone using a gas-phase kinetics-aerosol partitioning model. *Environmental Science & Technology* 1999, 33 (9), 1430-1438;(b) Odum, J. R.; Yu, J.; Kamens, R. M., Modeling the mass transfer of semivolatile organics in combustion aerosols. *Environmental Science & Technology* 1994, 28 (13), 2278-2285;(c) Rounds, S. A.; Pankow, J. F., Application of a radial diffusion model to describe gas/particle sorption kinetics. *Environmental Science & Technology* 1990, 24 (9), 1378-1386;(d) Shiraiwa, M.; Zuend, A.; Bertram, A. K.; Seinfeld, J. H., Gas-particle partitioning of atmospheric

- aerosols: interplay of physical state, non-ideal mixing and morphology. *Physical Chemistry Chemical Physics* 2013, 15 (27), 11441-11453;(e) Shiraiwa, M.; Seinfeld, J. H., Equilibration timescale of atmospheric secondary organic aerosol partitioning. *Geophysical Research Letters* 2012, 39 (24), n/a-n/a.
20. Kanakidou, M.; Seinfeld, J. H.; Pandis, S. N.; Barnes, I.; Dentener, F. J.; Facchini, M. C.; Van Dingenen, R.; Ervens, B.; Nenes, A.; Nielsen, C. J.; Swietlicki, E.; Putaud, J. P.; Balkanski, Y.; Fuzzi, S.; Horth, J.; Moortgat, G. K.; Winterhalter, R.; Myhre, C. E. L.; Tsigaridis, K.; Vignati, E.; Stephanou, E. G.; Wilson, J., Organic aerosol and global climate modelling: a review. *Atmos. Chem. Phys.* 2005, 5 (4), 1053-1123.
21. Jang, M.; Ghio, A. J.; Cao, G., Exposure of BEAS-2B cells to secondary organic aerosol coated on magnetic nanoparticles. *Chemical research in toxicology* 2006, 19 (8), 1044-1050.
22. (a) Perraud, V.; Bruns, E. A.; Ezell, M. J.; Johnson, S. N.; Yu, Y.; Alexander, M. L.; Zelenyuk, A.; Imre, D.; Chang, W. L.; Dabdub, D.; Pankow, J. F.; Finlayson-Pitts, B. J., Nonequilibrium atmospheric secondary organic aerosol formation and growth. *Proceedings of the National Academy of Sciences* 2012, 109 (8), 2836-2841;(b) Riipinen, I.; Pierce, J.; Yli-Juuti, T.; Nieminen, T.; Hakkinen, S.; Ehn, M.; Junninen, H.; Lehtipalo, K.; Petaja, T.; Slowik, J., Organic condensation: a vital link connecting aerosol formation to cloud condensation nuclei (CCN) concentrations. *Atmospheric Chemistry and Physics* 2011, 11, 3865.

23. Hinks, M. L.; Brady, M. V.; Lignell, H.; Song, M.; Grayson, J. W.; Bertram, A. K.; Lin, P.; Laskin, A.; Laskin, J.; Nizkorodov, S. A., Effect of viscosity on photodegradation rates in complex secondary organic aerosol materials. *Physical Chemistry Chemical Physics* 2016, *18* (13), 8785-8793.
24. Müller, C. B.; Loman, A.; Pacheco, V.; Koberling, F.; Willbold, D.; Richtering, W.; Enderlein, J., Precise measurement of diffusion by multi-color dual-focus fluorescence correlation spectroscopy. *EPL (Europhysics Letters)* 2008, *83* (4), 46001.
25. Ribeiro, A. C. F.; Ortona, O.; Simões, S. M. N.; Santos, C. I. A. V.; Prazeres, P. M. R. A.; Valente, A. J. M.; Lobo, V. M. M.; Burrows, H. D., Binary Mutual Diffusion Coefficients of Aqueous Solutions of Sucrose, Lactose, Glucose, and Fructose in the Temperature Range from (298.15 to 328.15) K. *Journal of Chemical & Engineering Data* 2006, *51* (5), 1836-1840.
26. Grayson, J. W. Viscosity of secondary organic material and related atmospheric implications. University of British Columbia, 2016.
27. (a) Song, M.; Liu, P. F.; Hanna, S. J.; Zaveri, R. A.; Potter, K.; You, Y.; Martin, S. T.; Bertram, A. K., Relative humidity-dependent viscosity of secondary organic material from toluene photo-oxidation and possible implications for organic particulate matter over megacities. *Atmospheric Chemistry and Physics* 2016, *16* (14), 8817-8830;(b) Grayson, J. W.; Zhang, Y.; Mutzel, A.; Renbaum-Wolff, L.; Böge, O.; Kamal, S.; Herrmann, H.; Martin, S. T.; Bertram, A. K., Effect of varying experimental conditions on the

- viscosity of α -pinene derived secondary organic material. *Atmos. Chem. Phys.* 2016, *16* (10), 6027-6040.
28. (a) Bodsworth, A.; Zobrist, B.; Bertram, A. K., Inhibition of efflorescence in mixed organic-inorganic particles at temperatures less than 250 K. *Physical Chemistry Chemical Physics* 2010, *12* (38), 12259-12266;(b) Pant, A.; Fok, A.; Parsons, M. T.; Mak, J.; Bertram, A. K., Deliquescence and crystallization of ammonium sulfate-glutaric acid and sodium chloride-glutaric acid particles. *Geophysical Research Letters* 2004, *31* (12), n/a-n/a;(c) Pant, A.; Parsons, M. T.; Bertram, A. K., Crystallization of Aqueous Ammonium Sulfate Particles Internally Mixed with Soot and Kaolinite: Crystallization Relative Humidities and Nucleation Rates. *The Journal of Physical Chemistry A* 2006, *110* (28), 8701-8709;(d) Wheeler, M. J.; Bertram, A. K., Deposition nucleation on mineral dust particles: a case against classical nucleation theory with the assumption of a single contact angle. *Atmos. Chem. Phys.* 2012, *12* (2), 1189-1201.
29. Greenspan, L., Humidity fixed points of binary saturated aqueous solutions. *Journal of research of the national bureau of standards* 1977, *81* (1), 89-96.
30. Winston, P. W.; Bates, D. H., Saturated solutions for the control of humidity in biological research. *Ecology* 1960, *41* (1), 232-237.
31. Price, H. C.; Murray, B. J.; Mattsson, J.; O'Sullivan, D.; Wilson, T. W.; Baustian, K. J.; Benning, L. G., Quantifying water diffusion in high-viscosity and glassy aqueous solutions using a Raman isotope tracer method. *Atmos. Chem. Phys.* 2014, *14* (8), 3817-3830.

32. Chenyakin, Y. Are diffusion coefficients calculated using the Stokes-Einstein equation combined with viscosities consistent with measured diffusion coefficients of tracer organics within organics-water mediums? University of British Columbia, Vancouver, Canada, 2015.
33. Schlessinger, J.; Koppel, D. E.; Axelrod, D.; Jacobson, K.; Webb, W. W.; Elson, E. L., Lateral transport on cell membranes: mobility of concanavalin A receptors on myoblasts. *Proceedings of the National Academy of Sciences* 1976, 73 (7), 2409-2413.
34. Jacobson, K.; Wu, E.; Poste, G., Measurement of the translation mobility of concanavalin a in glycerol-saline solutions and on the cell surface by fluorescence recovery after photobleaching. *Biochimica et Biophysica Acta (BBA) - Biomembranes* 1976, 433 (1), 215-222.
35. Seksek, O.; Biwersi, J.; Verkman, A. S., Translational Diffusion of Macromolecule-sized Solutes in Cytoplasm and Nucleus. *The Journal of Cell Biology* 1997, 138 (1), 131-142.
36. Picart, C.; Mutterer, J.; Arntz, Y.; Voegel, J.-C.; Schaaf, P.; Senger, B., Application of fluorescence recovery after photobleaching to diffusion of a polyelectrolyte in a multilayer film. *Microscopy Research and Technique* 2005, 66 (1), 43-57.
37. Axelrod, D.; Koppel, D. E.; Schlessinger, J.; Elson, E.; Webb, W. W., Mobility measurement by analysis of fluorescence photobleaching recovery kinetics. *Biophysical Journal* 1976, 16 (9), 1055-1069.
38. Tsien, R. Y., Constructing and Exploiting the Fluorescent Protein Paintbox (Nobel Lecture). *Angewandte Chemie International Edition* 2009, 48 (31), 5612-5626.

39. Meyvis, T. L.; De Smedt, S.; Van Oostveldt, P.; Demeester, J., Fluorescence Recovery After Photobleaching: A Versatile Tool for Mobility and Interaction Measurements in Pharmaceutical Research. *Pharm Res* 1999, *16* (8), 1153-1162.
40. Deschout, H.; Hagman, J.; Fransson, S.; Jonasson, J.; Rudemo, M.; Lorén, N.; Braeckmans, K., Straightforward FRAP for quantitative diffusion measurements with a laser scanning microscope. *Opt. Express* 2010, *18* (22), 22886-22905.
41. Fick, A., V. On liquid diffusion. *The London, Edinburgh, and Dublin Philosophical Magazine and Journal of Science* 1855, *10* (63), 30-39.
42. Bird, R. B.; Stewart, W. E.; Lightfoot, E. N., Transport Phenomena John Wiley & Sons. New York 1960, 413.
43. Schneider, C. A.; Rasband, W. S.; Eliceiri, K. W., NIH Image to ImageJ: 25 years of image analysis. *Nat methods* 2012, *9* (7), 671-675.
44. (a) Periasamy, N.; Bicknese, S.; Verkman, A. S., Reversible Photobleaching of Fluorescein Conjugates in Air-Saturated Viscous Solutions: Singlet and Triplet State Quenching by Tryptophan. *Photochemistry and Photobiology* 1996, *63* (3), 265-271;(b) Zhou, X. X.; Lin, M. Z., Photoswitchable fluorescent proteins: ten years of colorful chemistry and exciting applications. *Current Opinion in Chemical Biology* 2013, *17* (4), 682-690;(c) Mueller, F.; Morisaki, T.; Mazza, D.; McNally, James G., Minimizing the Impact of Photoswitching of Fluorescent Proteins on FRAP Analysis. *Biophysical Journal* 2012, *102* (7), 1656-1665.

45. Zobrist, B.; Soonsin, V.; Luo, B. P.; Krieger, U. K.; Marcolli, C.; Peter, T.; Koop, T., Ultra-slow water diffusion in aqueous sucrose glasses. *Physical Chemistry Chemical Physics* 2011, *13* (8), 3514-3526.
46. Quintas, M.; Brandão, T. R. S.; Silva, C. L. M.; Cunha, R. L., Rheology of supersaturated sucrose solutions. *Journal of Food Engineering* 2006, *77* (4), 844-852.
47. Migliori, M.; Gabriele, D.; Di Sanzo, R.; de Cindio, B.; Correr, S., Viscosity of Multicomponent Solutions of Simple and Complex Sugars in Water. *Journal of Chemical & Engineering Data* 2007, *52* (4), 1347-1353.
48. Telis, V.; Telis-Romero, J.; Mazzotti, H.; Gabas, A., Viscosity of aqueous carbohydrate solutions at different temperatures and concentrations. *International Journal of food properties* 2007, *10* (1), 185-195.
49. Mustafa, M. B.; Tipton, D. L.; Barkley, M. D.; Russo, P. S.; Blum, F. D., Dye diffusion in isotropic and liquid-crystalline aqueous (hydroxypropyl)cellulose. *Macromolecules* 1993, *26* (2), 370-378.
50. Tamba, Y.; Ariyama, H.; Levadny, V.; Yamazaki, M., Kinetic Pathway of Antimicrobial Peptide Magainin 2-Induced Pore Formation in Lipid Membranes. *The Journal of Physical Chemistry B* 2010, *114* (37), 12018-12026.
51. Pang, X.-F., *Water: molecular structure and properties*. World Scientific: 2014.
52. Price, H. C.; Mattsson, J.; Murray, B. J., Sucrose diffusion in aqueous solution. *Physical Chemistry Chemical Physics* 2016, *18* (28), 19207-19216.

53. (a) Ramanathan, V.; Li, F.; Ramana, M. V.; Praveen, P. S.; Kim, D.; Corrigan, C. E.; Nguyen, H.; Stone, E. A.; Schauer, J. J.; Carmichael, G. R.; Adhikary, B.; Yoon, S. C., Atmospheric brown clouds: Hemispherical and regional variations in long-range transport, absorption, and radiative forcing. *Journal of Geophysical Research: Atmospheres* 2007, *112* (D22), n/a-n/a;(b) Chakrabarty, R. K.; Moosmüller, H.; Chen, L. W. A.; Lewis, K.; Arnott, W. P.; Mazzoleni, C.; Dubey, M. K.; Wold, C. E.; Hao, W. M.; Kreidenweis, S. M., Brown carbon in tar balls from smoldering biomass combustion. *Atmos. Chem. Phys.* 2010, *10* (13), 6363-6370.
54. (a) Andreae, M. O.; Crutzen, P. J., Atmospheric Aerosols: Biogeochemical Sources and Role in Atmospheric Chemistry. *Science* 1997, *276* (5315), 1052-1058;(b) Rizzo, L. V.; Correia, A. L.; Artaxo, P.; Procópio, A. S.; Andreae, M. O., Spectral dependence of aerosol light absorption over the Amazon Basin. *Atmos. Chem. Phys.* 2011, *11* (17), 8899-8912.
55. Bones, D. L.; Henricksen, D. K.; Mang, S. A.; Gonsior, M.; Bateman, A. P.; Nguyen, T. B.; Cooper, W. J.; Nizkorodov, S. A., Appearance of strong absorbers and fluorophores in limonene-O₃ secondary organic aerosol due to NH₄⁺-mediated chemical aging over long time scales. *Journal of Geophysical Research: Atmospheres (1984–2012)* 2010, *115* (D5).
56. (a) Glasius, M.; Lahaniati, M.; Calogirou, A.; Di Bella, D.; Jensen, N. R.; Hjorth, J.; Kotzias, D.; Larsen, B. R., Carboxylic Acids in Secondary Aerosols from Oxidation of Cyclic Monoterpenes by Ozone. *Environmental Science & Technology* 2000, *34* (6), 1001-1010;(b) Zhang, J.; Huff Hartz, K. E.; Pandis, S. N.; Donahue, N. M., Secondary Organic Aerosol Formation from Limonene Ozonolysis: Homogeneous and Heterogeneous

- Influences as a Function of NO_x. *The Journal of Physical Chemistry A* 2006, 110 (38), 11053-11063;(c) Bateman, A. P.; Nizkorodov, S. A.; Laskin, J.; Laskin, A., Time-resolved molecular characterization of limonene/ozone aerosol using high-resolution electrospray ionization mass spectrometry. *Physical Chemistry Chemical Physics* 2009, 11 (36), 7931-7942;(d) Heaton, K. J.; Dreyfus, M. A.; Wang, S.; Johnston, M. V., Oligomers in the early stage of biogenic secondary organic aerosol formation and growth. *Environmental Science & Technology* 2007, 41 (17), 6129-6136;(e) Walser, M. L.; Desyaterik, Y.; Laskin, J.; Laskin, A.; Nizkorodov, S. A., High-resolution mass spectrometric analysis of secondary organic aerosol produced by ozonation of limonene. *Physical Chemistry Chemical Physics* 2008, 10 (7), 1009-1022;(f) Leungsakul, S.; Jeffries, H. E.; Kamens, R. M., A kinetic mechanism for predicting secondary aerosol formation from the reactions of d-limonene in the presence of oxides of nitrogen and natural sunlight. *Atmospheric Environment* 2005, 39 (37), 7063-7082.
57. Lee, H. J.; Laskin, A.; Laskin, J.; Nizkorodov, S. A., Excitation–Emission Spectra and Fluorescence Quantum Yields for Fresh and Aged Biogenic Secondary Organic Aerosols. *Environmental Science & Technology* 2013, 47 (11), 5763-5770.
58. Nguyen, T. B.; Laskin, A.; Laskin, J.; Nizkorodov, S. A., Brown carbon formation from ketoaldehydes of biogenic monoterpenes. *Faraday Discussions* 2013, 165 (0), 473-494.
59. (a) Abramson, E.; Imre, D.; Beranek, J.; Wilson, J.; Zelenyuk, A., Experimental determination of chemical diffusion within secondary organic aerosol particles. *Physical Chemistry Chemical Physics* 2013, 15 (8), 2983-2991;(b) Cappa, C. D.; Wilson, K.,

Evolution of organic aerosol mass spectra upon heating: implications for OA phase and partitioning behavior. *Atmospheric Chemistry and Physics* 2011, 11 (5), 1895-1911;(c) Vaden, T. D.; Imre, D.; Beránek, J.; Shrivastava, M.; Zelenyuk, A., Evaporation kinetics and phase of laboratory and ambient secondary organic aerosol. *Proceedings of the National Academy of Sciences* 2011, 108 (6), 2190-2195;(d) Vaden, T. D.; Song, C.; Zaveri, R. A.; Imre, D.; Zelenyuk, A., Morphology of mixed primary and secondary organic particles and the adsorption of spectator organic gases during aerosol formation. *Proceedings of the National Academy of Sciences* 2010, 107 (15), 6658-6663;(e) Virtanen, A.; Joutsensaari, J.; Koop, T.; Kannosto, J.; Yli-Pirilä, P.; Leskinen, J.; Mäkelä, J. M.; Holopainen, J. K.; Pöschl, U.; Kulmala, M., An amorphous solid state of biogenic secondary organic aerosol particles. *Nature* 2010, 467 (7317), 824-827;(f) Virtanen, A.; Kannosto, J.; Kuuluvainen, H.; Arffman, A.; Joutsensaari, J.; Saukko, E.; Hao, L.; Yli-Pirilä, P.; Tiitta, P.; Holopainen, J., Bounce behavior of freshly nucleated biogenic secondary organic aerosol particles. *Atmospheric Chemistry and Physics* 2011, 11 (16), 8759-8766;(g) Kuwata, M.; Martin, S. T., Phase of atmospheric secondary organic material affects its reactivity. *Proceedings of the National Academy of Sciences* 2012, 109 (43), 17354-17359;(h) Saukko, E.; Lambe, A.; Massoli, P.; Koop, T.; Wright, J.; Croasdale, D.; Pedernera, D.; Onasch, T.; Laaksonen, A.; Davidovits, P., Humidity-dependent phase state of SOA particles from biogenic and anthropogenic precursors. *Atmospheric Chemistry and Physics* 2012, 12 (16), 7517-7529.

60. (a) Zelenyuk, A.; Imre, D.; Beránek, J.; Abramson, E.; Wilson, J.; Shrivastava, M., Synergy between secondary organic aerosols and long-range transport of polycyclic aromatic hydrocarbons. *Environmental Science & Technology* 2012, 46 (22), 12459-12466;(b) Liu, P.; Li, Y. J.; Wang, Y.; Gilles, M. K.; Zaveri, R. A.; Bertram, A. K.; Martin, S. T., Lability of secondary organic particulate matter. *Proceedings of the National Academy of Sciences* 2016, 113 (45), 12643-12648;(c) Ye, Q.; Robinson, E. S.; Ding, X.; Ye, P.; Sullivan, R. C.; Donahue, N. M., Mixing of secondary organic aerosols versus relative humidity. *Proceedings of the National Academy of Sciences* 2016, 113 (45), 12649-12654.
61. Koop, T.; Kapilashrami, A.; Molina, L. T.; Molina, M. J., Phase transitions of sea-salt/water mixtures at low temperatures: Implications for ozone chemistry in the polar marine boundary layer. *Journal of Geophysical Research: Atmospheres* 2000, 105 (D21), 26393-26402.
62. (a) Fonin, A. V.; Sulatskaya, A. I.; Kuznetsova, I. M.; Turoverov, K. K., Fluorescence of Dyes in Solutions with High Absorbance. Inner Filter Effect Correction. *PLoS ONE* 2014, 9 (7), e103878;(b) Brandt, M. Fluorescence Spectroscopy 1999. https://www.rose-hulman.edu/~brandt/Fluorescence/Fluorescence_Introduction.pdf.
63. (a) Virkkula, A.; Van Dingenen, R.; Raes, F.; Hjorth, J., Hygroscopic properties of aerosol formed by oxidation of limonene, α -pinene, and β -pinene. *Journal of Geophysical Research: Atmospheres* 1999, 104 (D3), 3569-3579;(b) Varutbangkul, V.; Brechtel, F.; Bahreini, R.; Ng, N.; Keywood, M.; Kroll, J.; Flagan, R.; Seinfeld, J.; Lee, A.; Goldstein, A., Hygroscopicity of secondary organic aerosols formed by oxidation of cycloalkenes,

- monoterpenes, sesquiterpenes, and related compounds. *Atmospheric Chemistry and Physics* 2006, 6 (9), 2367-2388.
64. (a) Leungsakul, S.; Jaoui, M.; Kamens, R. M., Kinetic Mechanism for Predicting Secondary Organic Aerosol Formation from the Reaction of d-Limonene with Ozone. *Environmental Science & Technology* 2005, 39 (24), 9583-9594;(b) Hakola, H.; Arey, J.; Aschmann, S. M.; Atkinson, R., Product formation from the gas-phase reactions of OH radicals and O₃ with a series of monoterpenes. *Journal of Atmospheric Chemistry* 1994, 18 (1), 75-102.
65. Andreae, M. O.; Gelencsér, A., Black carbon or brown carbon? The nature of light-absorbing carbonaceous aerosols. *Atmos. Chem. Phys.* 2006, 6 (10), 3131-3148.
66. Saathoff, H.; Naumann, K. H.; Möhler, O.; Jonsson, Å. M.; Hallquist, M.; Kiendler-Scharr, A.; Mentel, T. F.; Tillmann, R.; Schurath, U., Temperature dependence of yields of secondary organic aerosols from the ozonolysis of α -pinene and limonene. *Atmos. Chem. Phys.* 2009, 9 (5), 1551-1577.
67. Zobrist, B.; Marcolli, C.; Pedernera, D.; Koop, T., Do atmospheric aerosols form glasses? *Atmospheric Chemistry and Physics* 2008, 8 (17), 5221-5244.

Appendices

Appendix A

Table 5.1: Selected parameters used in rhodamine 6G rFRAP experiments in sucrose water solutions. τ_{eq} is the characteristic diffusion time of water within sucrose-water droplet (see Eq. 2.1). t_{exp} is the time used for conditioning.

a_w	Slide #	Dropletradius (μm)	τ_{eq}	t_{exp}	Measured D value ($\mu\text{m}^2/\text{s}$)
0.80	1	350	11 min	1 h	0.492
	2	350	11 min	1 h	0.492
	3	350	11 min	1 h	0.441
0.75	1	350	17 min	1 h	0.0840
	2	350	17 min	1 h	0.0918
	3	350	17 min	2 hrs	0.0783
0.60	1	140	0.85 hrs	3 hrs	0.00194
	2	125	0.67 hrs	3 hrs	0.00545
	3	90	0.35 hrs	3 hrs	0.00259
0.52	1	190	11 hrs	6 d 15 hrs	0.000125
	2	150	7 hrs	6 d 15 hrs	0.000155
	3	200	12 hrs	6 d 15 hrs	0.000143
0.38	1	75	1 d	6 d	3.98E-06
	2	60	17 hrs	12 d	2.29E-06
	3	100	2 d	93 d	9.56E-07
	4	75	1 d	93 d	6.44E-07

A.1 Parameterization of the viscosity of sucrose in water as a function of water activity

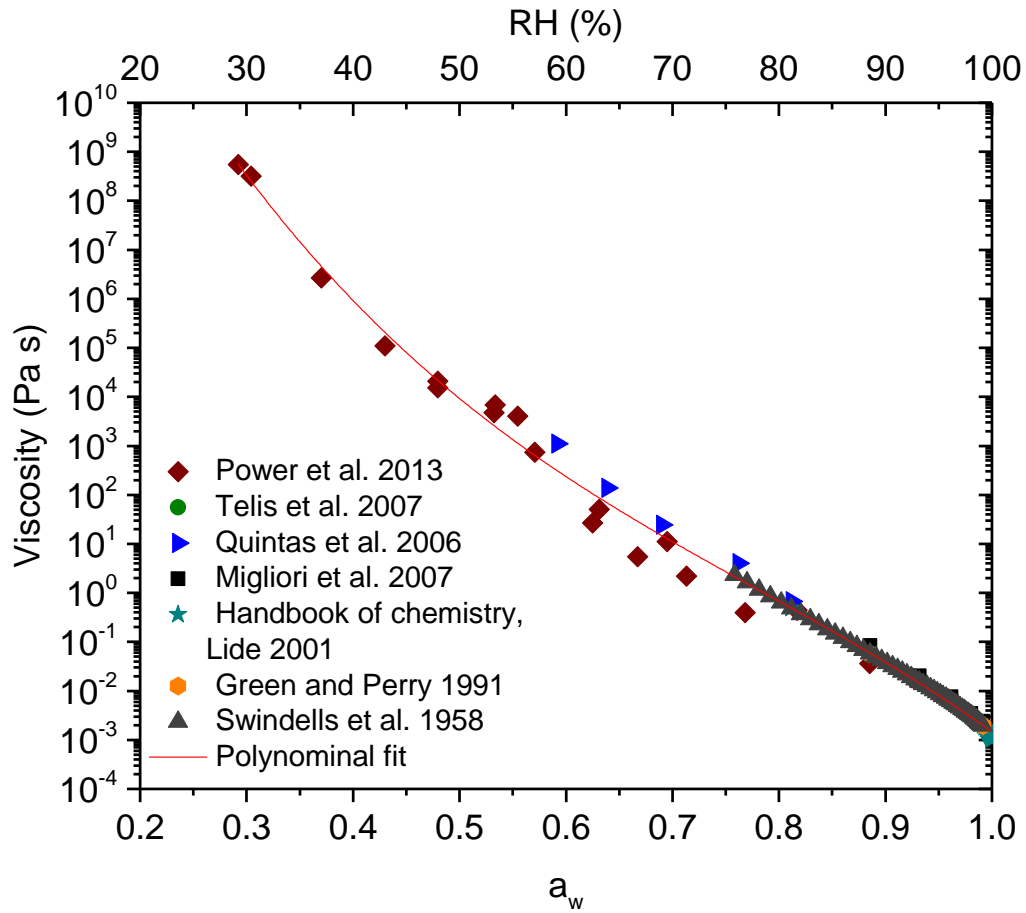


Figure 5.1: Parameterization of the viscosity as a function of water activity for sucrose water solutions using viscosity data from several sources.

Table 5.2: Fit parameters of the third order polynomial fit ($f(x) = A + Bx + Cx^2 + Dx^3$) in Figure 5.1.

	A	B	C	D	R^2
Fit parameters	20.97	-0.5641	0.0057	-2.4365×10^{-5}	0.9948

A.2 Determination of water activities of sucrose solutions

The amount of sucrose which was needed to obtain a certain water activity was calculated using a parameterization from Zobrist *et al.* (2011)⁶⁷:

$$a_w(T, w) = \frac{(1 + Aw)}{(1 + Bw + Cw^2)} + (T - T^\theta)(Dw + Ew^2 + Fw^3 + Gw^4). \quad 5.1$$

In this parameterization, the water activity, a_w , is calculated as a function of the temperature T and the concentration of sucrose in water w :

$$w = \text{weight percent of sucrose (wt \%)} / 100, \quad 5.2$$

T^θ is a reference temperature of 298.15 K and A to G are fit parameters ($A = -1$, $B = -0.99721$, $C = 0.13599$, $D = 0.001688$, $E = -0.005151$, $F = 0.009607$, $G = -0.006142$).

The experiments were performed at room temperature (19.9 °C to 22.4 °C) and because minor changes of the temperature only results in minor changes of the a_w , calculations regarding the a_w were performed using a temperature of $T = 20^\circ\text{C}$.

A.3 Polynomial fit for diffusion coefficients of water from Price *et al.*

Table 5.3: Parameters from the polynomial fit in Figure 2.15 with $f(x)=A+Bx+Cx^2+Dx^3$ based on Price *et al.*³¹

Molecule	A	B	C	D
Water	-20.89	25.92	-26.97	13.25

Appendix B

Table 5.4: Selected parameters used in rFRAP experiments with the intrinsic fluorophores in brown limonene

SOM. τ_{eq} is the characteristic diffusion time of water within sucrose-water droplet (see Eq. 2.1). t_{exp} is the time used for conditioning.

a_w	Slide #	Dropletradius (μm)	τ_{cd}	t_{exp}	Measured D value ($\mu\text{m}^2/\text{s}$)
0.90	1	200	23 s	17 min	0.60
	2	175	17 s	17 min	1.01
	3	160	15 s	22 min	0.82
	4	200	23 s	22 min	0.91
0.80	1	175	2.2 min	22 min	0.064
	2	175	2.2 min	18 min	0.073
	3	175	2.2 min	18 min	0.030
0.70	1	160	11.3 min	1.5 h	0.012
	2	160	11.3 min	3 h	0.017
	3	125	7 min	3 h	0.018
0.60	1	190	1.5 h	8 h	0.0092
	2	225	2.2 h	8 h	0.0086
	3	175	1.3 h	7 h	0.0094
0.52	1	150	6.6 h	38 d	0.0024
	2	185	10 h	38 d	0.0024
	3	150	6.6 h	38 d	0.0025
0.38	1	200	7.6 d	47 d	5.68E-4
	2	100	2 d	47 d	3.68E-4
	3	200	7.6 d	35 d	2.10E-4

Appendix C

The values for the concentration of R6G in citric acid and sucrose and water were calculated by subtracting the value of “Fluorescence without R6G” from “Fluorescence with R6G” and using the parameterization to calculate the concentration value.

Table 5.5: Values of diffusion coefficients, fluorescence intensities and calculated concentrations in citric acid water solution and sucrose water solution for 90% RH of R6G in brown limonene SOM. τ_{eq} is the characteristic diffusion time of water within sucrose water droplet (see Eq. 2.1). t_{exp} is the time used for conditioning.

a_w	Slide	Number of Bleach Spot	τ_{cd}	t_{exp}	Droplet radius (μm)	Fluorescence without R6G (a.u.)	Fluorescence with R6G (a.u.)	Conc. In citric acid	Conc. In sucrose water	Diffusion coefficient (μm)
0.9	1	1	90 s	18 min	400	7.8	72	0.273	0.290	0.203
		2				7.8	69	0.259	0.279	0.207
		3				7.8	89	0.354	0.373	0.1972
	4	1	60 s	20 min	320	12	57	0.203	0.215	0.3529
		2				12	64	0.236	0.243	0.3529
		3				12	55	0.194	0.206	0.403
	8	1	55 s	21 min	310	5	31	0.098	0.130	0.1961
		2				5	34	0.108	0.144	0.17001
		3				5	34	0.108	0.144	0.1716
		4				5	32	0.102	0.134	0.1736
	9	1	98 s	21 min	415	5.6	30	0.091	0.122	0.1962
		2				5.6	33.5	0.099	0.139	0.2131
		3				5.6	34	0.100	0.141	0.2399

a_w	Slide	Number of Bleach Spot	τ_{cd}	t_{exp}	Droplet radius (μm)	Fluorescence without R6G (a.u.)	Fluorescence with R6G (a.u.)	Conc. In citric acid	Conc. In sucrose water	Diffusion coefficient (μm)
0.9	12	1	62 s	24 min	330	4	78	0.302	0.334	0.3920
		2				4	79	0.307	0.338	0.4110
		3				4	76	0.292	0.324	0.3785
	14	1	100 s	59 min	420	4.6	132	0.543	1.165	0.2013
		2				4.6	100	0.405	0.490	0.2294
		3				4.6	104	0.423	0.537	0.2412
	20	1	62 s	80 min	330	9	32	0.102	0.115	0.6659
		2				9	32	0.102	0.115	0.7906
		3				9	39	0.127	0.148	0.8147
	22	1	82 s	70 min	380	9	32.5	0.103	0.118	0.8821
	23	1	62 s	70 min	330	9	30	0.095	0.106	0.6977
		2				9	26.5	0.084	0.089	0.4799
		3				9	27	0.086	0.092	0.3058

Table 5.6: Values of diffusion coefficients, fluorescence intensities and calculated concentrations in citric acid water solution and sucrose water solution for 80% RH of R6G in brown limonene SOM. τ_{eq} is the characteristic diffusion time of water within sucrose water droplet (see Eq. 2.1). t_{exp} is the time used for conditioning.

a_w	Slide	Number of Bleach Spot	τ_{cd}	t_{exp}	Droplet radius (μm)	Fluorescence without R6G (a.u.)	Fluorescence with R6G (a.u.)	Conc. In citric acid	Conc. In sucrose water	Diffusion coefficient (μm)
0.8	3a	1	6.5 min	45 min	300	7	64	0.236	0.262	0.02073
		2				7	66	0.245	0.270	0.02591
		3				7	76	0.292	0.310	0.06527
	5	1	6.5 min	67 min	300	14	36.5	0.117	0.113	0.009281
		2				14	30	0.095	0.082	0.01489
	7	1	6.5 min	36 min	300	11.5	35	0.112	0.118	0.05436
	11	1	4.16 min	49 min	240	7.2	65	0.240	0.265	0.1336
		2				7.2	61.5	0.224	0.252	0.09991
		3				7.2	58	0.208	0.238	0.1033
	14	1	4.9 min	49 min	260	2	75	0.288	0.329	0.01435
		2	4.9 min		260	2	84	0.330	0.378	0.01722

Table 5.7: Values of diffusion coefficients, fluorescence intensities and calculated concentrations in citric acid water solution and sucrose water solution for 70% RH of R6G in brown limonene SOM. τ_{cd} is the characteristic diffusion time of water within sucrose-water droplet (see Eq. 2.1). t_{exp} is the time used for conditioning.

a_w	Slide	Number of Bleach Spot	τ_{cd}	t_{exp}	Droplet radius (μm)	Fluorescence without R6G (a.u.)	Fluorescence with R6G (a.u.)	Conc. In citric acid	Conc. In sucrose water	Diffusion coefficient (μm)
0.7	3	1	35 min	45 min	280	11	42	0.139	0.153	0.05486
		2				11	42	0.139	0.153	0.04915
		3				11	41	0.135	0.148	0.04454
	5	1	40 min	119 min	300	8	56	0.199	0.227	0.01782
		2				8	48	0.163	0.194	0.01023
		3				8	50	0.172	0.202	0.02011
	6	1	48 min	119 min	330	11	28	0.089	0.087	0.01395
		2				11	26.5	0.084	0.080	0.01199
	9	1	18 min	120 min	200	10.5	68	0.254	0.264	0.005821
		2				10.5	72	0.273	0.280	0.004813
		3				10.5	86	0.340	0.341	0.00228